

TESIS DOCTORAL

EDICIÓN GENÓMICA EN RATÓN BASADA EN LA
ELECTROPORACIÓN DE CRISPR/CAS9 EN CIGOTOS
APLICACIÓN AL ESTUDIO DEL SÍNDROME DE MANO HENDIDA

PHP TESIS

GENOME EDITING BY THE ELECTROPORATION OF
CRISPR/CAS9 IN MOUSE ZYGOTES
APPLICATION TO THE STUDY OF THE SPLIT HAND-FOOT
MALFORMATION SYNDROME

AUTOR

SARA LUCAS TOCA

DIRECTOR/ES

MARIAN ROS LASIERRA

ENDIKA HARO GABICAGOGEASCOA

UNIVERSIDAD DE CANTABRIA

Escuela de [Doctorado](#) de la Universidad de Cantabria

Santander 2022



UNIVERSIDAD DE CANTABRIA

**Instituto de Biomedicina y
Biotecnología de Cantabria
(IBBTEC)**



TESIS DOCTORAL

**“Edición genómica en ratón basada en la electroporación de
CRISPR/Cas9 en cigotos. Aplicación al estudio del síndrome de
mano hendida”**

PhD THESIS

**“Genome editing by the electroporation of CRISPR/Cas9 in
mouse zygotes. Application to the study of the split hand-foot
malformation syndrome”**

Realizada por:

SARA LUCAS TOCA

Dirigida por:

MARIAN ROS LASIERRA

ENDIKA HARO GABICAGOEASCOA

María A. Ros Lasierra, Profesora de Investigación del Instituto de Biomedicina y Biotecnología de Cantabria (CSIC-UC-SODERCAN) y

Endika Haro Gabicagoeascoa, doctor por la Universidad de Cantabria

como directores de la Tesis Doctoral titulada: “Genome editing by the electroporation of CRISPR/Cas9 in mouse zygotes. Application to the study of the split hand-foot malformation syndrome”; “Edición genómica en ratón basada en la electroporación de CRISPR/Cas9 en cigotos. Aplicación al estudio del síndrome de mano hendida”

CERTIFICAN

Que dicho trabajo ha sido realizado por Doña **Sara Lucas Toca** y consideran que se encuentra terminado y reúne los requisitos para su presentación como memoria de doctorado por la interesada, al objeto de poder optar al grado de Doctor por la Universidad de Cantabria.



María A. Ros Lasierra

Directora y tutora de la tesis



Endika Haro Gabicagoeascoa

Director de la tesis

Santander a 17 de Santander 2022

"A todos esos pilares que han hecho esto
posible"

CONTENTS

ABBREVIATIONS AND ACRONYMS

RESUMEN

1. INTRODUCTION	21
1.1 Genome editing	23
1.2 The CRISPR/Cas9 system	26
1.3 Limb development	38
1.4 Specificity proteins (SP) family	42
1.5 Split hand-foot malformation (SHFM)	46
1.6 The Notch pathway	51
2. AIM OF THE PRESENT THESIS	55
3. MATHERIALS AND METHODS	59
3.1. Mouse strains	61
3.2. crRNA selection.....	61
3.3. Cas9 endonuclease	62
3.4. Ribonucleoprotein (RNP) complex preparation	62
3.5. ssODN repair template design	63
3.6. In vitro validation of crRNA.....	65
3.7. Zygote collection.	66
3.8. Electroporation procedure.....	67
3.9. Embryo transfer	69
3.10. Genotyping strategy	69
3.11. Isolation of genomic DNA (quick protocol)	70
3.12. Genotyping	71
3.13. Genotyping of established lines used in this project.	71
3.14. Sanger sequencing.....	73
3.15. Cloning PCR products.....	73

3.16.	Line establishment by backcrossing.....	74
3.17.	Analysis of possible off-target.	74
3.18.	Skeletal preparations.	75
3.19.	Paraffin embedding	76
3.20.	Whole mount in situ hybridization (WMISH)	76
3.21.	In situ hybridization in paraffin sections.....	77
3.22.	Immunohistochemistry	78
3.23.	Immunofluorescence	78
3.24.	Immunoblot	79
3.25.	Immunoprecipitation	79
4.	RESULTS.....	81
4.1.	OBJECTIVE 1: “Implementation of a CRISPR-based platform for genome edition in mouse zygotes”	83
4.2.	OBJECTIVE 2: “To generate animal models by mouse zygote electroporation with CRISPR/CAS9 system for the study of split hand-foot malformation (SHFM)”87	
4.2.1.	Loss of function of <i>Jag2</i>	87
4.2.2.	Double deletion of <i>Dlx5</i> and <i>Dlx6</i>	98
4.2.3.	Generation of a <i>Sp6</i> -tagged knock-in mouse.....	108
4.3.	APPLICATION OF THE CRISPR/CAS 9 TECHNOLOGY IN OTHER PROJECTS IN OUR LAB.....	117
4.3.1.	Individual deletion of the limb-specific <i>Lmx1b</i> enhancers <i>LARM1</i> and <i>LARM2</i> . 117	
4.3.2.	Generation of a <i>Hoxa13</i> tagged knock-in mouse	119
5.	DISCUSSION.....	123
5.1.	Development of a CRISPR/Cas9 based genome editing platform for generation of customized murine models	125
5.2.	Strategies to overcome the challenges of genotyping small INDELS.....	126

5.3 Disruption of the <i>Jag2</i> open reading frame by NHEJ mediated INDELs after CRISPR/Cas9 mediated DSB	127
5.4 The analysis of <i>Jag2;Sp6</i> compound mutants suggests genetic interaction between both genes	129
5.5 Perinatal lethality of heterozygous prevented the establishment of the double <i>Dlx5/Dlx6</i> edited deletion	131
6. CONCLUSIONS / CONCLUSIONES.....	137
7. REFERENCES	143
8. AGRADECIMIENTOS.....	169

ABBREVIATIONS AND ACRONYMS

Aa: amino acid

Ab: Antibody

Ag: Antigen

AER: Apical ectodermal ridge

AP: Antero-Posterior axis

Bp: Base paired

CRE: Cis-regulatory elements

CRISPR: Clustered regularly interspaced short palindromic repeats

crRNA: CRISPR RNA

DBD: DNA-binding domain

DKO: Double knock-out

DMD: Duchenne muscle dystrophy

DSB: Double strand break

DSL: Delta, Serrate and Lag-2

DV: Dorso-Ventral axis

EEC: Ectrodactyly-ectodermal Displasia-clefting

EGF: Epidermal growth factor

ESC: Embryonic stem cell

EtOH: Ethanol

F: Filial or inbreeding (sister X brother) generations.

FGF: fibroblast growth factor

FL: Forelimb

GM: genetically modified

HDR: homology-direct repair

HL: Hindlimb

HR: homologous recombination

IMC: inner mass cell

INDELS: Insertions and deletions

iPS: induced pluripotent stem

JAG2: Jagged 2

KLF: Krüppel-like factor

KI: Knock-in

KO: Knock-out

LFL: Left forelimb

LHL: Left hindlimb

N: Number of backcross generations

NGS: Next generation sequencing

NHEJ: non-homologous end joining

NLS: Nuclear localization signal

NT: Nucleotide

PAM: Protospacer adjacent motif

PBS: Phosphate Buffered Saline

PD: Proximo-Distal axis

PFA: Paraformaldehyde

PICS: Protease Inhibitor Cocktail

PN: Pronucleus

RFL: Right forelimb

RHL: Right hindlimb

RNP: ribonucleoprotein

RP: retinitis pigmentosa

RPA: Recombinase polymerase amplification

RT: room temperature

sgRNA: single-guide RNA

SHERLOCK: specific high-sensitivity enzymatic reporter unlocking

SHFLD: Split Hand-Foot Long-bone deficiency

SHFM: Split Hand-Foot malformation

Sm: Syndactylism

Shh: Sonic Hedgehog

Sp: Specificity protein

TALEN: transcription activator-like effector nucleases

TF: Transcriptional factors

tracrRNA: Trans-activating CRISPR RNA

ZFN: Zinc finger nucleases

ZGA: zygotic genome activation

ZP: Zona pellucid

RESUMEN

RESUMEN

La edición genómica ha sido, y aún es, uno de los grandes retos de la Biología. El descubrimiento de la tecnología CRISPR/Cas9 y su aplicación para la edición génica ha supuesto una revolución en el campo de la ingeniería genética, permitiendo generar mutaciones específicas en lugares deseados del genoma de una manera relativamente sencilla y rápida.

El CRISPR, acrónimo del inglés clustered regularly interspaced short palindromic repeats (en español repeticiones palindrómicas cortas agrupadas y regularmente espaciadas) son familias de secuencias de ADN en bacterias que, junto con las endonucleasas Cas, forman el sistema inmune adaptativo de las arqueas y las bacterias, usado para defenderse de agentes patógenos invasores como pueden ser los virus. Este sistema ha sido modificado y adaptado para la edición genómica. Aunque existen varios tipos de sistemas CRISPR/Cas, el CRISPR/Cas9 es el que más se ha adaptado para la edición del genoma y es el que hemos puesto a punto en nuestro trabajo.

El primer objetivo de este proyecto ha sido establecer un servicio de edición genómica en el Instituto de Biomedicina y Biotecnología de Cantabria (IBBTEC). La creación de esta plataforma pone a disposición de los investigadores de nuestra comunidad la posibilidad de generar modelos animales para el estudio de enfermedades humanas o cualquier otro propósito, de una manera sencilla, rápida y económica.

Para conseguir este objetivo, hemos tenido que poner a punto el cultivo in vitro de embriones de ratón y las condiciones óptimas para la transferencia de estos a madres pseudopreñadas una vez que ya han sido modificados genéticamente. Además, hemos tenido que seleccionar la cepa de ratón más conveniente en cada caso. También hemos seleccionado el método de aplicación de los componentes del CRISPR, el proveedor de estos y el dispositivo de trabajo más adecuado. Gracias al apoyo del Servicio de Estabulación y Experimentación Animal (SEEA) de la Universidad de Cantabria, especialmente de su director, Miguel García, y de Beatriz Romero hemos conseguido poner a punto todas las condiciones para lograr el establecimiento de este servicio con éxito, en el cuál, editamos el genoma a través de la electroporación de CRISPR/Cas9 en cigotos de ratón con el electroporador NEPA 21.

El segundo objetivo de este trabajo ha sido utilizar este servicio para la generación de tres modelos animales para el estudio del síndrome de mano y pie hendido (SHFM, Split Hand/Split Foot Malformation), una malformación de la mano y/o pie que implica la falta de dedos centrales y una abertura en forma de “U” en la mano. Estos modelos se han basado en modelos animales previamente publicados para poder validar el correcto funcionamiento de la técnica mediante la comparación del fenotipo de nuestros modelos y los previamente descritos.

El primer modelo animal que se ha generado ha sido el modelo de pérdida de función de *Jagged2* (*Jag2*) con la finalidad de estudiar su posible interacción génica con *Sp6* (uno de los genes implicados en el síndrome de mano y pie hendido, puesto que el mutante *Sp6*^{-/-};*Sp8*^{+/-} presenta SHFM (Haro et al. 2014)) dada la similitud de fenotipo de ambos mutantes. Para ello, hemos seleccionado un crRNA para dirigir la Cas9 hacia el exón 4 del gen, basándonos en el modelo previamente descrito por Gridley (Jiang et al. 1998). Entre los diversos alelos que obtuvimos con la modificación génica deseada, hemos seleccionado uno que conlleva la eliminación de 41 nucleótidos (nt), lo que altera la pauta de lectura del gen generándose la pérdida de función de este. El establecimiento de la línea *Jag2*^{emMar} a partir del ratón portador del alelo mutado, nos ha permitido constatar que en homocigosis se reproducía el fenotipo de pérdida de función de *Jag2*. El estudio de la serie alélica de los doble mutantes *Jag2*;*Sp6* ha demostrado que los dobles mutantes *Jag2*^{-/-};*Sp6*^{-/-} presentan fenotipos más severos que los mutantes individuales revelando la interacción entre ambos genes.

El segundo modelo animal generado ha sido la pérdida de función conjunta de los genes *Dlx5* y *Dlx6* que están localizados en proximidad en el genoma y se transcriben de manera convergente. *Dlx5* y *Dlx6* están también implicados en el síndrome SHFM y sus dominios de expresión se solapan con los de *Sp6* y *Sp8*, habiéndose mostrado una interacción entre *Sp8* y *Dlx* (Pérez-Gómez et al. 2020). Basándonos en el modelo previamente publicado por Lufkin (Robledo et al. 2002) hemos seleccionado dos crRNA, uno para dirigir la Cas9 hacia el primer intrón de *Dlx6* y otro hacia el primer intrón de *Dlx5*. La electroporación de los dos crRNAs a la vez nos ha permitido eliminar el fragmento entre los dos cortes (~16Kb) produciendo así el doble mutante. Hemos encontrado problemas para establecer la línea partiendo de diferentes fundadores, probablemente debido a la reducida viabilidad de los heterocigotos, lo que finalmente nos ha impedido establecerla. La electroporación de los dos crRNA generó, además de la

eliminación del fragmento, la inversión de este. Hemos conseguido establecer la línea con la inversión en homocigosis y no hemos observado ningún fenotipo aparente, lo que sugiere que las proteínas quiméricas que se forman con el primer exón de un gen y los dos exones del otro gen son funcionales o al menos hipomórficas.

El tercer modelo animal se ha dirigido a fusionar un epítipo al factor de transcripción Sp6 con la finalidad de facilitar su detección en experimentos de CHIP-seq. El epítipo seleccionado ha sido el tag V5. Para la generación de este modelo se ha seleccionado un crRNA para dirigir la Cas9 justo hacia los nucleótidos previos al codón STOP de la proteína. Además, en la electroporación de los cigotos para la generación de este modelo hemos incluido una hebra donante de ADN como molde. Esta hebra consiste en un oligonucleótido de cadena sencilla (ssODN) que contiene la secuencia de ADN codificante para el tag V5 flanqueada por secuencias homólogas a los lados del corte para dirigir su inserción en la región deseada del genoma. La línea de ratón *Sp6:V5^{emMar}* se ha conseguido establecer en heterocigosis y homocigosis sin fenotipo alguno, aunque la detección del tag resulta problemática.

En resumen, hemos implementado un servicio de edición genómica basado en la electroporación de cigotos de ratón usando la técnica CRISPR/Cas9. Este servicio pone a disposición de la comunidad científica de Cantabria la posibilidad de generar los modelos de ratón deseados de una manera sencilla, rápida y económica. La idoneidad del servicio queda demostrada mediante la generación de varios modelos animales para el estudio de la SHFM en este trabajo (*Jag2^{emMar}*, *Sp6:V5^{emMar}* y la doble delección de los genes *Dlx5* y *Dlx6*), así como la generación de otros modelos de gran utilidad (*DelLARM1^{emMar}*, *DelLARM2^{emMar}*, *Hoxa13:V5^{emMar}*, *HoxcDelEC1-2^{emMar}* y *HoxcInvEC1-2^{emMar}*) para el desarrollo de otros proyectos que llevados a cabo en nuestro laboratorio.

1. INTRODUCTION

1. INTRODUCTION

1.1 Genome editing

Genome editing refers to the ability to modify the genome as desired. It is an invaluable resource to improve our understanding of human genetics and it can be applied to treat, cure, and prevent genetic diseases.

Monogenetic diseases affect at least 250 million individuals globally (Doudna 2020). The scientific community characterizes genetically affected families by DNA sequencing. Detailed information about the mutation that produces each disorder can be applied to find a genetic cure by disrupting the toxic gene function or restoring the essential gene function with the application of genome editing technologies. Genome editing can be performed *in vitro* or *in vivo* giving the possibility to alter cell fates and organism traits by the generation of the desired mutations in their DNA.

Different types of genetically modified (GM) animals have been generated for the global study of many pathological entities. The first two decades in the application of genome editing technologies for the generation of GM organisms were based on the use of embryonic stem cells (ESC) in culture that were modified by homologous recombination. Selected cells containing the desired mutation were injected into the blastocyst to obtain chimeric mice and subsequent establishment of the line bearing the desired mutation. In recent years, the discovery of programmable nucleases that are directly introduced into the mouse zygote, has represented an incredible improvement in the generation of animal models for the study of human diseases.

Programmable nucleases can perform site-specific DNA cleavage generating double strand breaks (DSB). After that, since the damage could be lethal, the cell will try to repair it. The cell has two intrinsic DNA repair mechanism: the nonhomologous-end joining (NHEJ) pathway and the homology-directed repair (HDR) pathway. Genome editing takes advantage of these two mechanisms to modify the cell's genome.

The most common natural repair mechanism used by the cells is the NHEJ pathway, in which the joining between both DNA strands is performed without a homologous template. The NHEJ pathway is prone to error and therefore frequently

results in nonspecific insertions or deletions (INDELS). The INDELS may cause frameshift mutations, which can disrupt the gene function. The INDELS can be considered as footprints left by the genetic editing systems and its quantification can be used to determine the overall activity (off-target) and specificity of the system (Lin and Luo 2019). This pathway enables the generation of knock-out (KO) models.

Less frequent is the use of the HDR pathway to repair the DSB. This mechanism requires a DNA homologous template. It consists in the perfect copy of the homologous chromatid into the genomic sequence being repaired by homologous recombination (HR). This pathway is useful for the insertion of an exogenous DNA sequence into the genome, for the generation of knock-in (KI) models or to correct mutations. To favor this pathway, a donor sequence with homology arms (homologous template) is provided to direct the HR. The donor must have homology regions for the sequences upstream and downstream of the DSB. It can only occur in the S and G2 phase of the cellular cycle (Wefers et al. 2017).

Currently, there are three different genetic editing systems based on nucleases: i) the Zinc-finger nucleases (ZFN), ii) the transcription activator-like effector nucleases (TALEN), and iii) the clustered regulatory-interspaced short palindromic repeat associated with Cas system (CRISPR/Cas). All of them generate a DSB in the DNA with varying specificity and efficiency being the CRISPR technology the one that reaches the higher specificity and efficiency (Fig. 1).

The **ZFN** system is an artificially engineered DNA endonuclease made by the fusion of the nuclease domain of bacterial restriction enzyme *FokI* with three zinc finger domains. Each zinc finger recognizes a specific 3-4 bp sequence via its alpha-helix, so that 3 zinc fingers arranged in tandem can be designed to recognize a 9-12 bp specific sequence. The dimerization of the *FokI* non-specific endonuclease domain is required to generate a DSB. For *FokI* to dimerize and cut, two ZNF-*FokI* complexes targeting opposite strands of the target DNA sequence simultaneously in a non-overlapping manner are designed. The zinc fingers are designed in pairs, each recognizing a different DNA strand flanking a specific DNA sequence of the genome. This strategy was first used in 2009 to produce a KO rat (Geurts et al. 2009). The possible cleavage of sequences in the genome, instead of or in addition to the specific target sequence (off-target) and the

complexity of ZFN design and production, which is not accessible to all laboratories, are some of the limitations of this technology.

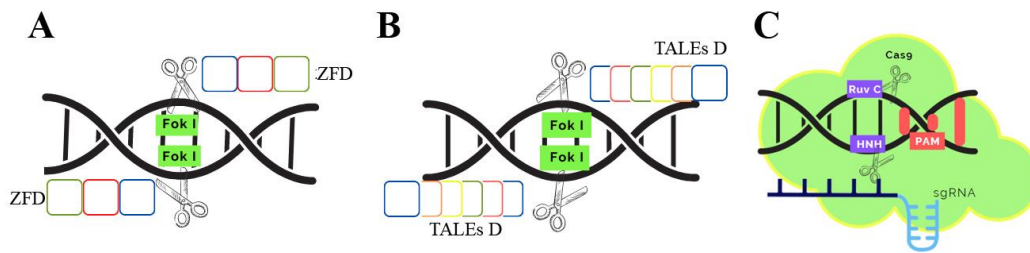


Figure 1: The three genome editing systems. **A.** The ZFN system formed by three zinc finger domains (depicted as blue, red, and green squares) and the nuclease domain of the *FokI* enzyme (green). **B.** The TALEN system consists of TALE repeat domains (blue, red, green, and yellow squares) and *FokI* nuclease domain (green). **C.** CRISPR/Cas9 system is formed by a single-guide RNA (blue) and Cas9 endonuclease (green).

In 2011, **TALEN** was used for the generation of a KO rat as an alternative to ZFN (Tesson et al. 2011). Whereas ZFN are completely engineered in the laboratory, the transcription activator-like (TAL) effectors are naturally occurring activators found in some plant-infecting pathogens to hijack and transform the plant cellular machinery. The TALEN system is also a chimeric protein generated by the fusion of a DNA-binding domain with the *FokI* endonuclease domain, operating also as dimers. The DNA-binding domain consists of several 33-35 amino acid (aa) repeats arranged in tandem. DNA recognition is achieved through the aa at position 12-13 of each repeat. This region is termed the repeat variable di-residues or RVD that recognizes a single DNA base pair. The diversity of the TAL effectors enables targeting of specific DNA sequences through the assembly of the repeats in tandem where each of the repeats targets a single nucleotide fused to the *FokI* nuclease. Both the ZFN and the TALEN systems require the recoding of protein sequences for each new target site. This, together with the long process to generate the large number of plasmids that are required in the technique suppose a barrier for the generalized application of these system.

The Clustered Regularly Interspaced Short Palindromic Repeats (**CRISPR**)-associated with **Cas** (CRISPR-associated protein) system was adapted for genome editing

in eukaryotic cells the first time in 2013 (Cong et al. 2013) and has resulted in an invaluable animal model generation tool able to generate precise genome modifications with high efficiency and low cost. Whereas ZFN and TALEN are protein-DNA dependent to detect the target sequences by different aa/nucleotide codes, the CRISPR/Cas system only needs a small RNA molecule to match the target DNA sequences to standard Watson-and-Crick nucleotide pairing code that is a more stable interaction (Seruggia and Montoliu 2014). The discovery and the application of the CRISPR/Cas system in multiple organisms have transformed the life science field. This system will be described in the following section.

1.2 The CRISPR/Cas9 system

The CRISPR/Cas system is an adaptable immune mechanism of many archaea and bacteria to protect themselves from pathogen organisms that has been modified for genome editing.

There are two main components in this system: The *Cas* genes and the CRISPR locus. CRISPR refers to arrays of short conserved repeated sequences interspaced by spacers. The spacers are DNA sequences of similar size, that correspond to DNA sequences present in invader organism genomes that the bacteria or archaea have previously encounter. Each CRISPR locus encodes acquired spacer sequences and repeat sequences. The *Cas* genes encode different Cas endonuclease proteins involved in different processes like CRISPR RNA processing, target DNA or RNA cleavage and new spacer integration.

The natural course of this adaptative prokaryotic immune response consists in three stages: adaptation, CRISPR RNA (crRNA) processing and interference (Makarova et al. 2011; Makarova and Koonin 2015) (Fig.2).

After viral infection, during the adaptation stage, the bacteria integrate into the CRISPR locus a short piece of DNA (approximately 30bp) from the invader organism's genomes as spacers. This genome integration is through Cas1 and Cas2 endonuclease proteins, which are present in most of the known CRISPR/Cas systems.

During the processing stage, the transcription of the CRISPR locus produces the pre-crRNA (pre-CRISPR RNA) that is catalyzed by endoribonucleases into the short

mature crRNA. The effector complex, that is the ribonucleoprotein (RNP) complex, comprised of crRNA and the Cas protein of each immune system type and is responsible for interfering with the invader DNA or RNA sequences that are targeted and cleaved.

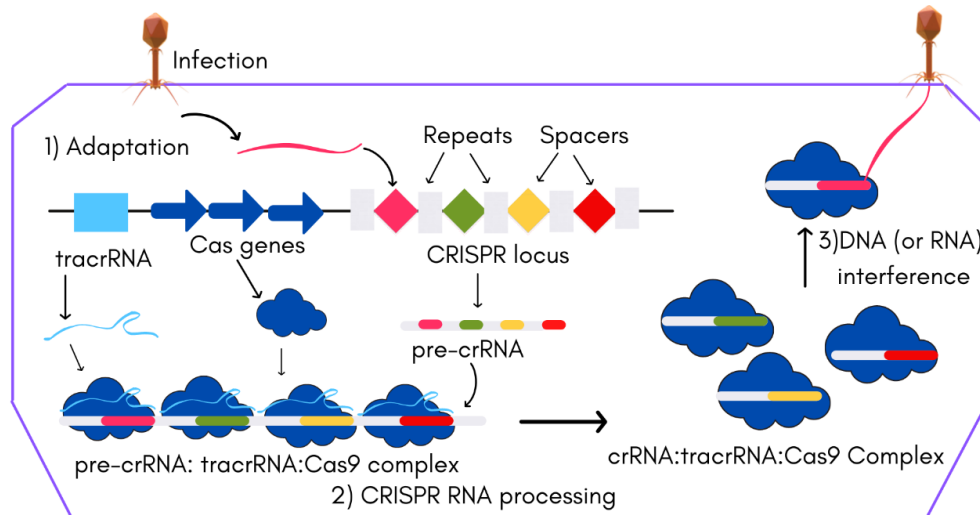


Figure 2: The CRISPR/Cas pathway (Type II). 1) Adaptation stage or spacer integration (invader organism DNA). 2) CRISPR RNA processing, from CRISPR locus to mature crRNA. 3) Foreign DNA or RNA interference. Adaptive immune mechanism system.

The third phase is the interference. To target and cleave a DNA sequence, the effector complex needs complementarity between the spacer and the target “protospacer” sequence in addition to a correct proto-spacer adjacent motif (PAM sequence) at the 3’ end of the protospacer sequence. The PAM sequence and its position is specific to each Cas endonuclease (Mojica et al. 2009).

Currently, the CRISPR/Cas classification captures only a part of the complexity of these systems, due to the intrinsic modularity and evolutionary mobility. The CRISPR/Cas system classification distinguishes three major types (I, II and III) and one last type (IV) less common, but clearly distinct. All of them have the components required for the key steps of the defense mechanism with one major difference: the associated Cas. Type I has the *Cas3* gene, type II has the *Cas9*, type III has the *Cas10* and type IV has the *Csf1*. The current classification combines evidences of Cas protein phylogeny, comparative genomics and structural analyses (Makarova and Koonin 2015).

- Type I CRISPR/Cas system: This type includes the signature *Cas3* gene that encodes a large protein with separate helicase and DNase activities. When the helicase domain of *Cas3* is fused to a Histidine/Aspartate (HD) family domain, it confers an endonuclease activity to cleave target DNA. The type I system is formed by a single operon encoding *Cas1* and *Cas2* genes for the Cascade (CRISPR-associated complex for antiviral defense) effector complex and *Cas6* that is responsible of pre-crRNA processing. Type I is subdivided in six subtypes (I-A to I-F) with differences in the signature genes or the features of the operon organization.

- Type II CRISPR/Cas systems: The signature gene of this type is the *Cas9* gene. *Cas9* encodes a multidomain protein that is essential for pre-crRNA processing to mature crRNA and can perform DNA cleavage. Type II structure, besides *Cas9* gene, also contains the ubiquitous *Cas1* and *Cas2* genes, apart from one or two genes that encode for the *trans*-activating CRISPR RNA (tracrRNA), which is a specialized ribonucleic acid molecule presents in this type II system (Chylinski et al. 2014) that interact with the crRNA to form a dual guide. The tracrRNA and the RNase III, the later not encoded in the CRISPR/Cas locus, are used for pre-crRNA processing. The *Cas9* endonuclease consists of two lobes: the recognition lobe and the endonuclease lobe. The recognition lobe is a *Cas9* specific functional domain that interacts with the heteroduplex formed by the crRNA and the DNA. It can be divided in three regions: a long α helix as a bridge helix, a REC1 domain that is essential for the heteroduplex recognition and a REC2 domain, which is not critical for the DNA cleavage like REC1 but participates in the heteroduplex recognition. The endonuclease lobe is composed by the HNH (Histidine-Asparagine-Histidine), the Ruv-C and the PAM-interacting domains (Nishimasu et al. 2014). The Ruv-C domain, near the amino terminus, cleaves the DNA-strand non-complementary to the guide RNA, and the HNH domain, in the middle of the protein, cleaves the complementary strand (Gasiunas et al. 2012). The *Cas9* recognizes NGG as its PAM sequence located 3' to the protospacer, where N is any nucleotide (Mali et al. 2013b) (Fig. 3). The *Cas9* interacts with the PAM sequence and employs PAM recognition to identify potential target sites to generate a DSB between nucleotides (nt) 3-4 upstream to the PAM (Garneau et al. 2010). Type II is subdivided in three subtypes (II-A to II-C) according to its operon organization. This Type II CRISPR/Cas system has been engineered for genome editing becoming a revolutionary tool as we show later.

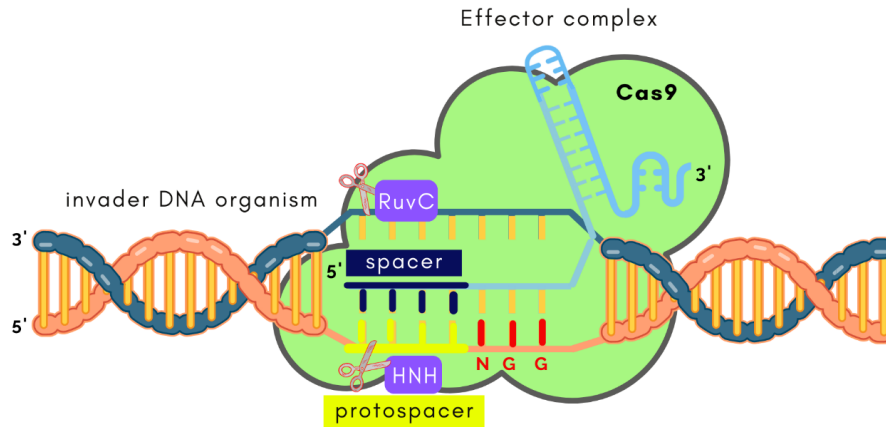


Figure 3: The effector complex of type II CRISPR/Cas system. There is a complementation between the spacer of the CRISPR system (blue) and the protospacer of the invader organism (yellow). The Cas9 (green) recognize the PAM sequence in the protospacer at 3' (NGG). The Cas9 by the PAM identification and the positioning of the Ruv-C and the HNH endonuclease domains undergoes conformational changes and generates a DSB in the foreign DNA.

- Type III CRISPR/Cas systems: The *Cas10* is the signature gene of this system that encodes for a multidomain protein with four domains identified: N-terminal cyclase-like domain, a helical domain, the palm domain, and the C-terminal alpha helical domain. The structure of type III is composed of genes that encode for subunits of the effector complex to process the pre-crRNA. Type III CRISPR/Cas systems often do not encode their own *Cas1* or *Cas2* genes. Type III can be divided in two subtypes (III-A and III-B) with distinct genes encoding the small subunits of effector complexes, *csm2* and *cmr5* respectively. The type III-B can target RNA.
- Type IV CRISPR/Cas systems: The type IV is found in several bacterial often in plasmids and not in proximity to the CRISPR array, if present. The type IV consists of a multisubunit crRNA–effector complex where *csf1* serves as signature for this type of the endonuclease. Type IV can be divided in two subtypes containing DinG family helicases or not.

The CRISPR/Cas system appeared as a potential genome-editing tool for site-specific DNA cleavage. In 2013, the CRISPR/Cas9 system was adapted for its use in eukaryotic cells. This modified type II prokaryotic system shows efficient RNA-guided

modifications in mammalian cells requiring only three main components: crRNA, tracrRNA and the Cas9 (Cong et al. 2013; Wang et al. 2013). Since then, the CRISPR/Cas9 technology has been successfully applied to a huge variety of organisms. The type II CRISPR/Cas system from *Streptococcus pyogenes* is the most engineered adapted for genome editing with high efficiency.

Applications of the engineered CRISPR/Cas9 system

Since its discovery, the CRISPR/Cas systems were described as potential tools for genome editing and multiple strategies were developed to facilitate its application to mammalian cells.

The RNP complex formed by the assembly of the crRNA, the tracrRNA and the Cas9 can be performed inside or outside the cell, depending on the procedure followed. The use of plasmids or viruses that encode the sequences to synthesize the crRNA, the tracrRNA and the Cas9, results in the formation of the RNP inside the cells. RNP delivery offers a more immediate function upon delivery and a lower risk for off targets compared with the use of plasmids because the Cas9 activity will be turndown by the cellular machinery (Farboud et al. 2018).

The RNP can be generated by first annealing the crRNA and the tracrRNA in vitro by oligo hybridisation or by using a synthetic single guide RNA (sgRNA) composed of both crRNA and tracrRNA. The sgRNA has more stability and it is recommended for experiments under difficult conditions as high nuclease environment.

The specificity of the CRISPR/Cas9 system is given by the crRNA that is the sequence that can be designed to target specific sites of the genome. The goal of the design is to achieve the most on-target activity, to assure that DSB occurs exclusively in the desired location, with minimal off-target activity. The crRNA recognizes and binds 20 nt on the DNA strand opposite to the PAM sequence. The 10–12 PAM-proximal nucleotides of the crRNA, referred to as the “seed region”, are particularly important for specificity and do not admit mismatches (Semenova et al. 2011; Jinek et al. 2012). The design of the crRNA must be meticulous, very high or low proportion of GCs are responsible for less cleavage efficiency and it is known that short sequence motifs in the seed region such as the TT-motif and GCC-motif sequences reduce the efficiency of the guide RNA (Graf et

al. 2019). Currently, there are several web tools available for the design of the crRNA like Chop-chop (Labun et al. 2019) or Breaking-Cas (Oliveros et al. 2016).

For the generation of animal models, that is the topic of this thesis, the CRISPR/Cas9 components can be delivered to the zygote in different ways:

1. **Microinjection:** This is a technical procedure originally proposed a hundred years ago to isolate bacteria cells using a glass micropipette (Korzsh and Strähle 2002). The microinjection technique requires high skilled and trained personnel to reduce cell damage. It was the first mechanism used to deliver the CRISPR/Cas9 components into zygotes (Wang et al. 2013; Horii et al. 2014). Microinjection has been used to deliver different cargos into different compartments of the cell (cytoplasm or nucleus) and in a variety of manners. Initially, mutant mice were generated by cytoplasmic microinjection of RNAs encoding the sgRNA and the Cas9. After that, a comparison between three kinds of microinjection: i) simultaneous injection of DNA and RNA into the cytoplasm, ii) injection of DNA and RNA into the pronucleus (PN), iii) injection of RNA into the cytoplasm followed 2 hours later by DNA pronuclear injection, uncovered that cytoplasmatic or pronuclear RNA and DNA injection were the most efficient procedures (Wang et al. 2013). Nowadays, it is common that all components are delivered together as RNP complex, according to its higher efficiency (Farboud et al. 2018).

2. **Electroporation:** This is another method used to introduce the CRISPR/Cas 9 components into the embryo with no high skills requirements. Initially, the efficient delivery of RNA into embryos (Grabarek et al. 2002) had the disadvantage that required the weakening of the zona pellucida (ZP). The development of the “Technique for Animal Knock-out system by Electroporation (TAKE)” with the NEPA 21 electroporator (NEPA GENE) relieved this requirement allowing the electroporation of embryos with high efficiency and higher embryo survival rates than mRNA endonucleases delivered by conventional microinjection (Kaneko et al. 2014; Kaneko and Mashimo 2015; Alghadban et al. 2020). Because of its advantages the electroporation was the method used in this thesis.

CRISPR timeline (based on or according to the Broad Institute)

CRISPR genome editing system is based on a natural immune process of bacteria to defend itself from invader organisms. Since the first reference by Francisco Mojica in

1993, many scientists have contributed to the understanding and application of this system. Below is a brief history of how this field evolved according to the Broad Institute (<https://www.broadinstitute.org/what-broad/areas-focus/project-spotlight/crispr-timeline>).

In **1993**, F. Mojica was the first scientific to characterize what is now called the CRISPR locus. After that, in **2000**, he reported on repeats in the genome of *Archaea* and *Hyperthermophilic* bacterias. They were short elements generally repeated in clusters spaced/separated by sequences of the same length (Mojica et al. 2000). F. Mojica together with Ruud Jansen coined the term CRISPR (Clustered Regularly Interspaced Short Palindromic Repeats) that was first used in **2002** (Jansen et al. 2002).

Later, in **2005**, it was revealed that the origin of these regularly spaced sequences was from foreign organisms (Mojica et al. 2005) and this discovery let F. Mojica to hypothesize correctly that the CRISPR was an adaptative immune system.

Subsequently, in **2005**, the *Streptococcus termophilus* was sequenced and reported to contain an unusual CRISPR locus (Bolotin et al. 2005). This CRISPR locus was unusual because unlike previously described CRISPR it was not associated with previously reported *Cas* genes. This CRISPR locus encoded a large protein with endonuclease activity known as *Cas9*. Furthermore, the spacers of this CRISPR locus shared a common sequence at one end, the PAM sequence, which is required for target recognition.

In **2007**, Hovart and collages demonstrated that the CRISPR/Cas system is an immunity system in bacteria that integrates invader phage DNA into the CRISPR array allowing them to fight off the new phage attacks (Barrangou et al. 2007). They showed that the *Cas9* activity was likely the only required for CRISPR interference phase.

The next discovery came in **2008** when Jon Van der Oost and colleges reported how the CRISPR/Cas system acts in bacteria (Brouns et al. 2008). They showed how in *Escherichia coli*, sequences of invader organisms that have been integrated in the CRISPR/Cas system were transcribed into small RNAs (crRNA) to generate a response for subsequent infection from the same virus (Brouns et al. 2008). Later in the same year, it was concluded that the CRISPR/Cas system targets the DNA directly (Marraffini and Sontheimer 2008). At that time, many Scientists thought that the CRISPR could be like

eukaryotic RNA interference (RNA_i), a silencing mechanism which targeted RNA, therefore, it was a relevant discovery. It is worth noting here that in 2009 CRISPR systems targeting RNA were reported (Hale et al. 2009).

The journal Nature published in **2010** a study by Moineau and colleges revealing that the CRISPR/Cas immune system generated DSB into the DNA between the nucleotide 3 and 4 upstream the PAM (Garneau et al. 2010). Then, they also confirmed that the Cas9 endonuclease was the only protein required for DNA cleavage in the CRISPR/Cas9 system.

In **2011**, Charpentier and her colleges, through the differential RNA sequencing of *Streptococcus pyogenes*, uncover the tracrRNA, with 24nt complementary to the repeat sequences in the CRISPR. They showed that the maturation of crRNA was directed by the tracrRNA. Moreover, they demonstrated that RNase activity in the CRISPR/Cas system, is necessary to cleave the tracrRNA and pre-crRNA just after the base-pairing (Deltcheva et al. 2011).

In the same year, Syksnis and colleges cloned the CRISPR locus of *S. thermophilus* and expressed it in *E. coli* to determine that the transferred CRISPR/Cas system could provide heterologous protection (Saprunauskas et al. 2011). Later in **2012**, they characterized the cleavage site and showed the requirement of the PAM sequence. They revealed that the RuvC endonuclease domain cleaves the non-complementary strand while the HNH domain cleaves the complementary stand. The crRNA must be complementary with the 20nt following the PAM sequence to drive the Cas9. These findings showed that the Cas9 can be reprogrammed to target a desire site by changing the crRNA sequence, a relevant discovery for genome editing (Gasiunas et al. 2012).

At the same time, Charpentier and Doudna published similar findings of Gasiunas. The CRISPR/Cas9 system was shown to be similar by both groups. In this case, Charpentier and Doudna fused the tracrRNA and the crRNA as a single RNA chimera (sgRNA) to simplify the system (Jinek et al. 2012).

In **2013**, Zhang was the first to successfully adapt the CRISPR/Cas9 for genome editing in eukaryotic cells. Zhang and his team engineered two different Cas9 orthologous (from *Streptococcus thermophilus* and *Streptococcus pyogenes*) and cleave human and mouse endogenous genomic loci simultaneously (Cong et al. 2013) and drive the

homologous repair mechanism. Similar research with human cells was published at the same time by George Church's lab at Harvard University (Mali et al. 2013b).

Overview of CRISPR Applications

The widespread adoption of CRISPR technology has transformed the field of life science. This bacterial immune system has been adapted to serve as an efficient, rapid, and cost-effective gene editing tool.

Currently, the CRISPR system for genome editing has been applied with different Cas proteins to the modification of many organisms. The two main Cas proteins used for CRISPR genome editing, the Cas9 and the Cas12a (Cpf1), are both deoxyribonucleases (DNases). Both the unmodified as well as the engineered mutant versions of these enzymes have been extensively used. If the target sequence is GC-rich, it is more likely to contain a NGG PAM, which can be targeted by Cas9 (Mali et al., 2013). On the other hand, if it is an AT-rich sequence, it is more likely to contain a TTTV PAM (Shmakov et al. 2015), which can be cleaved by Cas12a.

Because the CRISPR/Cas9 is the most used variant, we will next list different applications of this system in several fields, ranging from stem cells modifications to therapies with CRISPR.

Stem cells

Autologous stem cells are the goal in personalized regenerative medicine due to their ability to proliferate, differentiate and secrete cytokines/growth factors to restore damaged tissues. There are different types of stem cells, mainly embryonic stem cells (ESCs) and adult stem cells; among them bone marrow-derived mesenchymal stem cell (BMSCs), adipose-derived stem cells (ASCs) and hematopoietic pluripotent stem cells (HSCs). Moreover, it is possible to reprogram somatic cells to generate induced pluripotent stem cells (iPSCs). Autologous iPSCs can be subjected to genetic modifications to correct gene expression defects (Hsu et al. 2019).

In 2012, the catalytic domains of Cas9 were mutated to generate a catalytically deactivated Cas9 (dCas9) unable to generate a DSB (Qi et al. 2013). A RNP complex formed with dCas9 can be used to bind to the target site and inhibit the transcription of the desired gene, CRISPR *interference* (CRISPRi). This CRISPRi is used to knockdown

gene expression. In addition, dCas9 has been fused to transcriptional activators, generating the CRISPR *activation* (CRISPRa) that induces the activation of target genes (Gilbert et al. 2013; Maeder et al. 2013). The CRISPRa and CRISPRi are commonly used in stem cell reprogramming.

If dCas9 is fused to epigenetic modifiers it can generate epigenetic modifications. These modifications persist over time and are potentially inheritable in dividing cells (Nunez et al. 2021).

An engineered mutation of wild-type (WT) *Streptococcus pyogenes* Cas9 (SpCas9), D10A, produces nick genomic DNA rather DSB. It is necessary two Cas9 nickases targeting opposite strand to generate DSB. This Cas9 nickases are of high-fidelity and exhibit lower off target effects (Cong et al. 2013).

Somatic cells

The genome editing performed in somatic cells induces non-heritable changes and it is much closer to clinical implementation as gene therapy.

Virus-based gene therapies are the most extended procedures allowing efficient and safe somatic cell modifications. The gene therapy has suffered a wide development with the implementation of CRISPR technology for the modification of somatic cells. Potentially, the CRISPR/Cas9 system and the sequence to be modified (Donor/Template), inserted in plasmids, can be delivered into the organism (Johnson et al. 2020). It is important to consider that not all organs can be transfected in vivo with plasmid DNA, so genome editing in somatic cell is still an arduous process.

Plants

Target genome editing technology is an incredible tool for understanding plant and fungi gene function and crop improvement. CRISPR/Cas9 system is a powerful tool to improve different features in crops, such as yield, plant architecture, nutrient content, disease resistance and adaption to stress. Several studies about genome editing in several plants as *Arabidopsis thaliana* or *Nicotina benthamiana* have been published and stable genetic mutants have been obtained. The efficiency of the CRISPR/Cas9 depends on the plant species (Li, J.F. et al. 2013; Xie and Yang 2013).

Animal models of human disease

The development of genetic engineering enables the manipulation of the organism's genes and can be applied to generate animal models of human disease, which are invaluable tools for the global study of pathological entities. Alternative methods to the use of animals, such as cell cultures and computer simulations should be considered and used whenever possible. However, there are complex processes that can only be understood in the whole animal. In recent past years, with the discovery of the CRISPR/Cas9 system, the generation of animal models by genome editing has experienced an unprecedented development.

A transgenic animal is one that carries a foreign gene (transgene) deliberately inserted into its genome. The transgene is inserted and stably incorporated into the genome and therefore transmitted to their descendants. The first transgenic mouse was generated in 1974 (Jaenisch and Mintz 1974) by inserting a DNA virus but, the mouse did not pass the transgene to their offspring. Seven years later, in 1981, the stable germ line transmission in a Mendelian distribution of a modified allele generated by the mouse pronuclei injection was achieved (Gordon and Ruddle 1981). The production of transgenic mice by pronuclear injection is an extended method that allows with relatively high efficiency the transmission of the modified allele to the offspring.

A notable improvement in the generation of KO animal models was the introduction of mouse embryonic stem cells (ESCs). The ESCs with the desired modification are injected into the blastocysts to obtain chimeric mice that are crossbred and if germ line transmission is achieved the mouse lines are established. This process is long, high cost and generates many animals. The CRISPR can be applied to embryos, notably reducing the use of animals. The CRISPR/Cas technology offers the ability to generate animal models in a much easier, faster, and efficient manner.

Upon CRISPR discovery, it was rapidly employed to efficiently edit the embryo's genome. In addition to the microinjection, the CRISPR/Cas9 has also been introduced into the zygote by electroporation, a technique that doesn't require special training or skills that reached 100% efficiency in bi-allelic targeting in live mice (Chen et al. 2016).

Improved genome-editing via oviductal delivery (*i*-GONAD) is an alternative method for CRISPR/Cas9 delivery into zygotes that does not require the handling of the zygotes (Ohtsuka et al. 2018; Takabayashi et al. 2018).

Nucleic acid detection

A new platform to detect nucleic acid with the CRISPR technology has been established by Zhang and his colleagues. This platform, termed SHERLOCK (specific high-sensitivity enzymatic reporter unlocking) allows to detect RNA or DNA from clinical samples of interest. The CRISPR technology in this case is combined with Cas13 endonuclease and a recombinase polymerase amplification (RPA) (Gootenberg et al. 2017; Kellner et al. 2019).

Nowadays this technology is being used to detect the SARS-CoV-2 (Zhang et al. 2020). Researchers of the Broad Institute combine SHERLOCK technology with a big data platform to create CARMEN (Combinatorial Arrayed Reactions for Multiplexed Evaluation of Nucleic acids), which is a technology that allows simultaneous analysis up to 1000 proofs (Ackerman et al. 2020).

In this competition to develop the more competitive system to detect the SARS-CoV-2, the lab of Jennifer Doudna set up the CRISPR DETECTR (Chen et al. 2018). This technology works with the endonuclease Cas12a that cuts DNA instead of RNA in contrast to Cas13a. In this case, to detect the SARS-CoV-2, which is an RNA virus, it must be first transcribed to DNA for detection.

CRISPR-based therapies

Here, we will only list some of CRISPR therapeutic applications:

The Stanford University has been the first to carry out a system to fight against the SARS-CoV-2 based on CRISPR/Cas system. The experimental technology known as PAC-MAN (Prophylactic Antiviral CRISPR in human cells) uses Cas13d endonuclease. The guide RNA is designed to direct the Cas13d endonuclease to the sequence of the SARS-CoV-2 to cut the RNA virus. The researchers have developed a guide RNA to detect 90% of the coronavirus that exist nowadays (Nguyen et al. 2020).

The CRISPR/Cas9 system has been used to prevent retinal degeneration. Retinitis pigmentosa (RP) is an inherited retinal dystrophy commonly caused by mutation in *Rhodopsin* (*Rho*) gene. Subretinal electroporation of two plasmids edited the gene in transgenic mice with RP (Latella et al. 2016).

The Duchenne muscular dystrophy (DMD) results from mutations in the *dystrophin* (*Dmd*) gene. CRISPR/Cas9 delivered by adenoviral vectors (AVV) to delete the mutated *Dmd* exon 23 has been shown to enhance skeletal muscle function deficiencies in a mice model for DMD (Tabebordbar et al. 2016).

Oncogenes and mutant tumor suppressor genes are another area with excellent applications of genome editing tool. The first clinical trial using CRISPR for cancer therapy was in 2016 at Sichuan University's West China Hospital. In this trial, lymphocytes were genetically modified *ex vivo* and infused back into the patients. The process was laborious and raised doubts about the targeted region. This trial can be considered as the first approach to *ex vivo* CRISPR/Cas9 application in cancer treatment (Zhan et al. 2018).

1.3 Limb development

Developmental biology is the study of embryonic development and other processes by which organisms grow and develop. After fertilization, the single-celled zygote suffers a species-specific number of mitotic divisions, termed cleavage, and generates a spherical embryo composed of blastomeres, the morula. By the end of cleavage, the embryo enters the blastula stage adopting the shape of a hollow sphere formed by two different layers: the external layer or trophoblast and an inner cluster of cells called the inner cell mass (ICM). The ICM forms the epiblast (columnar epithelial cells) and the hypoblast (cuboidal epithelial cells), which are together known as the bilaminar disc. Afterwards, the embryo enters the process of gastrulation characterized by extensive morphogenetic movements and reorganization of the cells. As a result of gastrulation, the embryo contains three germ layers: endoderm, ectoderm, and mesoderm and is known as the trilaminar disc. Gastrulation is followed by organogenesis when the three germ layers form the different tissues and organs. The ectoderm generates the epidermis of the skin and forms the brain and nervous system, the mesoderm generates

the blood, heart, kidney, gonads, bones, muscles, and connective tissues and the endoderm produces the epithelium of the digestive tube and associated organs.

This Thesis focuses on the limb. During development, the first morphological evidence of a limb is the *limb bud* that is a small bulge of the lateral body wall at the appropriate level. Limb buds are made of two components: an internal core of mesodermal cells derived from the lateral plate mesoderm and the covering surface ectoderm. Vertebrate limb development is controlled by the continuous interaction between these two components, the ectoderm, and the mesoderm. The limb bud grows and patterns along three main axes: the proximo-distal axis (PD, from the shoulder to the tip of the digits), the anterior-posterior axis (AP, from the thumb to the little finger) and the dorso-ventral axis (DV, from knuckle to palm) (Fig.4). Correct outgrowth and patterning along each of these main axes is directed by a specific signaling center, the apical ectodermal ridge (AER), the zone of polarizing activity (ZPA) and the non-AER ectoderm.

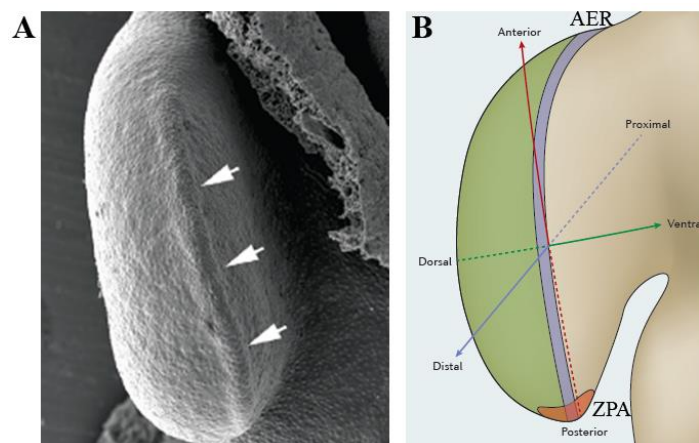


Figure 4: Developmental axes in the limb. **A.** Microphotograph of scanning microscopy showing a distal wing bud. The AER is indicated by white arrows (From Fernández-Terán and Ros. 2008). **B.** Diagram of the same distal view of a limb bud in which the three developmental axes and the main signaling centers are showed. AP axis is controlled by the ZPA (red), PD axis is controlled by the AER (purple) and DV axis is controlled by the dorsal ectoderm signaling center (green) (From Petit et al., 2017)

Since the developing limb is a non-vital organ that allows significant manipulation without compromising the embryo survival and it is also readily visible and accessible, it has become an incredible model to study vertebrate organogenesis. Moreover, the lesson learnt from the study of the different signaling pathways working during limb development to other developmental processes can be extrapolated to other tissues or organ.

The apical ectodermal ridge (AER)

The AER is one of the main signaling centers of the limb bud. It is the thickened ectoderm rimming the distal tip of the bud at the boundary between the dorsal and ventral ectoderm marked by *Wnt7a* and *En1* respectively (Fernandez-Teran and Ros 2008). The AER controls PD limb elongation and patterning, maintaining the underlying mesenchyme in a proliferative and undifferentiated state (Saunders 1948; Dudley et al. 2002; Sun et al. 2002; Niswander 2003; Boulet et al. 2004; Mariani et al. 2008). It is a dynamic and transitory structure (Guo et al. 2003). In birds, a mature AER forms a thick pseudostratified columnar epithelium, while in mammals it forms a poly-stratified epithelium (Fig. 5).

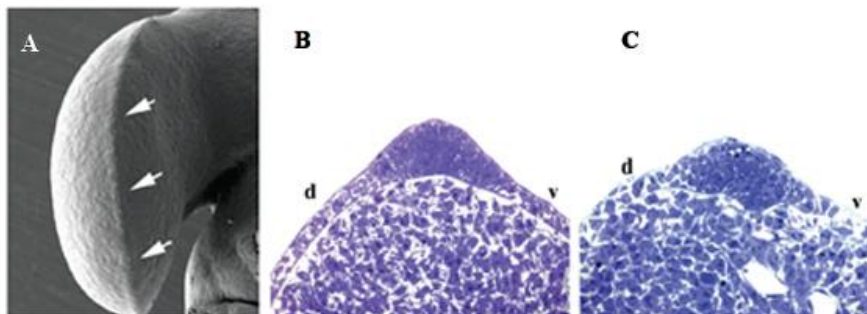


Fig 5: AER morphology. **A.** Microphotograph of scanning microscopy showing a distal view of 26HH wing bud. White arrows point to the prominence of the AER. **B.** Semithin section of 20HH wing bud (pseudostratified columnar epithelium). **C.** Semithin section of E 10.5 mouse forelimb (poly-stratified epithelium). From Fernández Teran and Ros, 2008.

When the AER is surgically removed limb development stops and a truncated limb is formed. The earlier the AER is removed, the more proximal the level of truncation, indicating the continuous requirement of the AER for the progressive PD development of

the limb (Saunders 1948; Rowe and Fallon 1982; Cohn et al. 1995). AER function is mediated by the secretion of a battery of FGF family members, *Fgf4*, *Fgf8*, *Fgf9* and *Fgf17*, known as AER-Fgfs, which have restricted patterns of expression in the AER. Of them, *Fgf8* is considered the best AER marker because its expression spatially and temporally accompanies the existence of the AER (Heikinheimo et al. 1994; Crossley and Martin 1995; Mahmood et al. 1995).

Experiments in chick showed that an ectopic source of FGF2 in the limb bud, induced the formation of extra skeletal elements (Riley et al. 1993). Moreover, other experiments showed that FGF4 and FGF2 were able to substitute for the AER with relatively normal formation of the skeletal structures (Lee Niswander and Martin 1993; Fallon et al. 1994).

Experiments generating targeted disruptions of different AER-Fgfs concluded that they mediate AER function in a redundant manner (Sun et al. 2000; Mariani et al. 2008). However, when they are individually eliminated, only loss of *Fgf8* produces abnormal limb development (Lewandoski et al. 2000; Moon and Capecchi 2000; Moon et al. 2000; Sun et al. 2000; Xu et al. 2000). *Fgf8* is the major contributor to AER-Fgf dose with minor contributions of *Fgf4*, *Fgf9* and *Fgf17* (Mariani et al. 2008).

Fgf8 is essential for gastrulation (Sun et al. 1999) therefore, to study its function in the limb, it was necessary to generate a conditional mutant (Lewandoski et al. 2000). The studies in this mutant showed that a specific inactivation of *Fgf8* in the early limb ectoderm results in a reduction in limb bud size, hypoplasia or aplasia of specific skeletal elements, and a delay in *Sonic hedgehog* (*Shh*) expression, which eventually, in absence of *Fgf8*, is induced and maintained by others AER-FGFs (Lewandoski et al. 2000; Sun et al. 2000). Moreover, *Fgf8* expression controls *Fgf4* expression, indeed, the phenotype observed after *Fgf8* removal can be explained due to the upregulation of *Fgf4* (Moon and Capecchi 2000).

The establishment of the AER results from the combination of complex interactions between the Fgf, Wnt/ β -catenin and Bmp signaling pathways and between the ectoderm and mesoderm. Wnt/ β -catenin activity in the ectoderm is required to induce and maintain the AER. BMP signaling, which seems to act upstream WNT- β -catenin, is

also required for AER induction and is involved in AER regression too (Barrow et al. 2003; Soshnikova et al. 2003; Fernandez-Teran and Ros 2008) .

Among the transcription factors expressed in the AER, we underscore *Sp6* (*Epiprofin/Epfn*) and *Sp8* (Harrison et al. 2000; Treichel et al. 2001; Bell et al. 2003; Kawakami et al. 2004; Nakamura et al. 2004), two members of the Specificity protein family that mediate *Fgf8* induction.

1.4 Specificity proteins (SP) family

The specificity proteins (SP) are evolutionary conserved transcriptional factors (TFs). They are characterized by a highly conserved carboxy terminal DNA-binding domain with three Cys2-His2 zinc fingers (ZF) motifs which bind to G-rich DNA elements, such a GC boxes and GT/CACC boxes. Theses binding sites can be found in many regulatory regions of genes suggesting that SP family are involved in their regulation. The SP TFs also contain the buttonhead (Btd) box immediately 5' to the ZF domain (Suske et al. 2005).

Thanks to a phylogenetic sequence analysis, *Sp* family was divided in three large clades. The first clade, *Sp* 1-4, contains *Sp1*, *Sp2*, *Sp3* and *Sp4* of vertebrate species and a single *Sp* representative of each of invertebrate species. The second clade includes vertebrate *Sp5* genes and the invertebrate *btd*, therefore this clade is known as *Sp5/btd* clade. The third clade, contains *Sp6*, *Sp7*, *Sp8* and *Sp9* of all vertebrate species and *Sp1* representative of each of the invertebrate species (Schaeper et al. 2010) (Fig. 6).

The *Sp* genes have variable functions including stem cell maintenance, cell proliferation, embryonic development, tissue differentiation and metabolism and each gene have different patterns of expression (Presnell et al. 2015). The genes in the *Sp1-4* clade in vertebrates are expressed ubiquitously during development. *Sp5* is expressed in the mid-brain and hind-brain boundary, in the primitive streak and later in the tail bud, otic vesicles, limb bud, the developing nervous central system, somites and pharyngeal region. Of the genes in the *Sp6-9* clade, *Sp6* is expressed in the hair follicles and in the AER. *Sp7* is expressed in osteoblasts. *Sp8* and *Sp9* are expressed in the nervous system and in the AER of the limb (Schaeper et al. 2010).

Previously we have indicated the important role of the AER for limb development. The *Sp6* and *Sp8* TFs are expressed in the limb ectoderm, where they control in a redundant and dose dependent manner the Wnt-dependent induction of *Fgf8* expression (Haro et al. 2014).

The *Sp6* mutant shows a defective autopod characterized by soft-tissue syndactyly in the FL (the fusion of two or more digits, digits 2-3 and occasionally 4) and oligodactyly in the hindlimbs (HL) caused by the osseous fusion of digits 3-4 (some cases the fusion is not complete). The penetrance and expressivity of the phenotype are variable with a clear bias for the left side. The *Sp6* mutant shows defects in the AER maturation showing double-ridge phenotype, that is when *Fgf8* expression is observed in two parallel stripes at the border of the expanded AER (Kawakami et al. 2004; Talamillo et al. 2010).

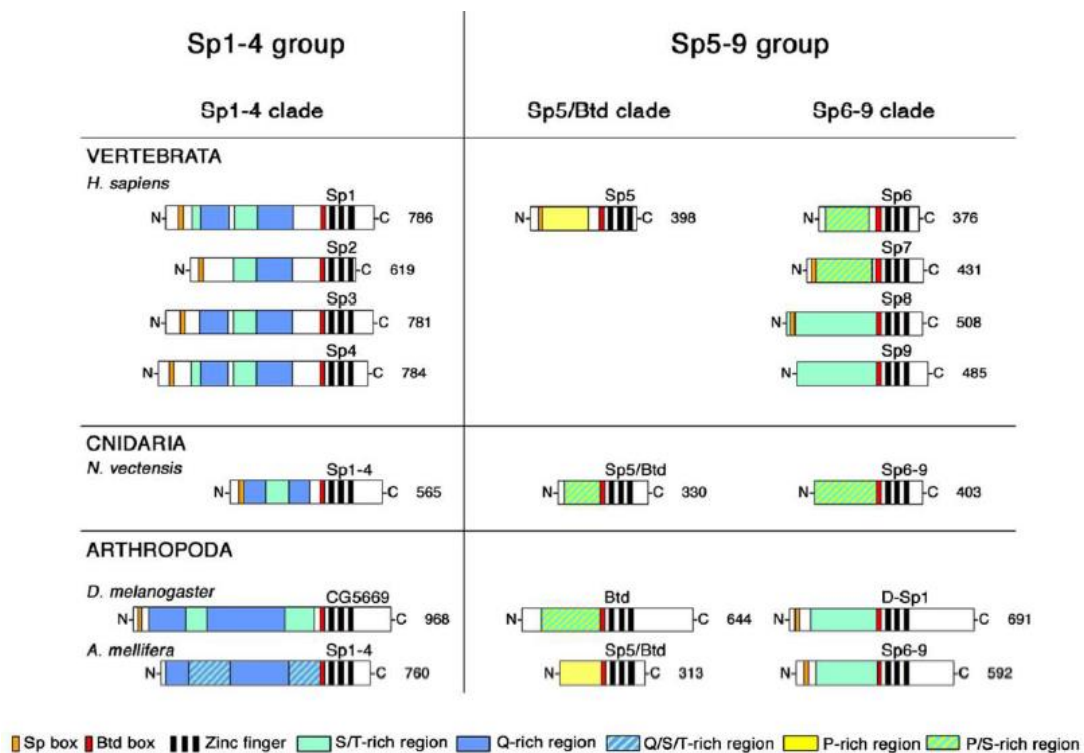


Fig. 6 Protein domain structure of selected SP-family species. All the proteins are oriented in the same way, with the amino terminus-N to de left and the carboxi terminus-C to the right. Sp proteins are divided in two big groups: Sp1-4 and Sp5-9, and in three clades, Sp1-4 clade, Sp5/Btd and Sp6-9. From Scaeper et al. 2010.

The *Sp8* mutant presents a dramatic phenotype with truncated limbs, absent tail and defects in anterior and posterior neuropore closure producing exencephaly and spina bifida (Bell et al. 2003; Treichel et al. 2003).

The study of double *Sp6;Sp8* mutants showed that a progressive reduction in *Sp6/8* gene dosage results in progressively more severe limb malformations ranging from a mild syndactyly to Split/Hand Split/Foot Malformation (SHFM), to oligodactyly, to truncation of the limbs and finally to amelia (Haro et al. 2014). Most interestingly, these malformations are associated with a DV phenotype (Fig. 7). DV patterning is controlled by the non-AER ectoderm through the restricted expression of *Wnt7a* in the dorsal ectoderm (Dealy and Brown 1993; Riddle et al. 1995) and the expression of *En1* in the ventral limb ectoderm (Davis et al. 1991; Gardner and Barald 1992). In the absence of *Sp6* and *Sp8*, the loss of *En1* expression in the ventral ectoderm together with ventral expansion of *Wnt7a* expression led to the development of bidorsal limb buds and digital tips.

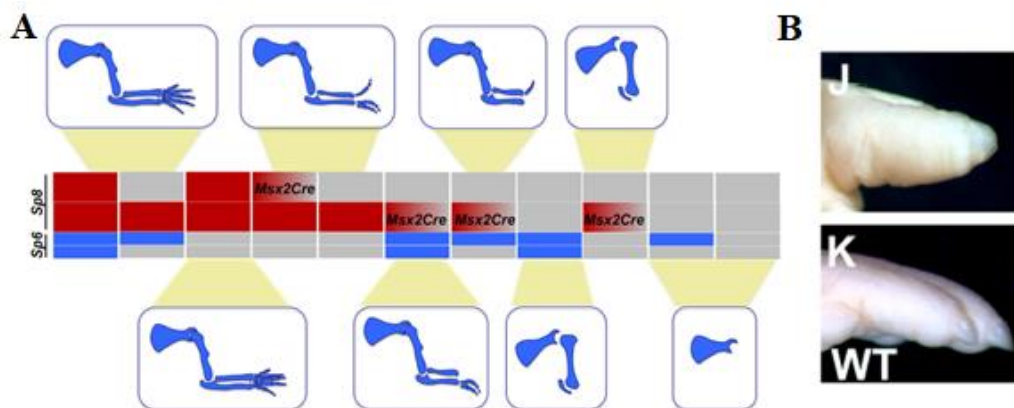


Figure 7: The study of *Sp6* and *Sp8* gene dosage. **A.** A progressive reduction of *Sp6/8* gene dosage results in progressively more severe limb malformations. Blue boxes indicate *Sp6* alleles and red boxes are *Sp8* alleles. **B.** On the top there is a *Sp6*^{-/-}; *Sp8*^{+/-} digit tip with conical nail phenotype. On the bottom there is a WT nail. From E. Haro *et al.* 2014.

The mutant that retains a functional copy of *Sp8* in the absence of *Sp6* (*Sp6*^{-/-}; *Sp8*^{+/-}) displays a SHFM phenotype that constitutes an excellent animal model for this malformation. It is most similar to a novel form of SHFM in human caused by a missense mutation in the homeobox domain of *DLX5*, including the DV phenotype (Shamseldin et

al. 2011; Haro et al. 2014). In this line, a recent study in our lab has revealed that Sp8, Sp6 and Dlx5 act together to regulate target genes (Pérez-Gómez et al. 2020)

A combination of ChIP-seq and RNA-seq genome-wide analyses was used to investigate the Sp8 regulatory network and mechanism of action (Pérez-Gómez et al. 2020). Sp8 activates crucial limb patterning genes, including *Fgf8*, *En1*, *Sp6* and *Rspo2* through distal enhancers. *Dlx* genes are also direct target of Sp8. In addition this study also reveals a Sp8 dual mode of gene regulation: first by directly binding to the consensus SP binding domain in the genome and second by indirectly engaging through association with Dlx5 or other Dlx family members (Hojo et al. 2017; Pérez-Gómez et al. 2020). Thus, at least part of the *Dlx5/Dlx6* loss of function phenotype may be due to the subsequent impairment of Sp8 function and vice versa providing an explanation for the similarity in phenotypes (Fig.8) (Pérez-Gómez et al. 2020).

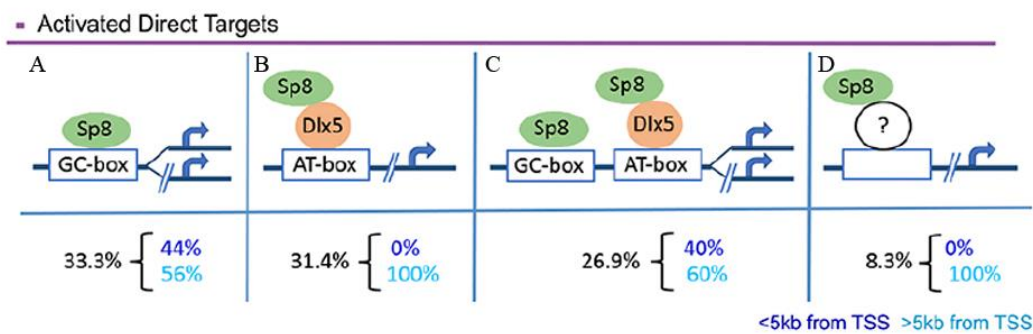


Figure 8: Sp8 direct target genes. Categorization of Sp8 regulatory regions according to the presence of Sp1-like and/or Dlx binding motifs. **A.** One third (33.3%) of the Sp8 regulatory regions contained GC-rich/Sp1 but no AT-rich/Dlx5. **B.** The 31.4% of the Sp8 regulatory regions contained AT-rich/Dlx5 but not GC-rich/Sp1 sites. **C.** The 26.9% Sp8 regulatory regions showed a predominant distal location, contained both sp1-like and Dlx5-binding sites. **D.** A small percentage (8.3%) of regulatory regions did not contain either Sp1-like or Dlx binding site indicating a possible indirect recruitment of Sp8 through the interaction with additional TFs or a low percentage of false positive Sp8 peaks. From Pérez-Gómez et al., 2020.

1.5 Split hand-foot malformation (SHFM)

Split-hand/split-foot malformation (SHFM), also known as ectrodactyly, is a highly variable malformation of the hand and/or foot characterized by the loss or deformity of the central rays that leads to a central cleft and the subsequent split appearance frequently accompanied by loss and webbing of fingers and toes (Temtamy and McKusick 1978; S Sifakis et al. 2001). The SHFM has a very heterogeneous genetic background with at least six associated loci named SHFM1-6 (Duijf et al. 2003; Elliott and Evans 2006; Kouwenhoven et al. 2015) (Table 1).

The SHFM can appear in isolation, when only the limb malformations are present, or syndromic when other disorders, most commonly hearing loss, craniofacial anomalies, and/or developmental delay, are also present. The association with dermatological defects and cleft lip and/or palate forms the triad that defines the ectrodactyly-ectodermal dysplasia-clefting (EEC) (Elliott and Evans 2006).

Table1. The SHFM types. The name appeared in the first column, then it is the chromosome location in the genome, the next column collected the different genes affected and in the last column there is the OMIM and the pattern of inheritance of each malformation.

PHENOTYPE	CHR LOCATION	GENE/LOCUS	INHERITANCE	PHENOTYPE MIM NUMBER
SHFM1	7q21.3	<i>Dlx5</i> <i>Dlx6</i>	autosomal dominant	# 183600
SHFM2	Xq26	<i>Fgf13</i> <i>TONDU</i>	X-linked pattern of inheritance	313350
SHFM3	10q24	<i>Dactylin</i> (<i>FBXW4</i>) <i>Fgf8</i>	autosomal dominant	600095 moved to # 246560
SHFM4	3q27	<i>p63</i>	autosomal dominant	# 605289
SHFM5	2q31	<i>Dlx1</i> <i>Dlx2</i> <i>HOXD</i> gene cluster	autosomal dominant	606708
SHFM6	12q13	<i>Wnt10b</i>	autosomal recessive	# 225300

The clinical presentation of SHFM is highly heterogeneous with incomplete penetrance and variable expression, even within families. One study revealed that the

birth rate of SHFM is 0.51/10,000 with 65.2% of the patients displaying isolated SHFM and 34.8% syndromic SHFM (Elliott et al. 2006).

The **SHFM1** (OMIM # 183600) is due to chromosomal rearrangements of the 7q21.3-22.1 region. These mutations usually appear as *de novo* mutation events but can also be inherited in an autosomal dominant manner, with low penetrance and variable expressivity. The affected region encompasses several coding genes, *DYNCH3*, *SLC25A13*, *C7orf76*, *DSS1*, *DLX5* and *DLX6*, of which the homeobox genes ***DLX5*** and ***DLX6*** are considered causative because several SHFM1 families have been reported with intragenic point mutations in these genes (Shamseldin et al. 2011; Badura-stronka et al. 2014; Sowińska-Seidler et al. 2014; Wang et al. 2014; Ullah et al. 2017). Also, mice lacking *Dlx5* and *Dlx6* display the SHFM in their hindlimbs (Robledo et al. 2002).

The SHFM1 locus alterations are associated with both isolated and syndromic limb malformations. About one third of patients with SHFM1 have sensorial deafness but the association of Ectrodactyly-Ectodermal Dysplasia-Cleft (EEC) malformations are much less frequent (Tackels-Horne et al. 2001). The EEC syndrome is an autosomal disorder associated with *p63* mutations (Brunner et al. 2002; Rinne et al. 2007). *P63* regulates *Dlx6* and *Dlx5* expression (Iacono et al. 2008; Kouwenhoven et al. 2010; Guerrini et al. 2011).

SHFM2 (OMIM # 313350) is very rare and maps to chromosome Xq26.3 (Nunes et al. 1995; Faiyaz-Ul-Haque et al. 2005). In 1987, a Pakistani family with 36 members affected by SHFM in 7 generations was described. Due to the distribution of the members effected (33 males and 3 females), the SHFM2 was considered compatible with X-linked inheritance (Ahmad et al. 1987; Khan et al. 2012). The Xq26.3 region includes ***FGF13*** and ***TONDU*** (Vaudin et al. 1999) but a screening of the exons and exon/intron boundaries of 19 candidate genes in the region did not identify any mutations (Faiyaz-Ul-Haque et al. 2005).

SHFM3 (OMIM # 600095 moved to OMIM #246560) maps to chromosome 10q24, a region that includes the *FBXW4/Dactylin* gene (Gurrieri et al. 1996). The SHFM3 was mapped in 1996 (Raas-Rothschild et al. 1996) to 10q25 and the critical region narrowed to 10q24 in 2004 (Roscioli et al. 2004). The phenotype was variable, and the feet showed more developmental abnormalities than the hands. Interestingly, the

SHFM3 has been associated to tandem duplications of this genomic region that it is close to *FGF8* and includes *FGF8*-regulatory modules driving its expression during limb development (Marinić et al. 2013).

SHFM4 (OMIM # 605289) maps to chromosome 3q27 and involves *P63* (Ianakiev et al. 2000). The *P63* gene is a homologue of the cell-cycle regulator *P53* and plays multiple functions including control of skin stratification and adult stem/progenitor cell regulation. It is expressed in the ectoderm and is a master regulator of AER formation and differentiation (Mills et al. 1999; Yang et al. 1999).

The P53 family of proteins include several functional domains: an N-terminal transactivation domain, a central DNA-binding domain, and an oligomerization domain. Besides SHFM4, mutations in P63 have been associated with EEC, as previously mentioned, and other syndromes (Brunner et al. 2002; Rinne et al. 2007). Mutations in the DNA-binding domain of *P63* were associated with both non-syndromic SHFM and EEC. The mutated amino acids in the families with isolated SHFM4 were associated with the maintenance of the overall structure of the DNA binding domain, in contrast to the mutated amino acids in families with EEC which were associated with direct DNA interaction (Ianakiev et al. 2000). Mice null for *p63* show severe developmental defects, including limb truncations, abnormal skin, and absence of epidermal derivatives (hair follicles, teeth, and mammary glands) (Mills et al. 1999; Yang et al. 1999).

SHFM5 (OMIM # 606708) has been mapped to chromosome 2q31 region, with deletions involving a 5-Mb interval centromeric to *EXV2* located upstream of the *HOXD* cluster (Goodman et al. 2002). The SHFM5 has been described as bilateral SHFM (Boles et al. 1995) caused by the deletion of *HOXD* cluster, *EVX2*, *DLX1* and *DLX2* and a microsatellite marker D2S294, where *DLX1* and *DLX2* are putative candidate genes (J C Ramer et al. 1990; Boles et al. 1995; Campo et al. 1999; Theisen et al. 2011). Nevertheless, neither mice heterozygous, nor homozygous for individual or combined mutations of *Dlx1* and *Dlx2* display limb malformations (Kraus and Lufkin 2006).

SHFM6 (OMIM # 225300) maps to chromosome 12q13.12 and is caused by mutations in *WNT10B* with an autosomal recessive inheritance (Ugur and Tolun 2008; Blattner et al. 2010; Khan et al. 2012). *WNT10B* acts through the canonical Wnt-bcatenin signalling pathway and it has been shown to be expressed in the AER during mouse limb

development (Witte et al. 2009). *WNT10B* and *WNT3A* are ligands of the canonical Wnt-signaling pathway which acts upstream of FGF in the AER.

Despite the multiple loci implicated in SHFM it is possible that all these genomic or genetic alterations converge to a regulatory network, the P63 network. *P63* is responsible for SHFM4 and it is an upstream regulator of *Dlx* genes (Iacono et al. 2008; Guerrini et al. 2011), that are associated with SHFM1 and SHFM5. *Fgf8* expression is progressively reduced in the AER of *p63* null mice (Yang et al. 1999). The SHFM phenotype is considered to result from a failure in the maintenance of the medial AER due to defects in *Fgf8* expression (Temtamy and McKusick 1978; S Sifakis et al. 2001) (Fig.9). It would be most interesting to investigate a possible relationship between the *Sp6/8* genes and the p63 network. This is based on the phenotypic similarity between the *Sp6/8*-dependent SHFM and the non-syndromic autosomal recessive human SHFM caused by a *DLX5* missense mutation, including the dorso-ventral alterations and supported by the functional interaction between *Dlx* and *Sp* factors (Pérez-Gómez et al. 2020).

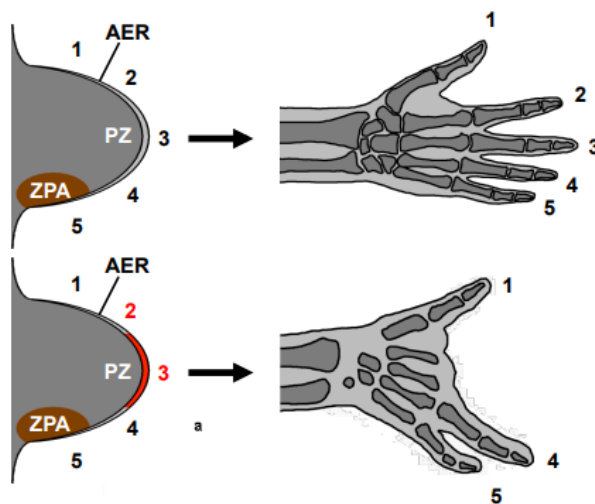


Figure 9: Illustration of AER defects and consequence SHFM phenotype. Normal development of the limb (top). The failure in the maintenance of the medial AER leads to the absence of the central rays and produces SHFM phenotype (bottom). From Duijf *et al.* 2003

Dlx genes

Dlx genes form a highly conserved family of mammalian homeobox genes homologous of *Drosophila Distal-Less (Dll)* genes. There are six *Dlx* genes in mammals, *Dlx1-6*, distributed in pairs (*Dlx1/Dlx2*; *Dlx3/Dlx4*; *Dlx5/Dlx6*) each one in one chromosome near a *Hox* clusters. The *Dlx1/2* pair locates near to *HoxD* cluster, the *Dlx3/4*

near the *HoxB*, and the *Dlx5/6* near to the *HoxA* cluster (Ozçelik et al. 1992; Simeone et al. 1994; McGuinness et al. 1996; Nakamura et al. 1996; Stock et al. 1996). *Dlx1/4/6* and *Dlx2/3/5* are paralogous groups reflecting the duplication origin (Sumiyama et al. 2003).

All vertebrate *Dlx* genes have a common organization in three exons and two introns with each exon containing some coding sequence and the homeobox split between exons 2 and 3 (McGuinness et al. 1996; Ellies et al. 1997; Liu et al. 1997).

During embryo development *Dlx* genes are expressed in ectodermal derivatives with a spatiotemporal expression pattern (Liu et al. 1997; Eisenstat et al. 1999). All *Dlx* genes are expressed in the AER where they control the pattern of limb development (Qiu et al. 1997; Acampora et al. 1999). The overlapping expression of several *Dlx* genes in some tissues suggests redundant and distinct functions of *Dlx* genes. Individual homozygous mutation of *Dlx* genes in tissues that express several family members usually lack phenotype unless at least two *Dlx* genes are removed (Anderson et al. 1997; Acampora et al. 1999).

As mentioned, SHFM1 and SHFM5 are directly associated with loci that involve *Dlx* genes. The SHFM1 is associated with *DLX5* and *DLX6* intragenic mutations (Shamseldin et al. 2011; Ullah et al. 2017) and the SHFM5 is related with *DLX1* and *DLX2* as possible responsible genes. However, *Dlx1/Dlx2* mouse double mutant do not show any limb phenotype (Kraus and Lufkin 2006).

The expression of *Dlx5* and *Dlx6* can be detected in the AER, in the pharyngeal arches, osteoblast of developing bones and between the neurons of the basal forebrain (Simeone et al. 1994; Acampora et al. 1999; Iacono et al. 2008). The analysis of *Dlx5*^{-/-}; *Dlx6*^{-/-} double mutants showed that besides maintaining the proliferation of the medial AER cell population, these genes had more functions because the mutant mice show craniofacial abnormalities, axial and appendicular skeletal irregularities and ectrodactyly phenotype that together result in perinatal lethality (Merlo et al. 2002; Robledo et al. 2002) (Fig. 10). Moreover, this SHFM1 animal model shows altered cell stratification and defects in cell polarity in the AER due to defects in the expression of *Wnt5a*. *Wnt5a* is a member of Wnt signaling pathway that controls the planar cell polarity (PCP) of the cells in the AER. *Dlx5*^{-/-}; *Dlx6*^{-/-} mice also show down regulation of *Dlx2* and *Fgf8* expression. It is remarkable that the addition of exogenous *Wnt5a* on ex vivo whole

cultures of embryonic HLs of *Dlx5;Dlx6* DKO supposed the functional and morphology recovery of the AER (Conte et al. 2016).

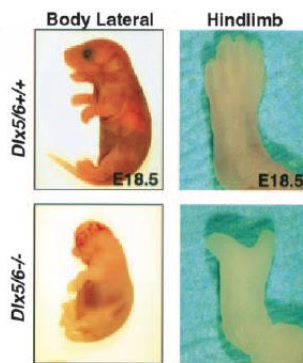


Figure 10: Mouse model of SHFM1. The double knock-out of *Dlx5* and *Dlx6* generates an animal model for the SHFM1 human disease. The ectrodactyly phenotype is restricted to the HLs (whole embryo on the left and HL detail on the right). From Robledo et al., 2002.

The mouse model of SHFM1 (*Dlx5*^{-/-};*Dlx6*^{-/-}), showed a recessive inheritance like the SHFM1 generated by a missense mutation in *DLX5* in humans (Shamseldin et al. 2011), nevertheless there is a common autosomal dominant inheritance in humans.

1.6 The Notch pathway

The Notch signaling pathway is an evolutionary conserved intercellular signaling pathway that is considered one of the most important signaling pathways during embryogenesis. It is required for the correct embryonic development involving processes such as cell fate specification, cell proliferation and negative regulation during cell differentiation and tissue morphogenesis.

In mammals, the Notch family is composed of four members, Notch1, Notch2, Notch3 and Notch4 that are single-pass transmembrane receptors. The Notch receptors interact with membrane-bound ligands encoded by the Delta-like (*Dll1*, *Dll3* and *Dll4*) and Jagged (*Jag1* and *Jag2*) gene families, which are also single-pass transmembrane proteins (Fig. 11A). The structure of the receptor binding domains of Notch ligands contains three epidermal growth factors (EGF) motifs, a Delta/Serrate/Lag-2 domain (DSL) and a C2 domain (also known as MNLL-module at the N terminus of Notch ligand) (Shilo and Sprinzak 2017). The core of the Notch pathway has a simple molecular design, with a small number of signaling components, but with an extraordinarily versatile function (Andersson et al. 2011). The canonical Notch signaling pathway is activated when a Notch transmembrane extracellularly receptor interacts with the canonical Notch transmembrane ligand located in other cell, generating the cleavage of the receptor freeing the Notch intracellular domain. In contrast, the non-canonical Notch

signaling pathway can be initiated by a non-canonical ligand or may not require cleavage of the notch receptor (Andersson et al. 2011).

During limb development, Notch signaling controls the AER by regulating apoptosis (Francis et al. 2005) and dorsal-ventral patterning (Irvine and Vogt 1997), besides regulating the size of bone and muscles (Schuster-Gossler et al. 2007). The *Notch1* receptor and the *Jag2* ligand are expressed in the AER while *Notch1* and *Notch2* receptors and the *Jag1* ligand are detected in the mesenchyme (Myat et al. 1996; Shawber et al. 1996; C Rodriguez-Esteban et al. 1997; Vargesson et al. 1998).

The first evidence of the Notch signalling pathway implication in early limb bud development was the analysis of a spontaneous mouse mutation known as *syndactylism* (*sm*) (Sidow et al. 1997) (Fig. 11B). The *sm* mutation consists of a missense mutation affecting one amino acid (glycine to serine) within the first EGF repeat of the *Jag2* DSL ligand domain. *Jag2* is expressed in the limb ectoderm but also in different tissues of the embryo as the somites, branchial arches, tail ectoderm, surface ectoderm, thymus, salivary glands, cranial ganglia, dorsal root ganglia and adult brain. The *sm* homozygous mouse is characterized by the development of a hyperplastic AER, visible at embryonic day 10.5, and syndactyly. The *sm* mutation generates an hypomorphic allele of *Jag2* that could explain the variable penetrance in the syndactylous phenotype. Nonetheless, the fact that Nocth signalling relies in proteolytic cleavage triggering dissociation from the membrane of the Notch intracellular domain (NICD) and its translocation to the nucleus without previous signal amplification renders the pathway very sensitive to variations in modifier levels from individual to individual (Sidow et al. 1997).

Posteriorly, a *Jag2* KO mouse model that produces syndactyly with complete penetrance was generated. The mouse showed perinatal lethally and more severe syndactyly than the *sm* allele that is considered hypomorph. It was demonstrated that *Jag2* is essential for correct craniofacial development and limb outgrowth. Similarly to *sm* mutants, *Jag2* mutants also have a hyperplastic AER and, the expression of *Fgf8* is expanded whereas the expression of *Bmp* genes (*Bmp2* and *Bmp7*) and apoptotic interdigital cells are reduced (Jiang et al. 1998).

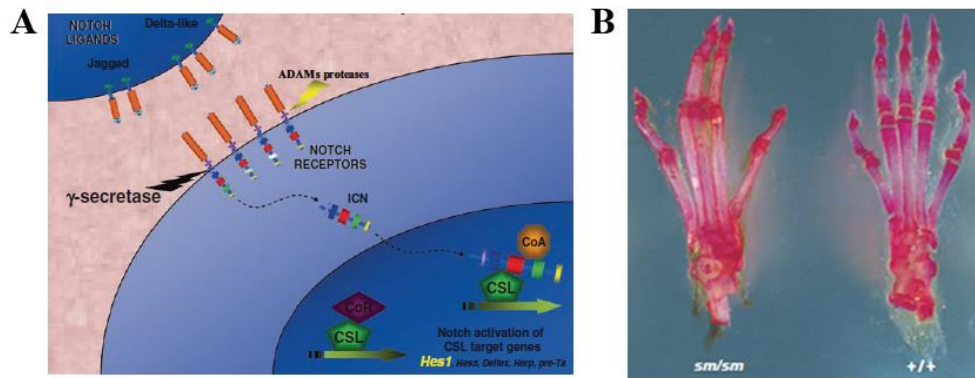


Figure 11: Schematic representation of Notch signaling pathway and *sm* phenotype in mouse. **A.** The five Notch ligands (Dll1, Dll3, Dll4, Jag1 and Jag2) are represented in the cell of the top and the four Notch receptors (Notch1, Notch2, Notch3 and Notch4) in the cell of the bottom. The union of the ligand and receptor is followed by the cleavage of the Notch intracellular domain that its translocated to the nucleus (From Hughes 2009). **B.** The *syndactylism (sm)* homozygous phenotype on the left versus the WT phenotype on the right (From Sidow et al. 1997).

Both *Jag2* and *Notch1* are co-expressed in the limb ectoderm where they control AER size. *Notch1* is a positive regulator of the apoptosis cell mechanism in the AER and its disruption results in a hyperplastic AER (Francis et al. 2005) and syndactyly similar but milder than the *Jag2* mutant. The syndactyly phenotype is identical to that of *Jag2* when both *Notch1* and *Notch2* are disrupted, suggesting that both Notch1 and Notch2, receive Jag2 signal and cooperate in the limb ectoderm (Pan et al. 2005).

Surprisingly, the AER and the digit phenotypes of *Jag2* KO mice (Jiang et al. 1998) are reminiscent by *Sp6* mutants (Talamillo et al. 2010). The *Sp6* KO exhibits variable penetrance and expressivity with defects in AER maturation that leads to limb buds with altered shape. Usually, there is a soft-tissue fusion in forelimbs involving digits 2-3 and sometimes digit 4, and osseous fusion of digits 3-4 in hindlimbs (Talamillo et al. 2010). Given the similarity of the *Sp6* and *Jag2* phenotypes and given that similar phenotypes caused by different genes may indicate that these genes work in the same functional module, we decided to investigate the genetic interaction between *Jag2* and *Sp6*.

2. AIM OF THE PRESENT THESIS

2. AIM OF THE THESIS

A significant part of the Biomedical progress of the recent past decades relies on the advancement of genetic engineering that has permitted the manipulation of the organism's genes and that can be applied to the generation of animal models for the study of human diseases. Without much doubt and without ignoring their inconveniences, animal models that reproduce the disease are invaluable tools for the global study of most pathological entities

OBJECTIVE 1

The first aim of this thesis is the implementation of a transgenic platform that allows gene editing in the mouse zygote in an easy, consistent, and efficient way. This platform is based on the direct application of CRISPR/CAS9 technology to mouse zygotes by electroporation. The availability of this technology at the IBBTEC would potentiate the current studies of several groups.

OBJECTIVE 2

The second objective of this thesis is to use the above-mentioned platform for the generation of three animal models that will permit a better understanding of the genetic and cellular causes of the Split Hand Food Malformation. These models are:

- 1- The *Jag2* KO (targeted single DSB)
- 2- The double deletion of *Dlx5* and *Dlx6* (targeted double DSB)
- 3- The *Sp6:V5* knock-in (single DSB and homologous recombination)

3.MATERIALS AND METHODS

3. MATERIALS & METHODS

3.1. Mouse strains

All animal procedures were conducted accordingly to the EU regulations and 3R principles and reviewed and approved by the Bioethics Committee of the University of Cantabria.

Wild type mice of the C57Bl6, CBA and CD1 strains were used in this project for the generation and establishment of transgenic mouse models. Transgenic mice were generated by the application of CRISPR/Cas9 technology in CBA/C57-B16 hybrid zygotes.

The mouse line B6.129-*Sp6*^{tm1Yoya} was used in this study. This line is characterized by the absence of the second exon of the *Sp6* gene that encodes the entire coding sequence (CDS) of *Sp6* (Nakamura et al. 2004).

3.2. crRNA selection

To select the required crRNAs, the target loci were obtained from <https://www.ncbi.nlm.nih.gov/gene/> and were interrogated with several independent online crRNA design tools: CHOP-CHOP (<https://chopchop.cbu.uib.no/>), Breaking-Cas (<https://bioinfogp.cnb.csic.es/tools/breakingcas/>) and CRISPR-Design (<http://crispr.mit.edu/>), which is no longer available.

We chose 3 crRNAs by comparing each crRNA scores in the different web tools. The different tools give us the same guide but with different scores because each platform uses its own algorithms to prioritize one guide or another. Thus, the top 3 crRNA candidates for each target showing the lower number of off-target and the higher number of on-target scores according to the 3 platforms were selected, although only the best one was ordered. A first selection of 3 crRNAs was made in case the chosen one failed, which never happened to us. In addition, the selected crRNAs of each target region were evaluated using, the CRISPR-Cas9 gRNA checker on-line tool from Integrates DNA technologies (IDT) (<http://idtdna.com>).

3.3. Cas9 endonuclease

The Cas9 endonuclease was obtained from IDT. The first Cas9 available was the wild-type Cas9, Alt-R® S.p. Cas9 Nuclease V3 (#1081058), with high genome editing potency. It is a recombinant *S. pyogenes* Cas9 enzyme plus a nuclear localization signal (NLS) to improve performance.

Over time, several mutant forms of Cas9 enzymes have been engineered by IDT. Currently, we use the HiFi Cas9, Alt-R® S.p. HiFi Cas9 Nuclease V3 (#1081060) which is a mutated Cas9 version with improved specificity and decrease off-target activity, while preserves its high on-target efficiency. The HiFi Cas9 also contains the NLS. Both Cas9 have a molecular weight of 162,200 g/mol.

3.4. Ribonucleoprotein (RNP) complex preparation

We have been working with IDT products using 2-part guide RNAs that are the Alt-R® CRISPR-Cas9 crRNA (crRNA) and the Alt-R® CRISPR-Cas9 tracrRNA (#1072532) (tracrRNA). The crRNA ordered to IDT is formed by 36nt RNA oligos that contains a 20nt target-specific protospacer region and a 16nt sequence that hybridizes with tracrRNA. Commonly, crRNA refers to the 20nt that will guide the Cas9 endonuclease to the desired genomic region, although in our case these crRNA will always carry 16nt more to hybridize with the tracrRNA.

The tracrRNA is universal and enables its combination with different crRNAs. It is formed by 67nt, which is shorter than the classical 89 base pairs (bp) of the natural *S. pyogenes* and contains chemical modifications that provide higher stability under high nuclease conditions. Some studies showed that an increasing the length of the single-guide RNA (sgRNA), formed by the crRNA linked to the tracrRNA, can results in decrease efficiency (Zhang et al. 2016; Matson et al. 2019). One part of the tracrRNA hybridizes with the crRNA (16nt) and the other part binds to the Cas9 endonuclease.

RNP complexes were prepared by mixing in equimolar concentrations the specific crRNA and the tracrRNA by heating for 5 minutes (min.) at 95°C and subsequent incubation with the Cas9 endonuclease (S.p. Cas9 Nuclease V3 or S.p. HiFi Cas9 Nuclease V3) in equimolar amounts for 10 min. at R.T. The dilution compound used for

the in vitro validation will be PBS in contrast with the Opti-MEM medium used to perform the RNP for the electroporation procedure.

The duplex formed by crRNA and tracrRNA are used in different concentrations depending on downstream procedures. For in vitro validation of the selected crRNAs, the final concentration of the duplex in the formation of the RNP complex was 1 μ M, while in zygote electroporation experiments the concentration was 6 μ M.

3.5. ssODN repair template design

The donor DNA is used as a repair template aimed to introduce a desired DNA sequence at specific genomic regions targeted by a crRNAs when a DSB is repaired by the HDR pathway. We have used single strand oligo DNA nucleotides (ssODN) as DNA templates for the generation of two knock-in (KI) models.

The HDR relies in a HR event that takes place between homologous DNA sequences present both in the donor and the genomic regions flanking the DSB. Therefore, the donor is composed of the desired DNA sequence to be introduced in the genome flanked by two DNA sequences, termed homology arms, that are identical to the endogenous sequences at both sides of the DSB targeted by the crRNA. In general DNA donors are used for the generation of KI models but can also be used to avoid the generation of INDELS originated because of NHEJ pathway mediated repair of DNA DSBs.

The length of the homology arms can vary depending on the length of the DNA sequence to be introduced. Homology arms that are usually longer than 500bp have been traditionally used in the generation of double-stranded circular DNA donor vectors for the introduction of large DNA fragments (Yang et al. 2014; Byrne and Church 2015). In contrast, 30-60 base homology arms have been shown to be highly efficient for the insertion of small fragments up to 200 bp (Chen et al. 2011; Wang et al. 2013; Boel et al. 2018). Moreover, it has been shown that optimal length for donor DNA ranges between 90-120 bp with shorter ones performing considerably worse and bigger ones showing a drop in efficiency (Shen et al. 2013; Wang et al. 2013; Boel et al. 2018). Until recently, dsDNA donors have been used for the generation of long DNA insertions, whereas ssODN donors have been used for the insertion of small fragments. Short ssODN can be easily synthesized simplifying the generation of the donor and can be directly purchased

from different companies in comparison to long dsDNA that require arduous cloning steps (Mikuni et al. 2016; Leonetti et al. 2021) and in terms of HDR showed higher efficiency over similar dsDNA templates (Beumer et al. 2013; Miura et al. 2015; Yoshimi et al. 2016). Recently, long ssDNA donors, up to 1kb, have been successfully used for the introduction of longer DNA fragments (Miura et al. 2018). Finally, the use of ssODN donors complementary to the opposite strand targeted by the gRNA containing asymmetric homology arms has been shown to slightly increase CRISPR-Cas9 mediated HDR efficiency (Richardson et al. 2016; Liang et al. 2017). However, further experiment did not show considerable effects in HDR efficiency using donor targeting the PAM containing or non-containing strands neither symmetrical or asymmetrical donors (Boel et al. 2018). One final consideration is the inverse relationship between the distance of the inserted DNA fragment relative to the DSB. It has been shown that the closer the sequence to be integrated is to the DSB the highest the integration rate is (Boel et al. 2018).

Therefore, to generate the *Sp6* KI allele with the V5 tag (42bp) we decided to use a ssODN donor of 124bp in length composed of 35-47nt in length homology arms and target both PAM containing and non-containing strands in different experiments (Fig. 12A).

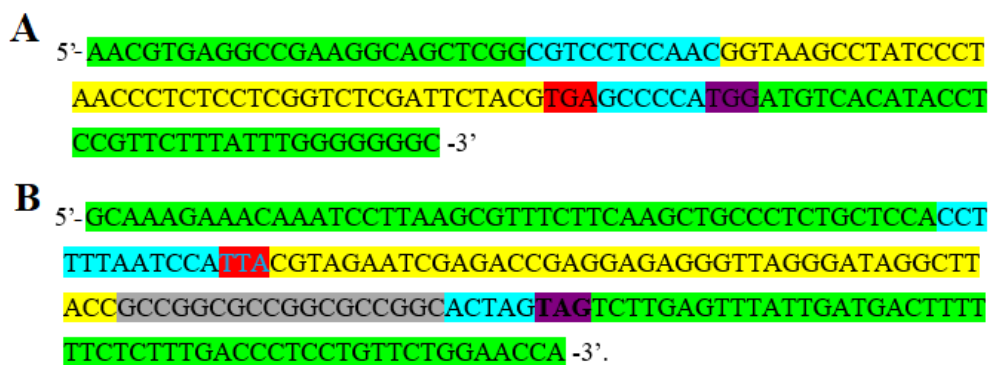


Figure 12: ssODN sequences. **A. *Sp6*:V5 (+) ssODN.** Both homology arms are highlighted in green, flanking the V5 sequence (yellow). The broken crRNA sequence is highlighted in blue and the PAM sequence in purple. The STOP codon, highlighted in red, is located just after V5 sequence. **B. *Hoxa13*:V5 (+) ssODN.** There are two homology arms of 60bp which are highlighted in green. The STOP codon is pointed in red, the linker in grey, the crRNA is pointed in blue and the changed PAM in purple.

To tag *Hoxa13* we introduced the V5 tag with a (+) ssODN, which sequence includes a sequence that encodes for an AlaGlyAlaGlyAlaGly peptide spacer between the protein and the epitope tag followed by a termination codon. The ssODN designed to insert the V5 TAG into *Hoxa13* sequence had the V5 sequence (42bp), the linker sequence (18bp) and two homology arms (63bp and 60bp). (Fig. 12B)

3.6. In vitro validation of crRNA

Primers flanking the genomic position targeted by the crRNAs were designed for all the different models. The distance between the primers and the DSB must be asymmetric. If so, after in vitro digestion of the target DNA in the presence of the RNP two bands of different sizes are visible by agarose gel electrophoreses. To avoid secondary structures and primer dimer formations, the suitability of manually designed primers was evaluated with the online tool “Oligoevaluator from Sigma Aldrich” (<https://www.sigmaaldrich.com/technical-documents/articles/biology/oligo-evaluator.html>) and checked with the UCSC tool “In-silico PCR” (<https://genome.ucsc.edu/cgi-bin/hgPcr>) (Table 2).

Table 2: Primers designed to crRNA in vitro validation. There was generated primers to amplify the target region for each crRNA. The table shows the name, direction, sequence and, the expected fragment for each pair of primers. Remark, that there is noted the expected fragment for the amplification of complete target region and below of it, the two expected fragment if the digestion is performed.

Name	direction	Sequence	Expected fragment
crRNA <i>Jag2</i>			
<i>Jag2</i> F-Fwd	5'-3'	CGATGTCGCCAAGGATAGG	1193bp
<i>Jag2</i> F-Rev	5'-3'	CACCTACTTCGTGGCCTACTAAAGC	733pb and 460pb
crRNA <i>Dlx6</i>			
<i>Dlx6</i> -Fwd	5'-3'	CAGCCGATAGATACTAGTGACATTGG	1060bp
<i>Dlx6</i> -Rev	5'-3'	CACGGGCATTGTTCATTAGC	625pb y 425pb
crRNA <i>Dlx5</i>			
<i>Dlx5</i> -Fwd	5'-3'	CGAGGTACTGAGTCTTCTGAAACC	1047bp
<i>Dlx5</i> -Rev	5'-3'	TGGCAGCAGCTTCATACACC	649pb y 398 pb
crRNA <i>Sp6</i>			
<i>Sp6</i> -Fwd	5'-3'	CCACACCGGGACCAAGAAGTTCC	436bp
<i>Sp6</i> -Rev	5'-3'	CCCTTTCTCACTATTTACCCCTCCC	214bp y 222bp

Validation of selected crRNA was performed following the IDT protocol “Alt-R CRISPR-Cas9 system: In vitro cleavage of target DNA with ribonucleoprotein complex”

(https://sfvideo.blob.core.windows.net/sitefinity/docs/default-source/protocol/alt-r-crispr-cas9-protocol-in-vitro-cleavage-of-target-dna-with-rnp-complex.pdf?sfvrsn=88c43107_26).

The target sequences were amplified by PCR standard protocol to be used as DNA templates for the corresponding crRNAs. PCR products were purified with the Kit Purification DNA (NZY gelpure, MB01102) and 50nM of DNA substrate were incubated in the presence of corresponding RNP complex for 60 min. at 37°C.

RNP complexes were prepared by mixing in equimolar concentrations the specific crRNA and the tracrRNA in nuclease free duplex buffer at a final concentration of 10µM followed by heating for 5 min. at 95°C and subsequent incubation with the Cas9 endonuclease in equimolar amounts for 10 min. at R.T.

To perform the in vitro digestion reaction, the RNP generated, 50nM of DNA substrate and 10X Cas9 Nuclease reaction buffer were incubated at 37°C for 1hour (h). The digestion was stopped by adding 1µL Proteinase K (20 mg/mL) at 56°C for 10 min. The cleaved products were visualized by agarose gel electrophoresis.

3.7. Zygote collection.

Super-ovulated females were obtained according to standard procedures (CNB-CBMSO transgenic service). (<https://www.cnb.csic.es/index.php/es/investigacion/servicios-cientificos/transgenesis>). Superovulation of 3-6 weeks old C57B16/J-CBA hybrid female mice was induced through intraperitoneal administration of 5UI body Pregnant Mare Serum Gonadotrophin (PMSG, #Folligon of MSD), followed by injection of 5UI body Human Cortical Gonadotropin (hCG, #CG10 Sigma Aldrich) 48h later. After that, females were mated with males ON.

The following morning, females showing a vaginal plug were sacrificed and the oviducts were removed and placed into a culture dish with M2 medium (M7167, Sigma Aldrich). The cumulus-oocyte complexes were collected by puncturing the ampulla of the oviducts with the use of a needle. The complexes were transferred to a clean M2 drop where the cumulus was removed using hyaluronidase (H4272 Sigma). diluted in M2 medium (1:100) and up and down the zygotes through the capillary to remove the

cumulus cells. The pronuclear stage embryos (E 0.5) were collected (Fig.13). The embryos were cultured in drops of KSOM (MR106-MR121, Sigma Aldrich) covered with paraffin oil in a humidified incubator at 5% CO₂ and 37°C until electroporation. After electroporation embryos were cultured for 1-2h before being transferred to CD1 pseudopregnant females. To check the correct in vitro development and the viability of the embryos, we initially cultured some embryos and let them to develop in vitro up to blastocyst stage (Fig.13).

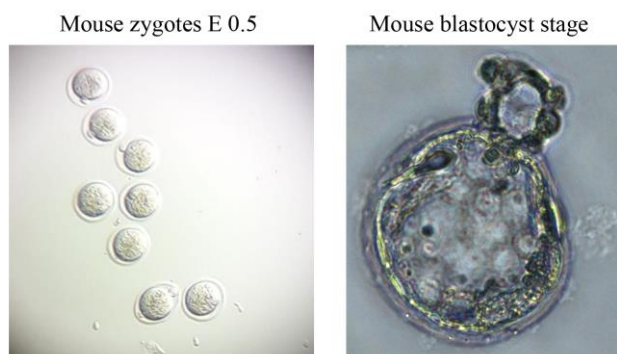


Figure 13: In vitro development of mouse E0.5 zygotes to blastocyst stage. On the right pronuclear stage embryos (E 0.5) and on the left, the same mouse zygotes after developing up to blastocyst stage in vitro post-fixed in 4% PFA/PBS.

3.8. Electroporation procedure

Mouse zygote electroporation was generated following the IDT DNA protocol “Ribonucleoprotein delivery using the Alt-R® CRISPR-Cas9 System and the NEPA21 Electroporator” (https://sfvideo.blob.core.windows.net/sitefinity/docs/default-source/user-submitted-method/crispr-cas9-rnp-delivery-mouse-zygote-electroporation-nepagene.pdf?sfvrsn=4b980e07_14).

The duplex crRNA:tracrRNA is first prepared. Both components are mixed in equimolar concentration to a final duplex concentration of 100μM and heated for 5 min. at 95°C in a final volume of 50μl. Next, the reaction is allowed to cool at room temperature (RT). To perform the RNP complex, the crRNA:tracrRNA duplex and the Cas9 endonuclease are incubated at RT in Opti-MEM medium for 10-20 min. The reaction containing the RNP was stored at 4°C up to 8 weeks or at -80°C for long term storage (1 year).

The RNP complex was delivered into pronuclear stage embryos with the use of the NEPA21 electroporator with the CUY501 P1-1.5 electrode following manufacturer’s

recommendations (Fig.14). This system minimizes embryo damage because there is no need for weakening the zona pellucida (ZP) with acidic Tyrode’s solution before electroporation.



Figure 14: The NEPA21 electroporator device. **A.** The NEPA 21 electroporator. **B.** The CUY501 P1-1.5 electrode that can perform the electroporation in a range of 5-50 embryos simultaneously.

The mechanism of this system is based on the use of three steps (Table 3). The first step is the generation of four poring pulses that are used to generate microscopic holes in the ZP and oolemma. These pulses are of high voltage (40V) but short duration (2.5ms). The poring pulses are applied with 50ms intervals. The second step is the transfer pulse. There are 5 transfer pulses which have lower voltage (7V) but longer duration (50ms) with a pulse interval of 50ms. These pulses transfer the RNP into the cytoplasm. The third step consists in a change in polarity of the transfer pulse increasing the efficiency for RNP delivery into the nucleus (Kaneko and Mashimo 2015).

Table 3. NEPA21 Electroporation conditions. The voltage, the number of pulses, the length the interval between pulses, the rate, and the polarity for both poring and transfer pulses are indicated.

#	Set Parameters											
	Poring Pulse						Transfer Pulse					
	V	Length (ms)	Interval (ms)	No.	D. Rate (%)	Polarity	V	Length (ms)	Interval (ms)	No.	D. Rate (%)	Polarity
1	40	2.5	50	4	10	+	7	50	50	5	40	+/-

To electroporate the embryos, 5µl of RNP complex solution were placed in the electroporation chamber and the impedance was measured. For electroporation the optimal impedance range is between 0.2-0.24 kΩ. Once the appropriate impedance was achieved the embryos were placed in a line in parallel to the electrodes. The use of the

CUY501 P1-1.5 electrode (1mm gap) allows the electroporation of 5-50 embryos simultaneously. In our experiments approximately 20-30 embryos were placed in the RNP drop at the same time. When the appropriate impedance was achieved (0.18-0.22 k Ω) the electroporation was performed. The electroporated embryos were cultured between 1-2h before being transferred to the infundibulum of CD1 pseudopregnant females.

3.9. Embryo transfer

The electroporated embryos were transferred to pseudopregnant female. To get pseudopregnant females we mated CD1 female mice with vasectomized males on the day before electroporation (Deb et al. 2006). The females showing a vaginal plug the next morning was selected as females ready to host the electroporated embryos. The embryos were transferred to the oviduct following the protocol of Kumamoto University (<http://card.medic.kumamoto-u.ac.jp/card/english/sigen/manual/transfer.html>). Embryo transfer into the oviduct was carried out by cutting the oviduct and inserting a capillary to expel the embryos towards the ampulla. 10 embryos were transferred into each oviduct.

3.10. Genotyping strategy

It is important to consider before starting with the design of the primers that they should be designed away from the DSB so that in case INDELS are produced they do not interfere with the genotyping strategy. The primers were designed with the same tools explained before at section 3.6 materials and methods.

For some models we have used the same primers that were designed for the validation of crRNA because they amplified the target region and allowed us to see in an agarose gel the differences between WT mice and mice with the desired mutation, as was the case of the animal model for *Dlx5/Dlx6* deletion. Different combinations of *Dlx6*-Fwd, *Dlx6*-Rev, *Dlx5*-Fwd and *Dlx5*-Rev were used for the analysis (Table 4)

The analysis of the newborn mice obtained from the electroporation of the crRNA_*Jag2* was done by Sanger sequencing. Since the quality for Sanger sequencing starts to decrease within 1 kb, the genotyping strategy for this model included primers that amplify a region smaller than 1Kb (*Jag2*-Fwd-G and *Jag2*-G-Rev, 662bp) (Table 4) so that the region around the DSB could be properly sequenced from both sides.

For the analysis of mice which have been electroporated with crRNA_*Sp6* we used the same primers designed for the in vitro validation of crRNA_*Sp6* but in addition we designed a specific primer that matched the V5 sequence to quickly identify the insertion of the TAG (Table 4).

Table 4. Primer used to genotype the different models. The table shows the name, direction, sequence and, the expected fragment for each pair of primers uses for the models indicated.

Name	direction	Sequence	Expected fragment
Jag2 KO model			
<i>Jag2</i> -Fwd-G	5'-3'	GTGGAAGGAAGCTTAGAGCATATGG	662bp
<i>Jag2</i> -Rev-G	5'-3'	CCGTGGAGCAAATTACATCC	
WT allele of <i>Dlx6</i>			
<i>Dlx6</i> -Fwd	5'-3'	CAGCCGATAGATACTAGTGACATTGG	1060bp
<i>Dlx6</i> -Rev	5'-3'	CACGGGCATTTGTCATTTAGC	
WT allele of <i>Dlx5</i>			
<i>Dlx5</i> -Fwd	5'-3'	CGAGGTACTGAGTCTTCTGAAACC	1047bp
<i>Dlx5</i> -Rev	5'-3'	TGGCAGCAGCTTCATACACC	
<i>Dlx5/Dlx6</i> deletion			
<i>Dlx6</i> -Fwd	5'-3'	CAGCCGATAGATACTAGTGACATTGG	1023bp
<i>Dlx5</i> -Rev	5'-3'	TGGCAGCAGCTTCATACACC	
<i>Dlx5/Dlx6</i> inversion			
<i>Dlx6</i> -Rev	5'-3'	CACGGGCATTTGTCATTTAGC	823bp
<i>Dlx5</i> -Rev	5'-3'	TGGCAGCAGCTTCATACACC	
WT allele of <i>Sp6</i>			
<i>Sp6</i> -Fwd	5'-3'	CCACACCGGGACCAAGAAGTTCC	436bp
<i>Sp6</i> -Rev	5'-3'	CCCTTTCTCACTATTCACCCCTCC	
<i>Sp6</i> allele with V5			
<i>Sp6</i> -Fwd	5'-3'	CCACACCGGGACCAAGAAGTTCC	262bp
<i>Sp6</i> -Rev KIV5	5'-3'	CGATTCTACGTGAGCCCCATG	

3.11. Isolation of genomic DNA (quick protocol)

Mice were weaned with 3 weeks and, tail-tip biopsy of 0.3 cm was taken for isolation of genomic DNA. 75µl of alkaline lysis reagent (25 mM NaOH, 0.2mM disodium EDTA) was added to the tail-tip and incubated for 45 min. at 90°C. After cooling at RT, 75µl of neutralization buffer (40 mM Tris-HCl) was added (Truett et al. 2000). Finally, centrifugation at 4000 rpm for 3 min was performed. Samples were store at 4°C for short-term or at -20°C for long-term.

3.12. Genotyping

The newborn animals obtained after electroporation are known as the F0 generation. The F0 mouse that carries the desired mutation and is used to establish the line will be known as the founder.

The genotyping of the F0 mice was performed by PCR standard protocol followed by Sanger sequencing for verification and detail of the modified allele. The different mouse lines generated were established and genotyped by PCR standard protocols, varying the annealing temperature according to the melting temperature (T_m) of the primers used.

The PCRs are performed with 1 μ l of sample obtained from tail biopsy, primer final concentration at 700nM, and Supreme NZYTaQ II 2x MasterMix (MB36002) in a total volume of 13 μ l. PCR products were visualized in agarose gel in TAE (Tris acetate EDTA), varying the concentration (0.8- 4%) depending on the size of the expected products. Agarose gels contained Green Safe Premium (MB13201) for DNA staining, and they were visualized in the Gel-Doc under ultraviolet light and the use of the Quantity–One software (BioRad). Finally, the molecular weight of the products was determined with the use of NZYDNA Ladder V (MB03101) and Gene Ruler Ladder (Molecular biology. SM0242 and SM0311). The set of primers used to genotype each mouse strain is specified below and it is indicated into 5' to 3' orientation.

3.13. Genotyping of established lines used in this project.

The *Jag2*^{emMar} mouse line carries a loss of function allele of *Jag2* that has been generated based on a previous published *Jag2* KO (Jiang et al. 1998). The *Jag2*^{emMar} allele has a 41bp deletion in the DSL domain that results in a frameshift mutation disrupting the open reading frame of *Jag2*. When an F0 mouse with the desired mutation was selected to be the founder of the line, new primers (*Jag2*-Fwd and *Jag2*-Rev) flanking the deletion and amplifying a shorter fragment were used to see the difference between the fragments amplified from the WT allele (201bp) and the mutant allele (160bp) (Table 5) by agarose gel electrophoreses. This line has been maintained in heterozygosity in a C57Bl6 background.

The *Sp6:V5^{em1Mar}* mouse line is a KI model. The allele *Sp6:V5^{em1Mar}* has an insertion of the V5 TAG sequence (42nt) just before the STOP codon of *Sp6*. When the mouse with the correct sequence inserted in its genome was selected as founder to establish the line, new primers were designed to amplify a shorter fragment and differentiate by PCR procedure the WT allele, 326bp, from the allele with the V5, 368bp (*Sp6-Fwd-L* and *Sp6-Rev-L*) (Table 5) This line has been maintained in homozygosity in a C57Bl6 genetic background.

Table 5: Primers designed to genotype established line. The table shows the name, direction, sequence and, the expected fragment for each pair of primers.

Name	direction	Sequence	Expected fragment
<i>Jag2^{emMar}</i>			
<i>Jag2-Fwd</i>	5'-3'	GACTGACGGGTAGCTGCTG	WT 201bp MUT 160pb
<i>Jag2-Rev</i>	5'-3'	AACTTGTTGCAGGTGGCACT	
<i>Sp6:V5^{em1Mar}</i>			
<i>Sp6-Fwd-L</i>	5'-3'	CCTGGCCAAACACATGAAAACC	WT 326bp MUT 368bp
<i>Sp6-Rev-L</i>	5'-3'	CTCCTGGCAGCCTAAATATTCAAGC	
<i>DelLARM2^{emMar}</i>			
356-Fwd	5'-3'	CTATGCAGACCCTTTCTTGG	WT 634bp MUT 500bp
356-Rev	5'-3'	GGAGAACCCTTGAACAAATGAC	
355-FarRev	5'-3'	GAGGGAGTTGGTTTAAATCACC	
<i>DelLARM1^{emMar}</i>			
356-Fwd	5'-3'	CTATGCAGACCCTTTCTTGG	WT 536bp MUT 1065bp
373-Rev	5'-3'	GCCAGAAGCAAAATCTAATGAG	
372-FarFwd	5'-3'	CAGGAGGTGTTCTTGAATTCTC	
<i>B6.129-Sp6^{em1Yoya}</i>			
WT-Fwd	5'-3'	GCTGGAAACCGTGAAGGAAAGG	WT 331 MUT 729bp
MUT-Fwd	5'-3'	GCTTCCTCGTGCTTTACGGTATC	
Common-Rev	5'-3'	GGTTAGGGGTCATAAGGGATAGG	

The *Del(LARM1^{emMar})* and *Del(LARM2^{emMar})* mouse lines were generated by application of CRISPR/Cas9 technology to delete *LARM1* and *LARM2* respectively, which are limb-specific enhancers of *Lmx1b*. The *Del(LARM1^{emMar})* allele has a 2,81 bp deletion of at *LARM1* enhancer region, and *Del(LARM2^{emMar})* has a deletion of 5,266 bp at the *LARM2* region. Primers flanking each target region were designed to analyze each DSB (Table 5).

The *Hoxa13:V5^{em1Mar}* mouse line is a KI model. The *Hoxa13:V5^{em1Mar}* allele was generated by inserting one copy of the V5 tag epitope in frame at the 3'-terminal end of

the *Hoxa13* gene before the stop codon. A 18nt linker was used to connect the sequence encoding the V5 tag epitope with the *Hoxa13*. The same primers designed for the in vitro validation of the crRNA_*Hoxa13* were used to maintain the line. This line has been maintained in homozygosity in a C57/Bl6 genetic background.

The line **B6.129-Sp6^{tm1Yoya}** that contains a loss of function allele for Sp6 was also used in this project and it is genotyped with its own primers listed in the table below.

3.14. Sanger sequencing

The region of interest was amplified by PCR standard protocol with previous designed primers positioned outside of target region. By pooling three PCR reaction of 25 μ l each, obtained 75 μ l of PCR product and check 5 μ l in agarose gel before continuing. The remaining PCR product was purified using a Kit Purification DNA (NZY gelpure. MB01102). The forward or reverse primers were used for Sanger sequencing method by Stab vida laboratory (www.stabvida.com/es).

Sanger sequencing results were visualized with the use of the Snap Gene Viewer. The chromatogram was inspected for possible mixed sequencing peaks indicative of potential INDELS In cases where the sequence analysed come from heterozygous or mosaic mouse, instead of a single peak for each nucleotide position in the chromatogram, two or more peaks will appear in the case of heterozygotes or mosaic animals, respectively.

3.15. Cloning PCR products

The pGEM-T Easy Vector system (From Promega company) was used to clone PCR products when mosaic founders were obtained. Following standard PCR protocol, 100 μ l of PCR product were purified using PCR purification kit (NZY gelpure. MB01102). The insert:vector ratio used in the ligation reaction was 3:1. 1X Rapid Ligation Buffer, T4 DNA Ligase and T4 DNA Ligase (3 Weiss units/ μ l) were added to ligation reaction and kept O.N at 4°C. Competent cells (Top10) were used for transformations by heat shock. 3 μ l of ligation reaction were added to the competent cells and placed them on ice for 30 min. After that, samples were incubated at 42°C for 20s. and placed back on ice for 2 min. 950 μ l of LB were added and cells were incubated 1h at 37°C. 100 μ l of each transformation reaction were plated (LB/Amp/X-Gal plates). The

plates were incubated O.N at 37°C. Successful integration of the insert into the pGEM-T Easy Vector interrupted the coding sequence of β -galactosidase and recombinant colonies could be identified by color screening from the Petri dish (white) from those with empty plasmids (Blue).

PCR standard protocol was used to validate the insertion of the product in the colonies picked. After that, it was growth in LB-Amp medium culture O.N at 37°C. Finally, the plasmid DNA was purified following a procedure based on the alkaline lysis of bacterial cells followed by adsorption of DNA onto silica in the presence of high salts (SPEEDTOOLS Plasmid DNA Purification kit. Biotools. Ref.21.222). Final product was analyzed by Sanger sequencing.

3.16. Line establishment by backcrossing

The establishment of the mouse lines generated was accomplished following the Jackson laboratory protocol.

The first step was mating the F0 founder mouse to an inbred mouse strain to eliminate mosaicism and off-target effects. Because ours F0 mice had a hybrid genetic background (75% C57BL/6 and 25% CBA), they were mated with C57BL/6 mice to establish the line in this background. When the first backcrossing generation (N1) was generated and analysed, a selected N1 male mouse that carried the desired edited allele was mated with other C57Bl/6 WT mice to generate N2 mice and the line was considered to be established.

The mouse lines generated in this project are named following the guideline for nomenclature of genes, genetic markers, alleles, and mutations in mice by the international committee on Standardized Genetic Nomenclature for Mice. Basically, includes the symbol of the edited gene with the abbreviation em (endonuclease-mediated mutation) and the initials of the lab (Mar) where the mice are created.

3.17. Analysis of possible off-target.

The possibility that the selected crRNAs cut a non-desired region (off-target) is directly evaluated by the crRNA design tool mentioned above and were studied by amplification of these possible off-target regions by conventional PCR and subsequent

analysis by Sanger sequencing. For this, primers flanking the possible off-target sequences selected were designed to amplify these regions (Table 6).

Table 6: Primers to off-target sequences analysis. The table shows the name, direction, sequence and, the expected fragment for each pair of primers.

Name	direction	Sequence	Expected fragment
Off-target 1 <i>Dlx6</i>			
OT <i>Dlx6</i> 1 Fwd	5'-3'	AAGCCTCAGATGTGTGTCCA	WT 781bp
OT <i>Dlx6</i> 1 Rev	5'-3'	TGAGTGCTCTTAACCGCTGA	
Off-target 2 <i>Dlx6</i>			
OT <i>Dlx6</i> 2 Fwd	5'-3'	GCCTCACTGCCTGTTTCAA	WT 643bp
OT <i>Dlx6</i> 2 Rev	5'-3'	AAGCCCTTAAGACCACCCAG	
Off-target 3 <i>Dlx6</i>			
OT <i>Dlx6</i> 3 Fwd	5'-3'	GGCTGTGGACCTGAGTTGA	WT 508bp
OT <i>Dlx6</i> 3 Rev	5'-3'	CATCCTCTGCCAGCATTCT	
Off-target 1 <i>Dlx5</i>			
OT <i>Dlx5</i> 1 Fwd	5'-3'	TCACTGAGCCACCCATGATT	WT 756bp
OT <i>Dlx5</i> 1 Rev	5'-3'	GAGGGCAATCACACACACAC	
Off-target 2 <i>Dlx5</i>			
OT <i>Dlx5</i> 2 Fwd	5'-3'	TATAGTGTGCACAGGAGGGC	WT 585bp
OT <i>Dlx5</i> 2 Rev	5'-3'	GCCTGTGTCCCATTCTCTCT	
Off-target 3 <i>Dlx5</i>			
OT <i>Dlx5</i> 3 Fwd	5'-3'	GGTGAGTAGGTGGGACTTCC	WT 723bp
OT <i>Dlx5</i> 3 Rev	5'-3'	TATGGGGATGGGAGTGTGTG	

3.18. Skeletal preparations.

New-born mice were collected in PBS and the skin and viscera were removed before being fixed in 95% ethanol (EtOH). Alizarin Red and Alcian Blue staining were performed following standard procedures. Mouse embryos were immersed in Alcian blue solutions (80% EtOH, 20% glacial acetic acid and 0.3 mg/ml Alcian Blue) for 24-72h for cartilage staining. This solution was replaced by 95% EtOH, through successive changes, to eliminate excess of Alcian Blue. The embryos were cleared by KOH 1% treatment for 3-4h until bones became visible. After that, Mouse embryos were stained with the Alizarin Red (0.05 mg/ml Alizarin Red in 1% KOH) in darkness into for 20h for bone staining. To clear the tissues, the embryos were embedded in 20% glycerin (in 1% KOH) around 24h and finally, they were dehydrated with serial changes every 24h of 70% EtOH: Glycerin: H₂O (1:2:7/3:3:4/4:4:2/5:5:0). The skeletal preparations were stored at RT.

3.19. Paraffin embedding

The embryos were harvested in cold PBS and fixed in 4% paraformaldehyde (PFA) and then washed in PBS. Successive changes of increasing concentration of EtOH (25%, 50%, 75%, 95%) until absolute EtOH were performed to dehydrate the tissues. Before embedding the mouse embryos into paraffin (Histosec pastilles without DMSO. Merck.Ref.1.15161.2504) at 60°C for at least 1h, they were cleared twice with xylene (time depend on the stage and size of the sample). Embryo sections of 10-12µm were performed with a Leica RM2125RT microtome and collect on siliconized slides (SuperFrostPlus).

3.20. Whole mount in situ hybridization (WMISH)

Embryos were dissected in cold PBS and fixed in 4% PFA in PBS at 4°C O.N. The next day, they were washed in PBS at 4°C, PBS-Tween (PBT- 0.1%Tween in PBS) at R.T and dehydrated in increasing concentrations of MetOH in PBT (25-50-75-100%). The embryos were stored at -20°C. Embryos must be rehydrated for WMISH in decreasing concentrations of MetOH, washed in PBT and then bleached with 6% H₂O₂ for 1h. Embryos were rinsed in PBT and incubated with proteinase K (PK, 10 µg/ml) in proteinase K buffer (50 mM Tris-HCl pH 7.4, 5 mM EDTA) at R.T for 5-15min., adjusting the digestion time to the stage of the embryo for mesodermal expressed genes. The ectodermal expressions need 5 min. of proteinase K (5 µg/ml). Embryos were washed in PBT and post-fixed in 0.2% glutaraldehyde + 4% PFA before immersion in hybridization buffer (50% formamide, 5x SSC, 2% blocking powder, 0.1% Triton X-100, 0.1% CHAPS, 1 mg/ml tRNA, 50 µg/ml Heparin pH 4.5, 500 mM EDTA pH 8) at 65°C O.N.

The following day, the samples were frozen at -20°C for at least 6h. After that, the hybridization buffer was replaced with new buffer containing the desired probe and incubated at 65°C O.N. The next day, several post-hybridization washes were done to get rid of unspecific binding: three washes of 2x SSC + 0.1% CHAPS (1M NaCl, 100 mM Sodium Citrate, 0.1% Chaps) of 30 min. each at 65°C, followed by three washes of 0.2x SSC + 0.1% CHAPS (10 mM NaCl, 1 mM Sodium Citrate, 0.1% Chaps) for 70 min. total at 65°C. Then, two washes of KTBT buffer (50 mM Tris-HCl pH 7.4, 150 mM NaCl, 10 mM KCl, 1% Triton X-100) were done for 10 min. at R.T. Samples were blocked in 20%

sheep serum (in KTBT) for 2h at R.T prior to incubation with anti-Digoxigenin-Alkaline Phosphatase antibody (anti-dig-AP) diluted (1:2,000) in blocking solution at 4°C O.N. After this, several washes were performed with KTBT at R.T.

Finally, detection of alkaline phosphatase activity was performed by incubating the embryos in darkness in NTMT buffer (100 mM Tris-HCl pH 9.5, 50 mM MgCl₂, 100 mM NaCl, 1% Triton X-100), with NBT (3 µg/ml) and BCIP (2.3 µg/ml). Once signal level was clear and robust, reaction was stop with several washes in KTBT and fixed in 4% PFA for analysis.

3.21. In situ hybridization in paraffin sections

A similar method to the above described for WMISH was followed in sections. Briefly, after dewaxing and rehydration, the samples were permeabilized by incubation in PK (10 µg/ml) for 7 min. 30s. (500µl/slide). Then, samples were washed in PBS for 5 min. at R.T, fixed in 4% PFA for 20 min. and washed with PBS again, followed by an acetylating step (0.1 M triethanol-amine, 0.066 mM Acetic Anhydride) of 10 min. to reduce background. After that, samples were washed twice in PBT for 5 min. and once with dH₂O. The sections were incubated in hybridization buffer containing the desired antisense ribonucleic acid (RNA) probe, at 65°C O.N in a humid chamber.

Next day, post-hybridization washes (at 65 °C) were performed to remove unspecific binding. Slides were washed 30 min. in 1x SSC/ 50% Formamide, 20 min. in 2x SSC and two additional 20 min. washes in 0.2x SSC. Finally, three washes (5 min. R.T) in MABT pH 7.5 (150 mM NaCl, 100 mM Maleic Acid, 0.04% Tween) were performed before incubation with blocking solution (20% sheep serum in MABT) for 1h at R.T. After that, sections were incubated O.N with the antibody α-DIG-AP (1:2500) at 4°C in a humid chamber (300µl/slide).

The following day, and after 3 washes in MABT (5 min., R.T), and a wash of NTM (pH 9.5) of 10min. After that, the signal was revealed with NTM/NBT (3 µl/ml)/ BCIP (2.3 µl/ml). When the desired signal level was obtained, the slides were rinsed in PBS for 5 min. and fixed in 4% PFA ON. Finally, the slides were washed again in PBS and air-dried. Dehydration and mounting were performed following routinary procedures.

3.22. Immunohistochemistry

Immunoassays were performed in paraffin sections. Sections were rehydrated following standard protocol through decreasing steps of EtOH concentration after two Xilol steps. To inhibit endogenous peroxidase, the sections were incubated with 2% H₂O₂ in methanol, followed by two washes with dH₂O for 5 min. Retriever treatment based on Citrate buffer 10mM pH6 or Proteinase K treatment were used to reveal the possible epitope masked. The sections were washed three times with PBS and one last wash with PBT before they were incubated for 30 min. in blocking solution (1% BSA, 1% Serum in TBST ,1% Tween 20 in TBS) at R.T with humidity. Sections were rinsed in PBT and incubated with primary antibody O.N at 4°C. We used as primary antibodies the Sp6 rabbit polyclonal antibody (#21234-1-AP) from Proteintech to Sp6 detection and the V5 tag monoclonal antibody (TCM5) from eBioscience to detect the V5 tag. The next day, two washes with PBS and one with PBT were performed. After that, the sections were incubated with secondary antibody conjugated with biotin, for 1h at R.T with humidity. After several PBS washes and a final one with PBT, sections were incubated with VECTASTAIN Elite ABC HRP Kit (Vector Laboratories PK-6100). The detection of the signal was performed with DAB detection solution (0.06% DAB + 0.005% H₂O₂ + Tris 0.05M pH=7.5). When the desired signal level was obtained, the slides were rinsed in PBS. Finally, sections were dehydrated and mounted using cytoaseal60 (Richard-Allan Scientific) following routine procedures.

3.23. Immunofluorescence

Immunoassays were performed in paraffin sections. Sections were rehydrated following standard protocols. The sections were incubated with Glycine 0.1M in PBS for 10 min. to avoid auto-fluorescence, then several washed of PBS were performed. Epitope retrieval was performed based on citrate buffer, or proteinase K treatment. Sections were rinsed several times with PBS and a final step with PBT. The sections were incubated with blocking solution (TBS, 10% Serum, 2% BSA, 0.2% Triton X-100) for 30 min. at R.T with humidity. The samples were rinsed with PBT and incubated with primary antibody O.N at 4°C. We used as primary antibodies the Sp6 rabbit polyclonal antibody (#21234-1-AP) from Proteintech to Sp6 detection and the V5 tag monoclonal antibody (TCM5) from eBioscience to detect the V5 tag. Several washes with PBS were performed and a last one with PBT. After that, the slides were incubated with secondary antibody

during 60-75 min. in darkness and with humidity. Then, slides were washed in PBS and final step of PBT. Finally, the sections were incubated with DAPI (Roche. Ref 10236276001) for 5 min. and rinse with PBS and dH₂O before being mounted using cytoaseal60 (Richard-Allan Scientific) following routine procedures.

3.24. Immunoblot

The HLs of an embryo stage according with the expression of the protein that we are going to detect were washed and dissected in cold PBS for immunoblot (western blot). Protein extraction was performed with RIPA buffer [50 mM Tris-HCl pH 7.5, 150 mM NaCl, 1% NP-40, 1% DOX, 0.1% SDS, Protease Inhibitor Cocktail (PICS)] keeping on ice during the process. The protein obtained was quantified with Lowry assay (DC-protein assay kit I #500-0115). Same volume of *Laemmli* (2x SDS gel-loading buffer: 100 mM Tris-HCl pH 6.8, 8% β-mercaptoethanol, 4% SDS, 20% glycerol, and 0.1% bromophenol blue) was mixed with the protein extract obtained before and heat at 100°C for 5min. Samples were run on 10% (v/v) SDS-Polyacrylamide Gel Electrophoresis (SDS-PAGE). To determinate the molecular weight, Precision Plus Protein Standards (Bio-Rad #161-0374) was used as marker. After that, the proteins were transfer from SDS-Polyacrylamide gel to nitrocellulose filters (Amersham Biosciences) and then blocked with 4% BSA in TBS-T (20 mM Tris pH 7.5, 500 mM NaCl, 0.1% Tween-20) for 1h at RT and shaking. The blocking solution was removed, and the samples were incubated with primary antibody (1:1000) diluted in 4% BSA in TBS-T O.N at 4°C and shaking. We have used as primary antibodies the Sp6 rabbit polyclonal antibody (#21234-1-AP) from Proteintech for Sp6 detection and several antibodies to detect the V5 tag (The V5 tag monoclonal antibody (TCM5) from eBioscience, Mouse anti-V5 tag from BioRad and Anti-V5 antibody from SigmaAldrich).

Next day, secondary antibody (1:10.000) was added after washing the membrane with TBS-T four times for 5 min. each and incubated 1h at R.T. After four additional washes with TBST protein detection was performed with ECL.

3.25. Immunoprecipitation

Immunoprecipitation (IP) technique was performed to precipitate Sp6:V5 protein through detection of the V5 tag. The V5-Trap magnetic agarose (#v5tma) from ChromoTek was use. This consists of an anti-V5-tag Nanobody (VHH) covalently bound

to magnetic agarose beads. The molecular weight of nanobodies (15kDa) is 10 times smaller than normal antibodies (150kDa) because they are made in camelids, which carry single-domain antibodies. Further detection of immunoprecipitated protein was performed by immunoblot assay with the Sp6 rabbit polyclonal antibody (#21234-1-AP) from Proteintech.

First, a total of 40 FLs and 40 HLs of *Sp6:V5* (V5/V5) embryos at stage 10.5 were dissected and lysed with RIPA buffer on ice and protein was quantified using the Lowry assay (DC-protein assay kit I #500-0115). From the total lysate, 10% was stored at -20°C to be used as positive control. The nanobody was resuspended according to manufacturer recommendations and 25 µl of the V5-trap magnetic agarose bead slurry were transferred into a 1.5 mL reaction tube followed by the addition of 500 µl ice-cold dilution buffer (Tris/Cl pH 7.5, 150 mM NaCl, 0.5 mM EDTA) for the equilibration of the beads (three times). Next, the beads were separated with the use of a magnet. Once the solution was cleared the supernatant was removed and the tissue lysate (1mg) was added to the equilibrated beads and incubated for 1 hour at +4°C in rotation. After this step, the sample was cleared with the use of a magnet and the supernatant removed. Next, the beads were with washed twice with washing buffer (10 mM Tris/Cl pH 7.5, 150 mM NaCl, 0.05 % Nonidet™ P40 Substitute, 0.5 mM EDTA). In the last wash, the beads were transfer to a new tube and the supernatant discarded. Finally, the beads were resuspended in *Laemmli* and heated for 5 min. at 95°C. The V5-Trap magnetic agarose beads were magnetized and the complex antibody:antigen was load in SDS- Polyacrylamide gel for western blot detection with the Sp6 antibody (Sp6 rabbit polyclonal antibody (#21234-1-AP) from Proteintech).

4. RESULTS

4. RESULTS

4.1. OBJECTIVE 1: “Implementation of a CRISPR-based platform for genome edition in mouse zygotes”

One objective of my thesis was to implement the genome edition of mouse zygotes based on the CRISPR/Cas9 tool with the goal to establish a platform that would offer this technology to the biomedical community. The availability of an in house, easy and customized way to generate murine models of disease, rewrite the mouse genome or other purposes, can certainly potentiate a large number of studies. With the support of the Servicio de Estabulación y Experimentación Animal (SEEA) at the University of Cantabria, specifically its director, Miguel García and the technician Beatriz Romero, we have successfully accomplished this objective.

To establish this platform, we had to set up the conditions to obtain, modify and transfer to pseudopregnant females the mouse zygotes, including their in vitro culture. Also, we had to select and set-up the specific method to deliver the CRISPR components to the zygote and select the appropriate source to obtain these products.

Regarding the procedures for obtaining, manipulating, and reimplanting the zygotes including conditions for in vitro culture, we collected advice from other well-established platforms, especially the transgenic service in the Centro Nacional de Biotecnología (CNB) and the Centro de Biología Molecular Severo Ochoa (CBMSO) directed by Belén Pintado (<https://www.cnb.csic.es/index.php/es/investigacion/servicios-cientificos/transgenesis>). Furthermore, my training and professional experience as an embryologist helped me to set up the culture conditions successfully and quickly. We decided to follow the protocol “In Vitro Maturation and In Vitro Fertilization of Mouse Oocytes and Preimplantation Embryo Culture” (Kidder 2014) (see M&M 3.7). We considered that having the best culture conditions was essential to avoid any embryo damage that could compromise the viability of the edited embryos even after short culture periods. To assess embryo viability under the selected conditions (Kidder 2014), we decided to culture the embryos from 1 cell stage to blastocyst stage. Under these conditions, 100% of the zygotes developed to blastocyst stage. Therefore, the zygotes collected from each female were cultured in drops of KSOM covered with paraffin oil in

a humidified incubator that preserve them in optimal conditions until subjected to CRISPR.

The CRISPR/Cas9 components can be delivered to the cells mainly in two ways: microinjection or electroporation. We selected the electroporation procedure because, in contrast to microinjection, it does not require high skills and has similar efficiencies in genome editing (Kaneko 2017).

Once we decided to use the electroporation, we selected the NEPA 21 electroporator (from NEPA GENE) because it has the great advantage of permitting the electroporation of the zygote without weakening of the zona pellucida, therefore reducing embryo damage (Kaneko and Mashimo 2015). This device is reported as the one that better preserves the viability of the embryo after electroporation showing high transfection efficiency and high viability according to its specifications. In addition, NEPA 21 electroporator does not require any specific buffer for embryo electroporation. The RNP complex, diluted in Opti-MEM (M&M 3.4), is loaded directly into the chamber and the impedance adjusted according to the manufacturer recommendation. After that, the embryos are directly placed within the RNP, between the electrodes, and electroporated after adjusting the impedance again (See M&M 3.8). We have strictly followed the procedure described in the IDT protocol “Ribonucleoprotein delivery using the Alt-R® CRISPR-Cas9 System and the NEPA21 Electroporator” (https://sfvideo.blob.core.windows.net/sitefinity/docs/default-source/user-submitted-method/crispr-cas9-rnp-delivery-mouse-zygote-electroporation-nepagene.pdf?sfvrsn=4b980e07_14).

IDT was selected as provider for the CRISPR products because, as mentioned above, they had a specific protocol for zygote electroporation with the NEPA 21 electroporator. Besides the high-quality of its genomics reagents, IDT also to purchase the RNP components separately. The RNP complex is composed of the tracrRNA, a universal oligo that forms an RNA duplex with the crRNA specific for the targeted region, and subsequently is combined with the Cas9 nuclease. Therefore, by varying only the crRNA we can assemble different RNP complexes to target different sites in the genome. Also, the existence of well-established protocols for the validation and use of the RNP complexes was additional support for the selection of IDT (see M&M 3.4 and 3.6).

According to the IDT protocol, once all the zygotes were collected, between 20 and 25 embryos were transferred to the electrode containing a drop of Opti-MEM containing the RNP and electroporated, while the rest of the collected embryos were maintained in the incubator for the next round.

After electroporation, the embryos were transferred to pseudopregnant females. Different times of embryo transfer after electroporation were tested. The uterine environment becomes receptive to implantation only after mating, so we mated the female mice with vasectomized males to produce pseudopregnant females (See M&M 3.9). The vaginal plug detection is defined as day 1 of pseudopregnancy. Initially, embryos were cultured for 1 day in the incubator and then, only those that had progressed to the 2-cell stage were considered viable and transferred to pseudogestational females in the day 1 of pseudopregnancy, following the protocol previously established in our animal facility for mouse embryo transfer. However, following this protocol, the rates of mice born from electroporated embryos were lower than expected. To optimize the protocol we synchronized the developmental stage of the embryos to be transferred with the pregnancy day of the pseudopregnant mice (Deb et al. 2006). For this, we cultured the embryos only for a few hours after electroporation, before transferring them at 1 cell stage into the oviduct of pseudopregnant female on day 1 of pregnancy. Following this protocol, the rates of mice born from electroporated embryos notably increased and therefore, it was adopted as the standard protocol.

Another final issue that we considered was the mouse strain. We started using C57BL/6J mouse embryos, but the number of mice born after the manipulations was low. In view of the results of some subsequent works, in which successful editing in C57BL/6J zygotes using CRISPR/Cas9 electroporation was reported (Alghadban et al. 2020), it is possible that the cause of the low number of born mice was our initial inexperience. Despite that, we decided to work with a hybrid genetic background strain (75% C57BL/6J and 25% CBA), since this mixed background has been shown to improve postnatal survival at least in ES cells derived animals (Eggan et al. 2001).

To accomplish the first objective of this thesis we decided to generate previously published animal models. We found suitable choosing previously characterized models for the evaluation and characterization of the procedure, as the phenotype obtained in the modified animals could be directly verified.

According to the second objective of this dissertation we have generated several animal models for the study of the SHFM. In addition, we have also generated additional animal models in the context of other projects currently in the lab all of them directed to study limb development:

- a. A *Jag2* knock-out (KO) model by the generation of a frameshift mutation in an exon of *Jag2* (*Jag2^{emMar}*)
- b. A double KO model by precisely deleting the two nearby genes *Dlx5* and *Dlx6* (*Dlx5/6^{emMar}*) using two crRNAs for the generation of a double KO. In the process of generating this model, we also obtained an animal carrying the allele with the inversion of the fragment between the two crRNAs (*InvDlx5/Dlx6*).
- c. The deletion of two regulatory regions by removing two fragments of 2.8 (*DelLARM1^{emMar}*) and 5.3Kb (*DelLARM2^{emMar}*).
- d. Two knock-in (KI) models by the insertion of a tag sequence (V5) before the stop codon of the desired gene (*Sp6:V5^{emMar}* and *Hoxa13:V5^{emMar}*).

This first general objective has been totally accomplished as demonstrated by the successful generation of several animal models described in the second objective of this work. This first objective resulted in the establishment of a genome editing platform that offers the scientific community the possibility of generating animal models of biomedical interest in an efficient, rapid, and accessible manner. The service is operative and has reached 100% efficiency in some of the latest models generated (<https://web.unican.es/unidades/scti/servicio-de-estabulaci%C3%B3n-y-experimentaci%C3%B3n-animal>).

4.2. OBJECTIVE 2: “To generate animal models by mouse zygote electroporation with CRISPR/CAS9 system for the study of split hand-foot malformation (SHFM)”

4.2.1. Loss of function of *Jag2*

Jag2 is a ligand of Notch that is expressed in the limb ectoderm where it controls AER morphology. *Jag2* KO animals die perinatally due to abnormal craniofacial development and are characterized by develop an hyperplastic AER and syndactylous limbs (Jiang et al. 1998). The syndactyly phenotype commonly affects both fore and hindlimbs involving soft tissue fusions of digits 2-3-4. Sometimes, the feet phenotype is more severe with primary chondrogenic or secondary osseous fusions (Jiang et al. 1998).

Both the AER and the digit phenotypes of *Jag2* KO mice (Jiang et al. 1998) are reminiscent of those displayed by *Sp6* mutants (Talamillo et al. 2010). The *Sp6* KO exhibits variable penetrance and expressivity with defects in AER maturation that leads to limb buds with altered shape. Usually, there is a soft-tissue fusion in forelimbs involving digits 2-3 and sometimes digit 4, and osseous fusion of digits 3-4 in hindlimbs (Talamillo et al. 2010). Given the similarity of the *Sp6* and *Jag2* phenotypes and given that similar phenotypes caused by different genes may indicate that these genes work in the same functional module, we decided to investigate the genetic interaction between *Jag2* and *Sp6*. To this end, we decided to generate the *Jag2* KO by CRISPR/Cas9 electroporation of zygotes. Based on the previously published deletion of 5Kb region encompassing the Delta Serrate Lag-2 (DSL) domain and half of the first EGF repeat of that generated a null allele of the *Jag2* gene (Jiang et al. 1998), we decided to disrupt the open reading frame of *Jag2* by targeting the DSL domain.

crRNA_*Jag2* selection

The target region, the *Jag2* DSL domain, is encoded in exon 4 by 186 nucleotides corresponding to aa 178-240 (Fig. 15). For the selection of the crRNA we compared the crRNA candidates from different web tools (see M&M 3.2). Finally, the crRNA selected was: `tgatcaacccccgaggaccgc` (chr12:112,884,047-112,884,066) named crRNA_*Jag2* because it was present in all three web tools used (CHOP-CHOP, Breaking-Cas and CRISPR-Design) that had the highest score and the lower off-targets with the lowest scores.



Figure 15: Genomic structure of *Jag2* obtained from the UCSC genome browser. Schematic representation of the targeted genomic region indicating the position of the selected crRNA_*Jag2*. *Jag2* is encoded by 26 exons represented in blue. The targeted region corresponds to the DSL domain encoded in exon 4 and marked by discontinuous red line and scissors.

In vitro validation of the crRNA_*Jag2*

The selected crRNA must be validated before being used in mouse zygotes. We followed the “Alt-R CRISPR-Cas9 system: *In vitro* cleavage of target DNA with ribonucleoprotein complex” protocol from IDT DNA (See M&M 3.6), that relies on PCR amplification of the targeted genomic region for subsequent cleavage by incubation with the RNP *in vitro*.

For this, we PCR amplified a 1193 bp fragment containing the crRNA_*Jag2* targeted region using genomic DNA as template. Primers were designed so that the amplified PCR product (primers: *Jag2*-F-Fwd and *Jag2*-F-Rev; See M&M 3.6) using genomic DNA as template, would give two bands of different sizes upon cleavage with the Cas9, enabling for rapid verification by agarose gel electrophoresis. Following purification of the amplified product, the DNA was incubated in presence of the RNP complex (crRNA_*Jag2*:tracrRNA:Cas9) (Fig. 16, lane B).

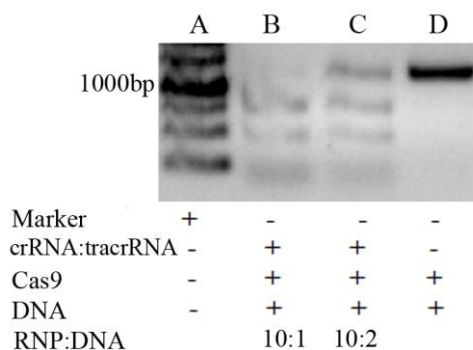


Figure 16: Successful *in vitro* digestion of the crRNA_*Jag2*. Gel electrophoresis image showing cleavage of the *Jag2* PCR amplified product of the DSL domain upon incubation with the crRNA_*Jag2*. Lane A: Marker. Lane B: Digestion of target sequence in two fragments of expected sizes, 733bp and 460bp, using a 10:1 molar ratio of RNP:DNA substrate. Lane C: Incomplete digestion using a 10:2 molar ratio of RNP:DNA substrate. Lane D: Target sequence (1193bp) incubated with Cas9 alone.

Two molar ratios were tested, 10:1 and 10:2 (RNP:DNA). The correct cleavage of the target sequence by the RNP was confirmed by agarose gel electrophoresis. Incubation of the PCR amplified product with the RNP lead to the appearance of 2 bands of the expected sizes (733bp and 460 bp). While the 10:1 molar ratio resulted in a complete digestion, the 10:2 molar ratio showed only a partial digestion (Fig. 16, lane C). As control we incubated the DNA with the Cas9 endonuclease alone, showing that it was not able to cut the target sequence in the absence of the crRNA (Fig. 16, lane D).

Generation of the *Jag2* KO model by zygote electroporation

We performed 6 electroporation rounds with the RNP for *Jag2*. 181 zygotes were electroporated and transferred to 8 pseudopregnant mice. We had 6 deliveries with a total of 16 mice born. Three of the 16 mice born carried a genomic modification at the targeted site (19 % efficiency).

Genotyping strategy of F0 animals, analysis of the offspring and founder selection

The genotyping strategy consisted in the PCR amplification of the crRNA targeted genomic DNA (obtained from tail biopsies) using primers flanking the targeted region. We designed a pair of primers flanking the DSB, *Jag2*-Fwd-G and *Jag2*-Rev-G (See M&M 3.10), that amplified a region of 662bp (Fig. 17).

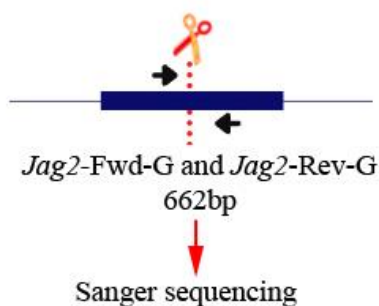


Figure 17: Genotyping strategy of *Jag2* KO model. Schematic representation of the 4th exon of *Jag2* showing the position of the primers relative to the DSB indicated by the scissors. The PCR product obtained after amplification of the target region is analysed by Sanger sequencing.

The size and sequence were confirmed by agarose gel electrophoresis and subsequent Sanger sequencing. It is important to keep in mind that there is a common feature to all models generated by CRISPR/Cas9 and is that the size of the PCR amplified product can differ from the expected size because of possible INDELS

generated by the NHEJ. Therefore, the analysis of the targeted genomic region of the 16 mice born after being electroporated.

The F0 mouse #1240, had a heterozygous deletion of 3 nucleotides at the targeted site that corresponded to aa 177 (Arg) located within the DSL domain (chr12:112,920,427-112,920,429) (mutant allele 1). The PCR product obtained from the amplification of the target region was cloned using the pGEM-T easy vector and the edited allele with the deletion of the 3 nucleotides verified by Sanger sequencing. This mutation did not result in a frameshift mutation. Accordingly, offspring from #1240 homozygous for this mutation and generated by mating heterozygous mice from the first generation (N1), were phenotypically indistinguishable from WT mice (n=4). Therefore, this line was discarded as the deletion of the aa 177(Arg) did not have an overt phenotype (Fig. 18).

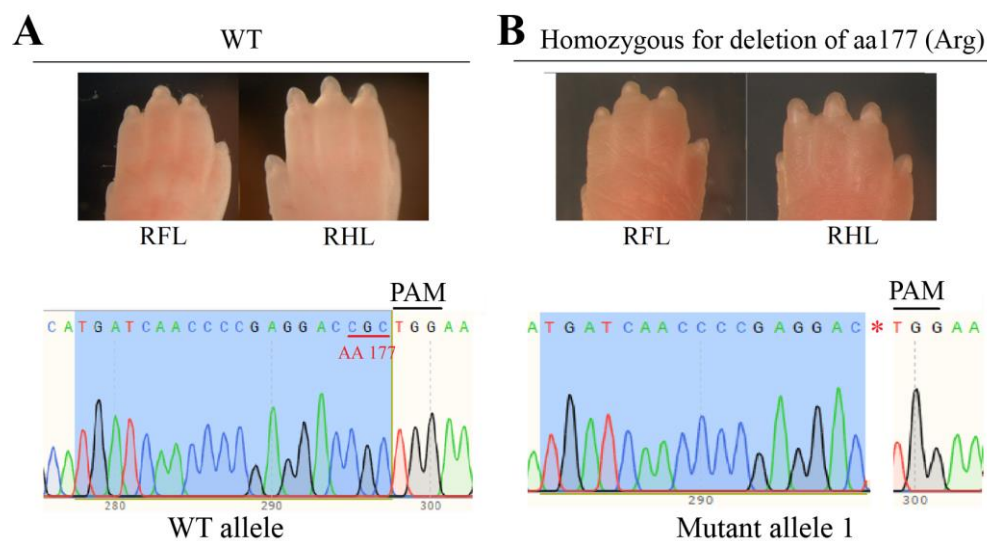


Figure 18: Deletion of aa 177 (Arg) of *Jag2* leads to a silent mutation with no phenotype. **A.** Dorsal view of the right forelimb (left) and right hindlimb (right) autopods of a WT animal. Below, corresponding Sanger sequencing electropherogram of the area targeted by crRNA_ *Jag2*. **B.** Dorsal view of the right forelimb (left) and right hindlimb (right) autopods of a mouse carrying the deletion of aa 177 lacking the syndactyly phenotype characteristic of the *Jag2* KO. Below the corresponding Sanger sequencing electropherogram showing the absence of the CGC trinucleotide coding for the aa 177. RFL, right forelimb; RHL, right hindlimb.

Cloning and further Sanger sequencing analysis of the F0 #1260 identified a single nucleotide deletion (C) at position chr12:112,920,428, that was inside the codon for the aa 177 (Arg) of Jag2 altering the open reading frame of the gene. Since it is a single nucleotide deletion further establishment of the line with this animal was discarded because genotyping of the animals will require Sanger sequencing and will make the maintenance of the line more laborious and expensive compared to PCR genotyping.

Finally, the Sanger sequencing revealed that the F0 #1257 was mosaic. So, we used the pGEM-T easy vector to clone the PCR product obtained from the amplification of the target region and sent the clones for Sanger sequencing. This revealed three different alleles in the genomic region targeted by the crRNA_*Jag2* (Fig. 19).

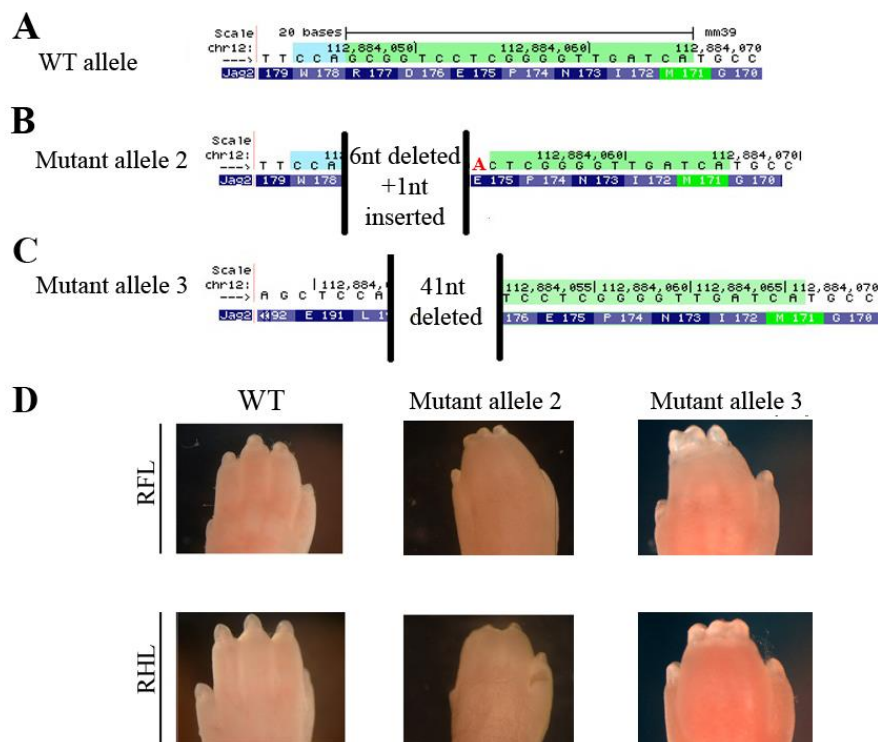


Figure 19: Sequence and phenotype of the different *Jag2* alleles of F0 #1257. A-C. Representation of the three different alleles present in this animal. The WT sequence, obtained from the UCSC Genome browser, is shown on top with the corresponding aa below. The PAM sequences are highlighted in blue and the crRNA in green. **A.** WT Allele. **B.** Mutant allele 2: Deletion of 6nt and insertion of 1nt (A, written in red). **C.** Mutant allele 3: 41nt deletion. **D.** Dorsal views of the newborn autopod of the different alleles in homozygosis. Both mutant alleles (2 and 3) reproduce the phenotype of the *Jag2* mutant and display soft tissue syndactyly of 2-4.

One of the sequences obtained corresponded to the WT allele (Fig. 19A), another sequence included the deletion of 6 nucleotides (CGCTGG) and the insertion of 1 nucleotide (A) (mutant allele 2) (Fig. 19B) and the third sequence carried the deletion of 41 nucleotides (CCGCTGGAAGAGCCTGCACTTCAGCGGCCACGTGGCACACC) (mutant allele 3) (Fig. 19C). The F0 #1257 was the mouse selected to be the founder of the line because the two mutant alleles (#2 and #3) in homozygosity caused the *Jag2* phenotype (Fig. 19D).

Establishment of the *Jag2* KO mouse line

Following the Jackson laboratory protocol (See in M&M 3.15) we established our lines by backcrossing the selected F0 mouse with C57BL/6J WT. First, we established the line from the #1257 mutant allele 2. The difference between the WT and mutant PCR amplified products was only of 5nt which made difficult to discriminate between them by regular PCR genotyping strategy. Therefore, we used the heteroduplex analysis for genotyping (Bhattacharya and Van Meir 2019)

Heteroduplex are formed by the hybridization between DNA sequences that contain mismatches and can be detected in an agarose gel because they migrate slower than their corresponding homoduplex. According to the results obtained with this method in the genotyping of CRISPR edited mice and the aim of obtaining a better resolution we decided to design new primers that amplified a smaller fragment (*Jag2-Fwd* and *Jag2-Rev*, 201bp) (See in M&M 3.12) (Bhattacharya and Van Meir 2019). We distinguished products from homozygous origin (+/+ or -/-), from heterozygous (+/-), because the first gave a single band while the later gave two bands due to the formation of heteroduplexes between the WT and the mutant allele (Fig. 20A). Next, to discriminate between the homozygous samples (mutant or WT), 5µl of the remaining PCR from the first step were mixed with 5µl of PCR product amplified from WT DNA as template, followed by denaturation at 95°C for 5 min. and subsequent incubation at 72°C for 5 min. for reannealing (Fig. 20B). Heteroduplexes formation was visualized in a 4% agarose gel in TAE running at 100V for 40-45min. The homozygous mutant resulted in the appearance of two bands where the lower band corresponded to the homoduplexes between copies of the mutant and WT alleles while the upper band corresponded to the heteroduplex formed between the WT and mutant alleles. In contrast, the WT showed up as a single band (Fig. 20C).

Finally, the mutant allele 3 of the F0 #1257 lacking 41 nucleotides (CCGCTGGAAGAGCCTGCACTTCAGCGGCCACGTGGCACACC) was easier to genotype by conventional PCR with the primers *Jag2-Fwd* and *Jag2-Rev* and agarose gel electrophoresis and also displayed the previously described *Jag2* KO phenotype (Jiang et al. 1998) (Fig. 20D). Therefore, we decided to establish the line with this allele, *Jag2^{emMar}*.

The mouse lines generated in this project, have been named following the guideline for nomenclature of genes, genetic markers, alleles, and mutations in mice by the international committee on Standardized Genetic Nomenclature for Mice. Basically, this nomenclature includes the symbol of the edited gene with the abbreviation em (endonuclease-mediate mutation), and the initials of the lab where the line was generated: Mar for Marian Ros.

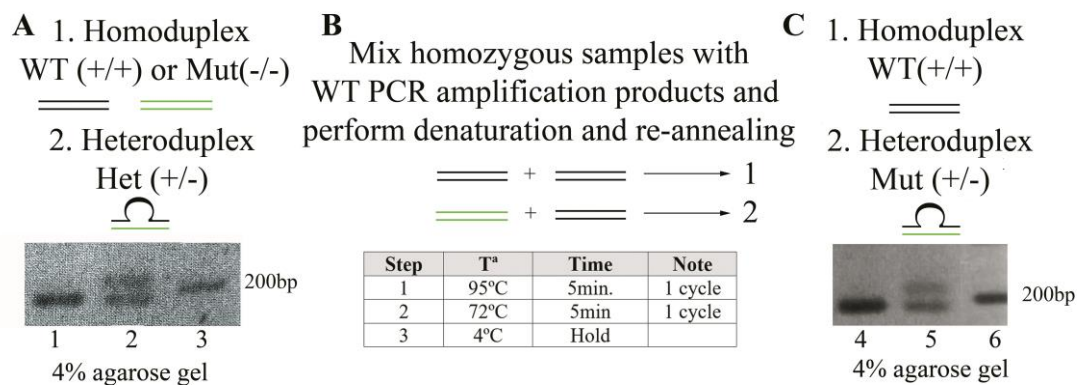


Figure 20: Resolving five nucleotide difference by heteroduplex analysis for the establishment of the *Jag2* KO line using the mutant allele 2 from the F0 #1257. Schematic representation of the heteroduplex analysis procedure. **A.** after conventional PCR, the heterozygous samples are visualized in a 4% agarose gel as two bands (lane 2), while products of WT and mutant homozygous origin appear as a single band of ~200bp (lane 1). Lane 3: marker **B.** PCR products from samples giving a single band in the first step are mixed with PCR amplified WT DNA, denatured and re-annealed. **C.** Finally, the products are visualized in a 4% agarose gel in TAE where the mutant homozygous samples appeared as two band (lane 5) due to the heteroduplex formation with the WT allele and the WT products appear as a single band (lane 4). Lane 6: marker.

Phenotypic characterization of *Jag2^{emMar}* mouse line

We initially characterized the *Jag2^{emMar}* mutants by gross inspection and skeletal staining (alcian blue and alizarin red stain). *Jag2^{emMar}* mice exhibited soft tissue syndactyly of digits 2 to 4 similar to that previously reported for the *Jag2* mutant (Jiang et al. 1998) (Fig. 21A). It should be mentioned however that, while a considerable proportion of *Jag2* mutants (5 out of 13; (Jiang et al. 1998)) displayed primary chondrogenic or secondary osseous fusions of the distal phalanges, this was not observed in any of the 6 *Jag2^{emMar}* mutant that we analyzed (Fig. 21A).

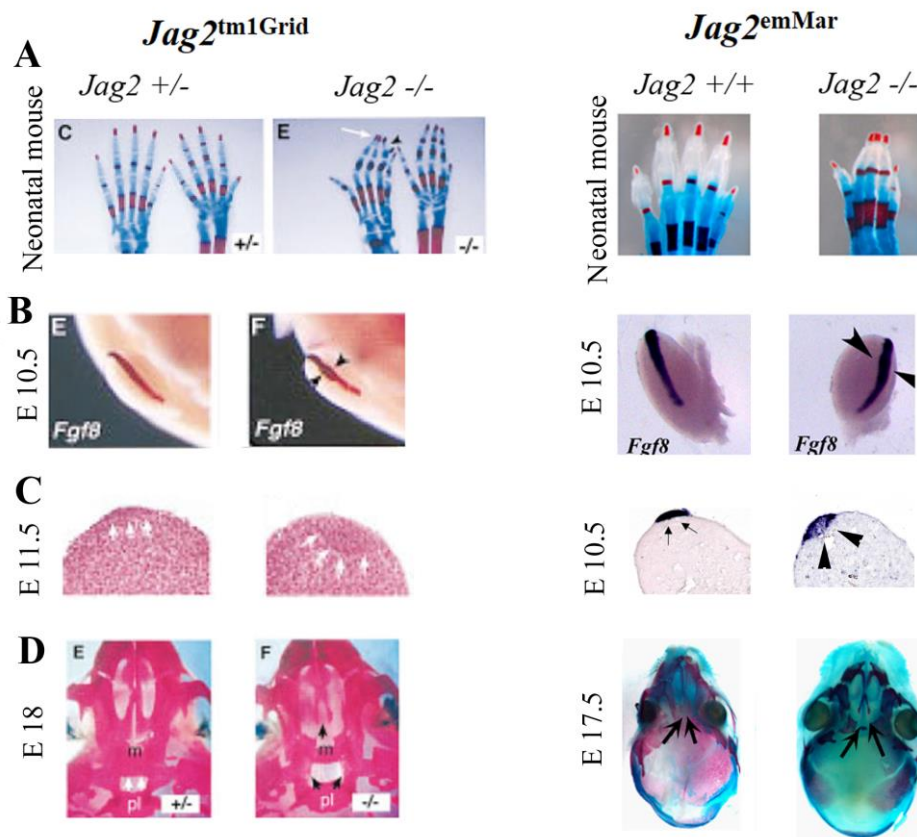


Figure 21: *Jag2^{tm1Grid}* (left) from (Jiang et al. 1998) and *Jag2^{emMar}* (right) comparative analysis. **A.** Neonatal mice skeletal staining. Syndactyly is observed in both mutants with complete soft-tissue fusion of digits 2-3-4. **B.** *Fgf8* WHISH. Black arrowheads point the *Fgf8* expression expansion in *Jag2* KO mice. **C.** Histological analysis of FLs in the left and *Fgf8* ISH in sections on the right. White arrows in *Jag2^{tm1Grid}* mutant and black arrows in our mutant show the basal limit of the AER, revealing the protrusion into the mesenchyme in the mutant limb. **D.** Ventral view of stained skeletal preparations of the head. The maxillary shelves (m) are more lateral in *Jag2* mutants (black arrowheads).

In addition, the *Jag2* mutant is characterized by the development of a hyperplastic AER that protrudes into the mesoderm with subsequent expansion of *Fgf8* expression. Therefore, we next analyzed the expression of *Fgf8* by whole mount in situ hybridization (WMISH) and confirmed the presence of a hyperplastic AER in our mutants (Fig. 21B). Further histological analysis confirmed the protrusion of the AER into the mesoderm (Fig. 21C). The *Jag2* mutants die at birth with cleft palate of the secondary palate. The normal palate development involves first the elevation and grow toward the midline of the palatal shelves (palatine and maxillary shelves), and then their fusion, which ossifies and forms the roof of the oral cavity. *Jag2* mutant have unelevated palatal shelves fused with the tongue (Jiang et al. 1998). As expected, the same phenotype was observed in the *Jag2*^{emMar} (Fig. 21D).

Therefore, we concluded that the *Jag2*^{emMar} KO model we have generated by CRISPR/Cas9 genome edition through direct zygote electroporation is a complete loss of function that faithfully recapitulates the previously published loss of function phenotype (Jiang et al. 1998).

Epistatic relationship between *Sp6* and *Jag2*

Sp6 and *Jag2* mutants display a similar limb phenotype and have overlapping expression domains in the limb. The expression of *Jag2* and *Sp6* in the developing limb of WT mice has been previously described (Sidow et al. 1997; Jiang et al. 1998; Talamillo et al. 2010). Briefly, *Jag2* transcript is reported in the AER and surface ectoderm (Shawber et al. 1996). *Sp6* expression in the ectoderm evolves from occurring in the whole ectoderm (E9.5), to only in the AER and ventral ectoderm (E10) and finally restricted to the AER (E10.5). At later stages *Sp6* expression persists over the tips of the digits (E15.5) (Talamillo et al. 2010). Similar phenotypes are more likely to share a genetic etiology, with both causative genes collaborating in the same network. Therefore, we decided to study a possible genetic interaction between *Sp6* and *Jag2*.

First, to determine whether the expression of *Jag2* is regulated by *Sp6* or vice versa, we analyzed the expression of each of these genes in mice homozygous for the absence of the other. We found that the expression of *Jag2* was not altered in *Sp6* null limbs shown in E11 limb buds (Fig. 22A). Similarly, *Sp6* expression was not affected in

Jag2 mutants, as shown for E11 in Fig. 22B. Thus, no effect of the deficiency of each gene was detected in the expression of the other.

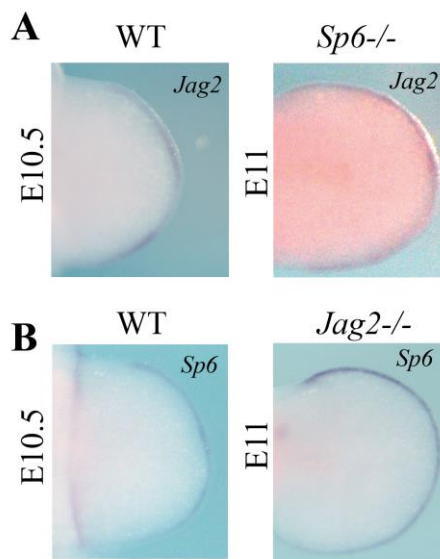


Figure 22: Normal *Jag2* expression in absence of *Sp6* and normal *Sp6* expression in *Jag2* null embryos. A. Ventral view of a WMISH for *Jag2* in WT (left) and *Sp6*^{-/-} (right) limb buds showing the correct *Jag2* expression in the *Sp6* mutant. **B.** Ventral view of a WMISH for *Sp6* in WT (left) and *Jag2*^{-/-} (right) limb buds hybridized *Sp6* showing normal *Sp6* expression in *Jag2* mutant.

Next, we checked whether the combined deficiency of *Jag2* and *Sp6* resulted in novel phenotypes by analyzing the double mutant *Jag2*^{-/-};*Sp6*^{-/-} allelic series resulting from crossing double heterozygous. All classes of progeny were recovered at expected mendelian rates.

The AER phenotype and the syndactylous limbs present in both single mutants prompted us to analyze the possible interaction between *Sp6* and *Jag2* during limb bud development focusing on the molecular analysis of *Fgf8* expression in the AER at E10.5 (Fig. 23) and skeletal staining at birth. *Fgf8* is considered the best AER marker (Lewandoski et al. 2000; Moon and Capecchi 2000). The double heterozygous *Jag2*^{+/-};*Sp6*^{+/-} were normal (Fig. 23D-D'), they did not present any alteration in *Fgf8* expression at E10.5, neither in the skeletal pattern at E17.5 (Fig. 24D). The same was true for animals bearing a single functional copy of *Sp6* in the absence of *Jag2* (*Jag2*^{-/-};*Sp6*^{+/-}) (Fig. 23B-B' and Fig. 23 E-E'). The *Sp6* mutant with one copy of *Jag2* showed the same phenotype as *Sp6* but given the variable penetrance of *Sp6* a high number of embryos would be required to completely confirm this results. In contrast, double *Jag2*^{-/-};*Sp6*^{-/-} homozygous presented a more pronounced double ridge phenotype in comparison to that previously described in *Sp6* mutants (Talamillo et al. 2010). Additionally, the skeletal staining showed a more severe syndactyly phenotype in the hindlimbs of double homozygous that

involved the fusion of the three phalanx elements of digits 3-4 with digit 2 lost from the metatarsal (2 out of 2; Fig. 24F). This phenotype was never seen in either single mutant (Fig. 24F). In contrast, the forelimbs of the double homozygous mutants displayed a syndactyly phenotype like that of *Sp6* or *Jag2* single mutants. Thus, the new phenotype observed in the hindlimb of double homozygous indicate synergic interaction between *Jag2* and *Sp6*.

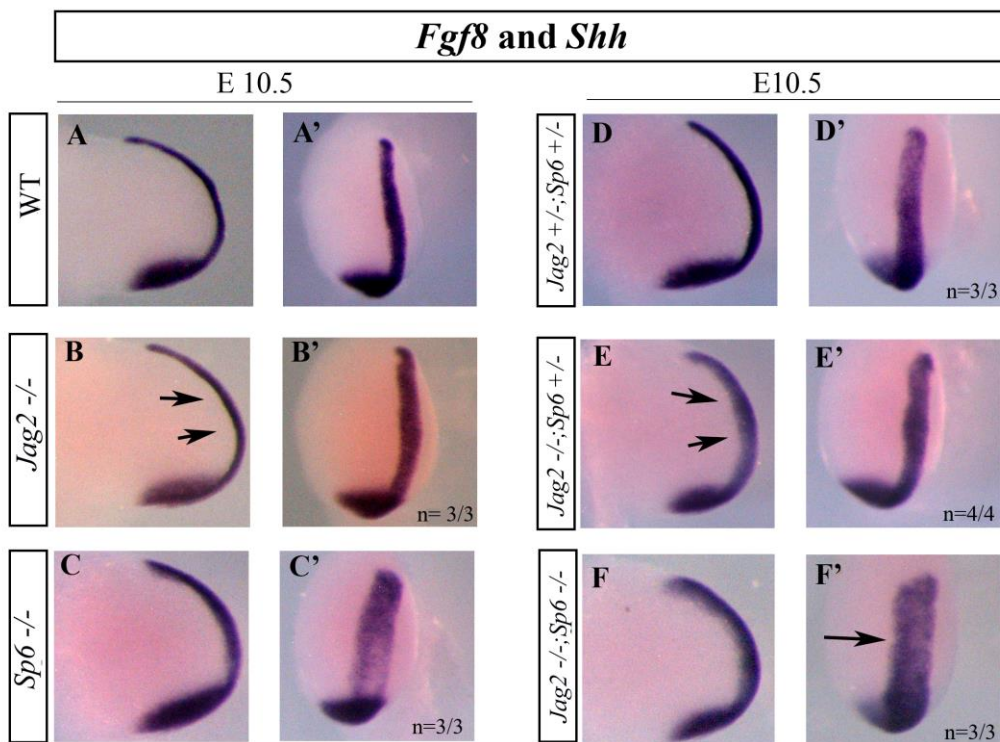


Figure 23: analysis of the AER in *Jag2*^{-/-}; *Sp6*^{-/-} double mutant. Dorsal (left, A-F) and distal (right, A'-F') views of E10.5 mouse forelimbs (FLs) of the genotypes indicated hybridized for *Fgf8* and *Shh* (A-F). *Fgf8* expression is restricted to the AER and *Shh* expression to the ZPA. Note the increase in the thickening of the *Fgf8* expressing area with the reduction of *Jag2* and *Sp6* allelic dosage. Black arrows point to the expansion of *Fgf8* expression. Representative examples are shown with the number of embryos displaying the phenotype over the total number of embryos analyzed for each genotype indicated at the bottom (n=X).

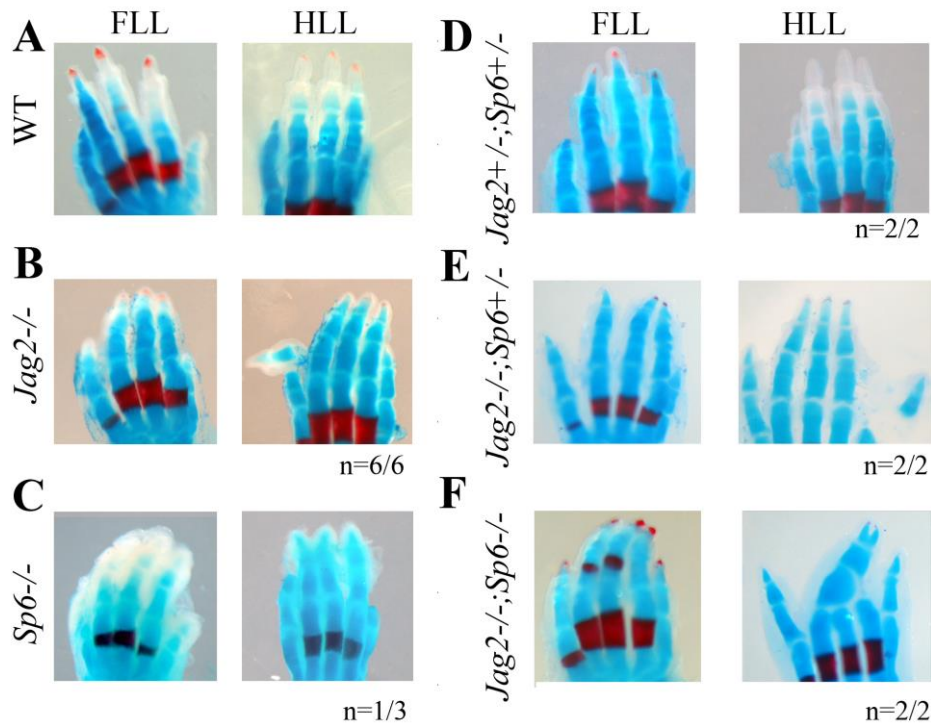


Figure 24: Skeletal staining of *Jag2* and *Sp6* double mutants. All the embryos are at E 17.5. **A.** WT left forelimb (FLL) on the left and left hindlimb (HLL) on the right. **B.** FLL and HLL of *Jag2* mutant with syndactyly phenotype. **C.** FLL and HLL of *Sp6* mutant with phenotype only on the left side. **D.** Double heterozygous mutant without any phenotype. **E.** *Jag2* mutant with only one functional copy of *Sp6*, with the same phenotype as single mutant of *Jag2*. **F.** FLR and HLR of double mutant embryos with a severe fusion of the bones reveals in the HLs. The number of embryos found with this phenotype are pointed with n (n=X).

4.2.2 Double deletion of *Dlx5* and *Dlx6*.

SHFM type 1 maps to chromosome 7q21q22 to an interval including the candidate genes *DSS1*, *DLX5* and *DLX6* with haploinsufficiency considered as the underlying mechanism (Crackower et al. 1996). Mutations in the intragenic region of *DLX5* (Shamseldin et al. 2011; Wang et al. 2014) and *DLX6* (Ullah et al. 2017) have also been reported as causative of SHFM1. However, it is necessary to disrupt both genes to obtain a SHFM phenotype in mice (Merlo et al. 2002; Robledo et al. 2002).

The aim of this objective is the generation of an animal model for the study of SHFM1 by zygote electroporation with CRISPR/Cas9 system. We decided to base our design on one of the previously published *Dlx6* and *Dlx5* double knock-out (DKO) animal model (Robledo et al., 2002). This *Dlx5/6* DKO was generated by gene targeting of ES cells and subsequent injection of ES cells carrying the targeted deletion into mouse blastocysts for the generation of chimeric animals. The targeted allele lacks a genomic region of ~11 kb containing the *Dlx5* and *Dlx6* homeodomains and associated C-terminal regions. In addition, an *ires-LacZ-neo* cassette was inserted under the transcriptional control of *Dlx6* 5' regulatory elements. Because the information on the exact point of the deletion is not clear, for the generation of our model we decided to target the first intron of both genes to remove both homeodomains and the associated C-terminal domains of *Dlx5* and *Dlx6*.

crRNA_*Dlx6* and crRNA_*Dlx5* selection

We have selected two crRNA to target intron 1 of *Dlx6* (crRNA_*Dlx6*) and *Dlx5* (crRNA_*Dlx5*) respectively (Fig. 25).

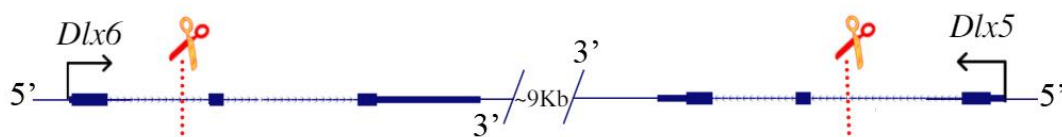


Figure 25: Schematic representation of the genomic region targeted by selected crRNA_*Dlx6* and crRNA_*Dlx5*. Genomic structure of *Dlx6* and *Dlx5* obtained from the UCSC genome browser. The *Dlx6* and *Dlx5* genes are encoded by three exons represented in blue. The target region corresponds to intron 1 of each gene as indicated by the discontinuous red line and scissors.

The selection of the crRNAs was based on the candidate present in all three web tools used that had the highest score and the lower off-targets with the lowest score (See M&M 3.2). The crRNA_*Dlx6* selected was: ggtatagcggggatattacg (chr6:6,864,949-6,864,968, mm:10) and the crRNA_*Dlx5*: tacagcggcaagcggtcggt (chr6:6,880,211-6,880,230, mm:10).

In vitro validation of the crRNA_*Dlx6* and crRNA_*Dlx5*

As mentioned, validation of each guide was performed following the IDT DNA protocol (Fig. 26) (See M&M 3.6).

First, we PCR amplified a 1060bp genomic region around the area targeted by the crRNA_*Dlx6*. The primers used annealed 625bp upstream and 425bp downstream of the crRNA targeted region (*Dlx6*-Fwd and *Dlx6*-Rev). After purification, the amplified product was incubated with the RNP complex (crRNA_*Dlx6*:tracrRNA:Cas9) in a 10:1 molar ratio (RNP:DNA substrate). The generation of the DSB in the target sequence by the crRNA was confirmed by visualization of the two expected fragments of 625bp and 425bp by agarose gel electrophoresis (Fig. 26, lane B). As negative control the incubation was performed in the absence of the crRNA (Fig. 26, lane C).

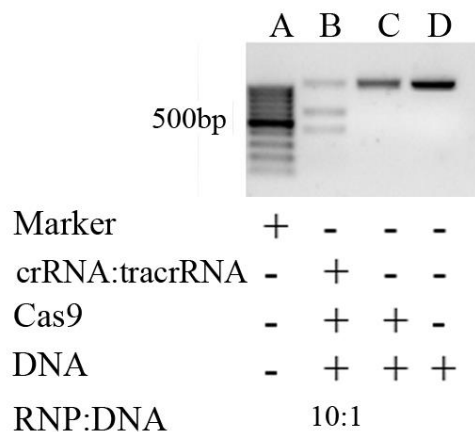


Figure 26: Successful in vitro digestion of the crRNA_*Dlx6*. Gel electrophoresis image showing cleavage of the *Dlx6* PCR amplified product encoding the target domain upon incubation with the crRNA_*Dlx6*. Lane A: Marker. Lane B: Incomplete digestion of template sequence in two fragments of 625bp and 425bp using a 10:1 molar ratio of RNP:DNA substrate. Lane C: Target sequence (1060bp) incubated only with Cas9. Lane D: DNA template.

The same procedure was followed for the validation of the crRNA_*Dlx5*. In this case the PCR amplified genomic region containing the targeted site was of 1047 bp and was amplified with primers *Dlx5*-Fwd and *Dlx5*-Rev (Fig. 27). As expected, two fragments of 649bp and 398bp were obtained after incubation with the RNP (Fig. 27, lane C).

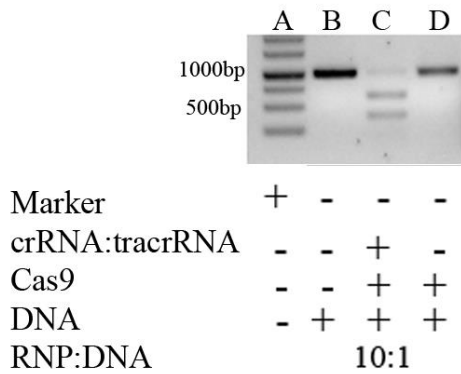


Figure 27: Successful in vitro digestion of the crRNA_ *Dlx5*. Gel electrophoresis image showing cleavage of the *Dlx5* PCR amplified product encoding the target domain upon incubation with the crRNA_ *Dlx5*. Lane A: Marker. Lane B: Target sequence (1047bp) incubated only with the Cas9. Lane C: Expected digestion of target sequence in two fragments of 649bp and 398bp using a 10:1 molar ratio of RNP:DNA substrate. Lane D: DNA template.

The generation of *Dlx5/Dlx6* DKO model by zygote electroporation

Initially, we performed 6 different electroporation rounds with the two RNP complexes at the same time, one formed with the crRNA_ *Dlx6* and the other with the crRNA_ *Dlx5*. 245 zygotes were electroporated and transferred to 12 pseudopregnant mice. We had 9 deliveries with 30 mice born. Twenty-eight mice were weaned of which 3 carried modifications in the desired region corresponding to 10.7 % efficiency of cleavage in at least one of the target sites. Only one of them, the mouse F0 #1248 carried the desired deletion.

Unexpectedly, we had trouble to establish the line from the F0 #1248 because all the offspring which carrying the desired edited allele died perinatally. These results led us to consider the possibility that the heterozygous deletion could be lethal or that might be an off-target effect. Nevertheless, as we had only one mouse F0 with the desired mutation, we decided to perform an additional electroporation with the same RNP complexes to get more mice to study if the problem with the F0 #1248 was an isolated problem or not. Therefore, we performed 2 additional electroporation rounds. 116 zygotes were electroporated and transferred to 6 pseudopregnant mice. We had 6 deliveries with 26 mice born. Twenty-three mice were weaned of which 10 carried modifications in their DNA. The efficiency was of 43.5% this second time.

Genotyping strategy of F0 animals, analysis of the offspring and founder selection

The genotyping strategy for this animal model implied several PCRs. First, we used the *Dlx6*-Fwd and the *Dlx5*-Rev primers to detect the deletion of the desired region

of 16Kb. The expected amplicon would be of 1023bp (Fig. 28B) in the allele with the deletion but 16285bp in the WT allele and therefore not expected to be amplified. Also, each targeted region is analyzed independently.

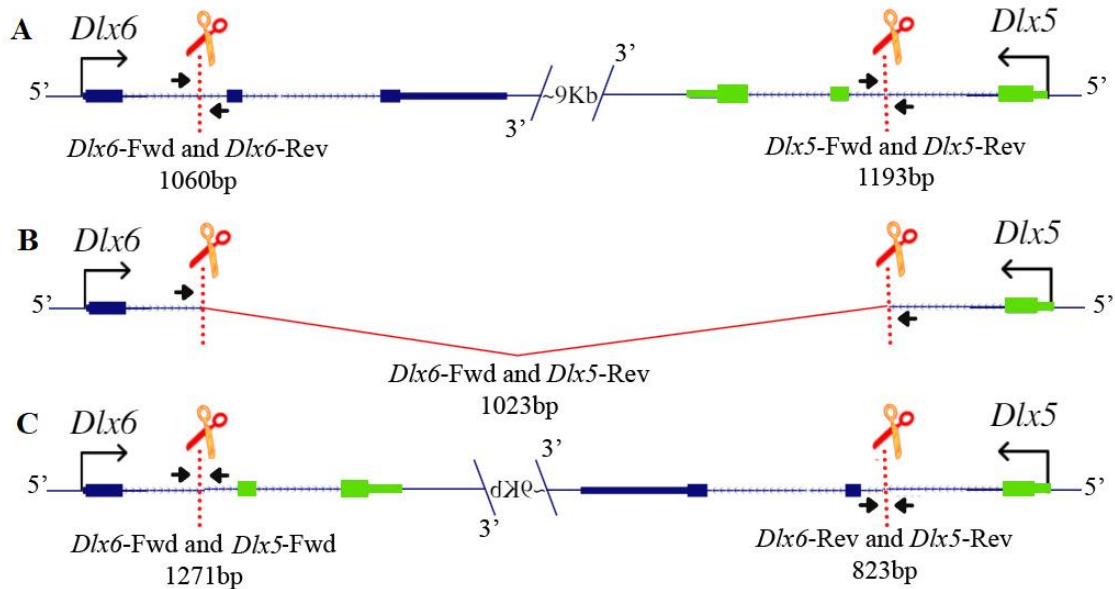


Figure 28: Genotyping strategy of the *Dlx5/6* DKO animal model. This image is a scale-free schematic representation of the *Dlx6* gene, with exons represented in dark blue and the *Dlx5* gene, with exons represented in green, showing the position of the primers (black arrows) used for genotyping the different possible alleles. **A.** WT configuration. Primers (black arrows) flanking each crRNA target site (discontinuous red line and scissors) are indicated with their name and the size of the amplified band. **B.** The allele with the desired deletion (red line) can be detected by the used of the primers *Dlx6*-Fwd and *Dlx5*-Rev, obtaining a fragment of 1023bp. In the absence of deletion, the expected size of the amplicon is too big to be obtained by regular PCR. **C.** Allele with the inverted configuration. If the fragment between both DSB has been inverted, the inversion is detected with both forwards primers or both reverse primers. We used *Dlx6*-Rev- and *Dlx5*-Rev.

The *Dlx6* breakpoint is analyzed by with the *Dlx6*-Fwd and the *Dlx6*-Rev, and the *Dlx5* breakpoint with the *Dlx5*-Fwd and *Dlx5*-Rev (Fig. 28A). Finally, because an inversion of the fragment between both DSB can also be generated, we used the *Dlx6*-Rev and the *Dlx5*-Rev primers to detect it. In the case of an inversion the size of the amplicon would be 823 bp (Fig. 28C). After the PCR analyses, the desired PCR amplified

products were subjected to Sanger sequencing to precisely define the genomic modification.

The analysis of the three edited mice obtained in the first cycle of electroporation showed that only two showed successful crRNA_*Dlx5* cleaved of the targeted site. Because the cut was in intron 1, no alteration is expected even in the case of INDELS, thus these mice were discarded.

F0 #1248, obtained in the first round of electroporation, was mosaic (Fig. 29B). The genotyping analysis showed that it carried a WT allele, according to the PCRs with *Dlx6*-Fwd and *Dlx6*-Rev and *Dlx5*-Fwd and *Dlx5*-Rev primers (Fig. 28A) but also the deleted allele (*Dlx6*-Fwd- and *Dlx5*-Rev) and the inverted allele (*Dlx6*-Rev and *Dlx5*-Rev), respectively (Fig. 28, lanes B and C). The band obtained by PCR with the primers to detect the deletion (*Dlx6*-Fwd- and *Dlx5*-Rev) was shorter than expected indicating that in the NHEJ directed repair of the DSB additional nucleotides were deleted. Analyses of its progeny showed transmission of the three types of alleles it carried: the WT, the inverted allele, and the deleted allele. Therefore, the F0 #1248 was initially selected as the founder of this line.

The analysis of the mice obtained in the second cycles of electroporation, resulted in 10 mice carrying mutations in their genomes.

The F0 #4069 and #4070 animals showed smaller fragments when each target region was amplified by PCR, revealing that after the crRNA cut the NHEJ generates small deletions. Because the DSB are in the introns, no modifications are expected and therefore these mice were discarded.

The F0 #4055 carried the inversion of the fragment in heterozygosity since we were able to amplify both the WT fragments at the *Dlx6* and *Dlx5* DSB and the fragment expected if the inversion occurred (*Dlx6*-Rev and *Dlx5*-Rev).

Other modifications found in the F0 #4050, #4053, #4056, #4059, #4062 and #4065 reflected cuts of the crRNA_*Dlx6* carrying small deletions that included the site for one of the primers as we did not obtain any fragment after the PCR amplification of this region, while *Dlx5* seemed to be intact according to the size of the band amplified. In addition, one of them, the F0 #4050, also showed the expected fragment for the desired

deletion after the use of primers *Dlx6*-Fwd and *Dlx5*-Rev (Fig. 29D). The presence of the deleted allele could indicate that this animal #4050 was heterozygous for the deletion and was eventually selected as founder of the line because no offspring of the initial founder (F0 #1248) with the deleted allele survived.

Finally, according to the PCR results, the F0 #4048 male was heterozygous for the deleted allele because it also carried the WT allele (Fig. 29C). Thus, Sanger sequencing of the band obtained with primers *Dlx6*-Fwd and *Dlx5*-Rev confirmed the presence of the deleted allele. Accordingly, it transmitted to his offspring's the WT allele and the deleted allele. This F0 #4048 was also selected as founder of the line.

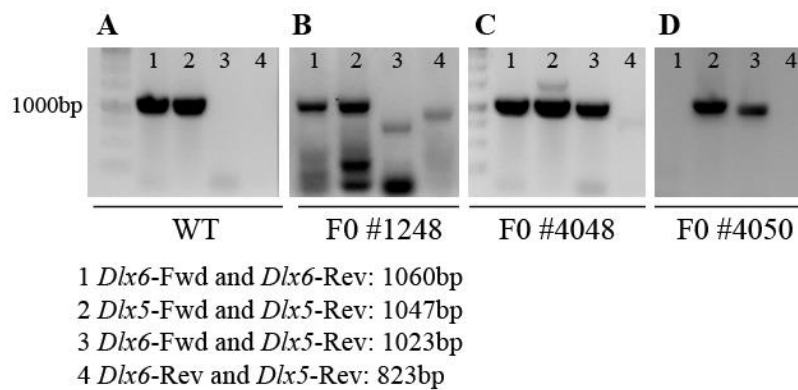


Figure 29: Genotype of the F0 mice carrying at least the deleted allele for *Dlx5/Dlx6* in heterozygosis. The different primers used for all 4 PCR (lanes 1-4) are indicated below the image with the expected fragments pointed. **A.** Results of the PCRs performed with WT mouse DNA. **B.** PCR results performed with the DNA of the mouse F0 #1248 which showed bands in all lanes indicating that it was mosaic. **C.** Results of PCR performed with the DNA of the mouse F0 #4048 which is heterozygous for the deletion, showing the bands corresponding to the WT and deletion alleles. **D.** Results of the PCRs performed with the DNA of the mouse F0 #4050 which did not show any amplified fragment for *Dlx6* and it is heterozygous for the deletion.

Establishment of the *Dlx5/6* DKO mouse line

First, we tried to establish the line from the mouse F0 #1248. Unexpectedly, all offspring bearing the edited allele with the deletion in heterozygosis died perinatally. Out

of the 60 offspring this mouse produced, 18 died perinatally including the 11 that carried the edited allele with the deletion. Thus, 18,3% of the offspring were heterozygous instead of the expected 50% mendelian rate indicating intrauterine lethality. No offspring with the deletion survived.

Then we tried to establish the line from the F0 #4050 which also was heterozygous for the deletion. This female was mated with a WT male (C57BL6/J) but, unfortunately, she did not transmit the edited allele. The PCR analysis of her 21 offspring from 3 deliveries only detected WT alleles.

After that, we tried to establish the line from the F0 #4048 that was a heterozygous male carrying the edited allele with the desired deletion. The analysis of his offspring from crosses with C57BL6/J females produced 45 offspring 12 of them (26.7% instead of 50% expected) inheriting the edited allele but only one of those survived, the others died perinatally. This N1 mouse was a female (**#6700**) that showed reduced fertility generating only 6 offspring in 4 deliveries of which 4 died perinatally. Unfortunately, any of the two mice that survived carried the deleted allele, while 3 out of the 4 that died perinatally had inherited it.

The high number of death offspring from F0 mice #1248 and #4048 carrying the allele with the deleted fragment prompted us to investigate the possibility that off-target effects could explain the lethality. To do so we focused on the analysis of the 3 sequences with the highest scores to be possible off-targets of the two crRNAs, crRNA_*Dlx6* and crRNA_*Dlx5*. We compared the off-target sequences obtained for our crRNAs in the Breaking-Cas, Chop-Chop and IDT platforms, focusing on those that appeared with a high score in the three platforms preferentially if located in the same chromosome as *Dlx5/6*.

This analysis was based on the hypothesis that an off-target lethal in heterozygosis segregated with the *Dlx* locus. Despite our hypothesis, the majority of off-target sequences with high score for the crRNA_*Dlx6* located outside chromosome 6 and therefore we decided to include two of them in our analysis. We designed primers to amplify these regions from DNA of the N1 female (**#6700**), but Sanger sequencing demonstrated no modification in these regions (Fig. 30) ruling out the possibility that the

Finally, we considered performing a more exhaustive analysis of mouse F0 #4048 with state-of-the-art techniques such as the rhAmpSeq™ CRISPR Analysis System from IDT, which is an analysis that allows quick and accurate quantification of CRISPR-Cas edits, but after studying the cost-benefit ratio of the process for the project, we discarded to perform this study.

Despite having obtained 3 live mice carrying the double deletion of *Dlx5* and *Dlx6* with transmission of the edited allele at least to the N1 generation, the line could not be established. Therefore, we decided to continue our investigations on the relationship between the *Dlx* and *Sp* gene families using alternative lines carrying the floxed deletion of *Dlx5* and *Dlx6* (Bellessort et al. 2016).

Analysis of the allele with the sequence between both DSBs inverted

The F0 #1248 bearing the allele with the inversion of the sequence between the two DSBs generated offspring that survived and inherited the inverted mutation at the expected mendelian rate. We asked whether this allele which implies the formation of *Dlx5/Dlx6* chimeric genes, would produce a genotype when in homozygosis.

The inversion in homozygosis did not show any phenotype (Fig. 31A). It is important to consider that the inverted allele implies the generation of two chimeric genes, one formed by exon 1 of *Dlx6* and exons 2 and 3 of *Dlx5* and the other, by exon 1 of *Dlx5* and exons 2 and 3 of *Dlx6* (Fig. 31B). Since the *Dlx6* and *Dlx5* genes show a convergent organization, the inversion of the fragment between the two DSBs positions the inverted region in the correct transcriptional direction corresponding to new position. The analysis of homozygous embryos was performed by PCR and only showed the expected fragment amplified with the used of *Dlx6*-Rev and *Dlx5*-Rev (Fig. 31C). Gross analysis of the homozygous mice showed a WT phenotype that could be understood if the chimeric proteins formed are fully functional or at least hypomorph proteins. The *Dlx5* and *Dlx6* genes share exon-intron structure and there is evidence showing their functional equivalence (Robledo et al. 2002; Bendall 2016).

Because the inverted allele had no phenotypic consequences, we did not establish the line.

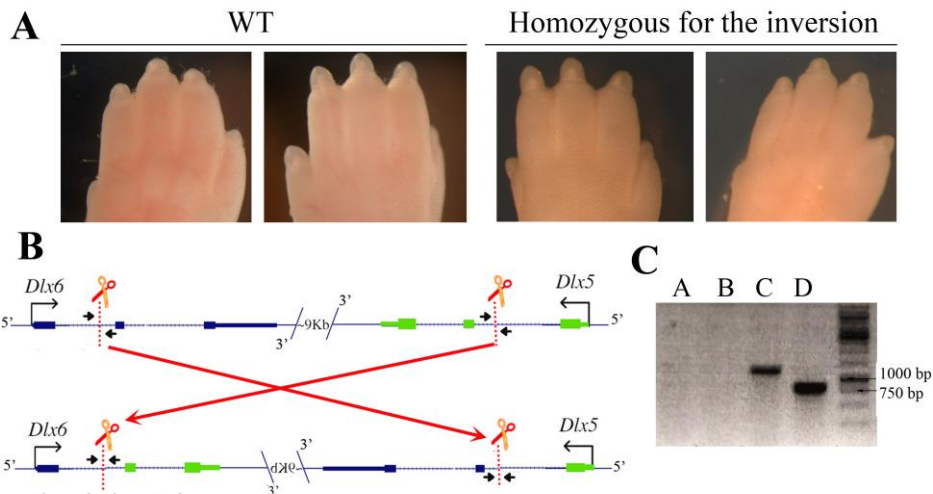


Figure 31: Analysis of a homozygous mouse for the inversion of the fragment between the two DSBs. **A.** The homozygous mouse for the inversion displays a WT phenotype. Dorsal views of FLs and HLs autopods of mouse homozygous for the inversion (right) and WT (left). **B.** Scheme of the inverted allele. **C.** Gel electrophoresis image showing in lanes C and D the bands of the expected size corresponding to the inversion obtained by the PCR amplification with the primers *Dlx6*-Fwd and *Dlx5*-Fwd (1271bp) and *Dlx6*-Rev and *Dlx5*-Rev (823 bp) respectively. PCR with the combinations of primers to detect the *Dlx6* WT allele (Lane A), the *Dlx5* WT allele (Lane B) had no yield.

4.2.3 Generation of a *Sp6*-tagged knock-in mouse

The correct development and function of the AER is crucial for limb development. The AER controls PD limb elongation and patterning (Saunders 1948; Dudley et al. 2002; Sun et al. 2002; Niswander 2003; Boulet et al. 2004; Mariani et al. 2008). *Sp6* and *Sp8*, are transcription factors expressed in the limb ectoderm and in the AER, where they mediate in a redundant and dose dependent manner the Wnt-dependent induction of *Fgf8* expression (Haro et al. 2014).

Sp6 mutant mice display soft-tissue syndactyly in the forelimb and synostosis in the hindlimb with variable penetrance and expressivity (Talamillo et al. 2010). The *Sp8* mutant mice display limb truncations at variable proximo-distal level, most frequently at the level of the elbow/knee (Bell et al. 2003; Treichel et al. 2003). Both mutants show

defects in the AER and in DV patterning. The analysis of the double *Sp6;Sp8* allelic series showed that *Sp6^{-/-};Sp8^{+/-}* mutants, those with only one functional copy of *Sp8*, displayed a SHFM phenotype. Curiously, the SHFM phenotype of *Sp6^{-/-};Sp8^{+/-}* mutants also carries double dorsal digit tips, like the SHFM1 described in humans as caused by a missense mutation in the *DLX5* homeobox, the only case reported in humans with DV defects (Shamseldin et al. 2011). This observation suggests a link between Sp and Dlx transcription factors and is corroborated by recent studies in our lab using a *Sp8:3xFLAG* allele indicating that part of the Sp8 transcriptional activity is mediated by Dlx5 (Pérez-Gómez et al. 2020).

To further investigate the redundancy between *Sp6* and *Sp8* and their possible interaction with the *Dlx* genes, we decided to determine the Sp6 bound genomic regions by ChIP-seq and compare them with those of Sp8. To overcome the limitation of the lack of commercially available ChIP-grade antibodies for Sp6, we decided to generate a *Sp6* tagged KI allele. We designed a KI model in which the endogenous Sp6 was tagged with the V5 epitope. The aim was to incorporate the epitope at the C terminus in frame with the Sp6 protein, a strategy that has been widely used in ChIP-seq studies and that we knew was functional in in vitro essays (Pérez-Gómez et al. 2020).

crRNA_*Sp6* selection

We selected a crRNA to target the *Sp6* coding region, just before the STOP codon into exon 2 (Fig. 32). For the selection of the target sequence, we compared candidates from different web tools (see M&M 3.2) and finally selected a crRNA named crRNA_*Sp6*: GGTATAGCGGGGATATTACGAGG (chr6: + 6,864,949-6,864,971), based on its high score.



Figure 32: Schematic representation of the genomic region targeted by the crRNA_*Sp6*. Genomic structure of *Sp6* obtained from the UCSC genome browser. *Sp6* is encoded by 2 exons. The targeted region corresponds to the region just before the stop codon and the discontinuous red line and scissors point to the expected DSB.

In vitro validation of the crRNA_*Sp6*

The validation of the crRNA for *Sp6* was performed following the same protocol explained for the previous crRNAs shown above (See M&M 3.6) (Fig. 33).

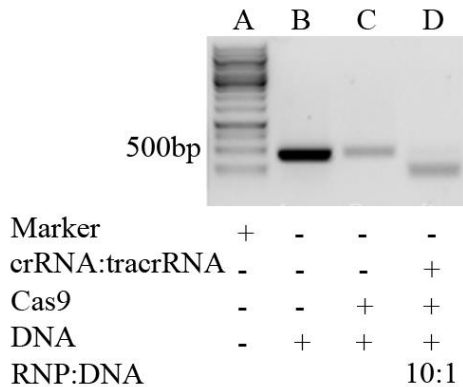


Figure 33. Successful vitro digestion of the crRNA_*Sp6*. Gel electrophoresis image showing cleavage of the *Sp6* PCR amplified product encoding the target domain upon incubation with the crRNA_*Sp6*. Lane A: The marker. Lane B: The DNA template. Lane C: The digestion of our DNA amplified with de Cas9 but without the crRNA as control. Lane D: The correct digestion of the template gives a single band containing the two 214bp and 222bp fragments.

We designed primers (*Sp6*-Fwd and *Sp6*-Rev) to PCR amplify a region of 436 bp around the breaking point. We performed a DNA substrate digestion with the RNP complex (crRNA_*Sp6*:tracrRNA:Cas9) in a 10:1 molar ratio (RNP:DNA substrate) that resulted in the presence of two fragments of the expected sized (214 and 222 bp). The correct generation of the DSB was confirmed by the single band of about 220bp that we inferred included the two similar size fragments (Fig 33, lane D). As negative control, the reaction was performed in the absence of the crRNA showing that the Cas9 was unable to cut the target DNA by its own (Fig. 33, lane C).

Donor design

To generate the *Sp6*-tagged KI mouse we designed a donor single strand DNA (ssODN) containing the V5 sequence to be introduced in the locus (Fig. 34) flanked by homology arms homologous to the WT sequence to direct the homologous recombination. We introduced the V5 sequence disrupting the crRNA sequence in the ssODN to avoid the Cas9 from cutting the donor DNA, rather than changing the PAM sequence. The ssODN size was 124nt in length composed of the V5 sequence (42bp) flanked by the homology arms (35bp and 47bp). Because not universal strand preference for the ssODN donor template has been identified (Paix et al. 2017; Schubert et al. 2021), we decided designed to use ssODN complementary to the target strand. We note that different epitope tags have been fused to members of the Sp family of transcription factors

both at their N-terminal or C-terminal ends without altering their function (Hojo et al. 2017; Pérez-Gómez et al. 2020).

```
5' AACGTGAGGCCGAAGGCAGCTCGGCGTCCTCCAACGGTAAGCCTA
TCCCTAACCTCTCCTCGGTCTCGATTCTACGTGAGCCCCATGGATGT
CACATACCTCCGTTCTTTATTTGGGGGGGC -3'
```

Figure 34: *Sp6:V5* ssODN (+). Both homology arms are highlighted in green, flanking the V5 sequence in yellow. The broken crRNA sequence is highlighted in blue and the PAM sequence in purple. The STOP codon, highlighted in red, is located just after V5 sequence.

The generation of *Sp6V5* KI model by zygote electroporation

We have performed 2 electroporation sessions with the RNP formed by the crRNA_*Sp6*, the tracrRNA, the ssODN and the Cas9 endonuclease. 103 embryos were electroporated. The embryos were transferred to 6 females.

Finally, we had 2 deliveries with a total of 3 offspring alive and 2 deaths. Two of these 5 mice, one of them alive and the other death, had the V5 inserted. Thus, the efficiency of our CRISPR/Cas9 system in this model to target the desired sequence and insert the donor by HDR was of 40%.

Genotyping strategy of F0 animals, analysis of the offspring and founder selection

One of the primers designed for the genotyping of the F0 mice was designed to anneal to the V5 sequence for a fast screening of the insertion of the V5. The amplification of the target region with the primers *Sp6*-Fwd and *Sp6:V5*-Rev should generate a fragment of 262bp (Fig. 35) if the V5 sequence has been inserted. Other primers were designed to amplify the complete target region, a fragment of 436bp if the allele is WT and 478bp (Fig. 35) if the V5 sequence has been inserted, to be analyzed by Sanger sequencing.

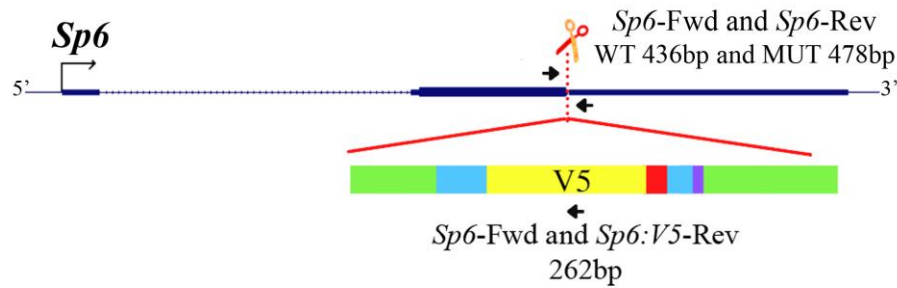


Figure 35: Genotyping strategy for the *Sp6:V5* KI animal model. The scheme represents the target site in exon2 of *Sp6*, just before the STOP codon (top) and the donor (bottom). The donor is formed by two homology arms (green), and the V5 sequence (yellow). The primers *Sp6*-Fwd and *Sp6*-Rev have been designed to amplify the target region (436 and 478bp in the WT and the mutant, respectively). *Sp6:V5*-Rev was designed to detect the V5 insertion amplifying a fragment of 262bp.

As mentioned, the analysis of the offspring by PCR resulted in 2 mice carrying the edited allele with the desired mutation but only one of them was alive, the F0 #1272 (Fig. 36).

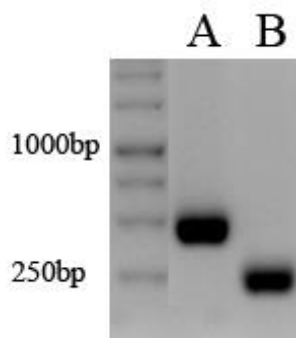


Figure 36: PCR genotyping of the *Sp6:V5* KI animal model. Gel electrophoresis image showing the results of the two PCRs used for F0 #1272 genotyping. Lane A: The primers *Sp6*-Fwd and *Sp6*-Rev are used to amplify the target region (478bp because the V5 sequences has been inserted). Lane B: The use of *Sp6*-Fwd and *Sp6:V5*-Rev showed a fragment of 262bp which indicates that the V5 tag had been inserted.

Sanger sequencing of the PCR amplified band using the primers *Sp6*-Fwd and *Sp6*-Rev showed that the mouse F0 #1272 was mosaic, so we proceeded to make a deeper analysis by cloning the amplified fragment of F0 #1272 by PGEM T-easy (see in M&M 3.14).

Sanger sequencing of the different clones showed that at least 3 alleles were present (Fig. 37). One of the alleles contained the complete V5 tag (allele 1) while the other two alleles showed partial insertions of V5 (alleles 2 and 3, Fig. 37). The F0 #1272 was selected to be the founder of the line.

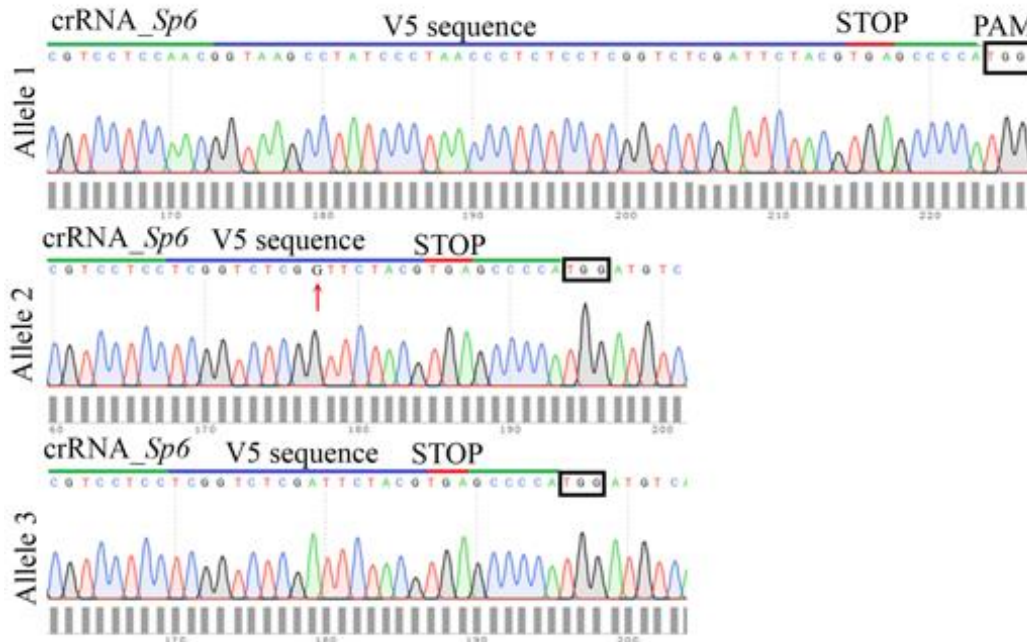


Figure 37: HDR mediated insertion of the donor DNA in the F0 #1272. Electropherogram showing the 3 alleles obtained after Sanger sequencing of mosaic F0 #1272. Allele 1 has the complete V5 tag sequence (top) while allele 2 has a partial insertion of the V5 tag sequence and a change of one nucleotide (G > A, denoted with a red arrow). Similarly, allele 3 has a partial insertion of the V5 tag.

Establishment of the *Sp6:V5^{emMar}* mouse line

We have established the line *Sp6:V5^{emMar}* from F0 #1272 selected as founder of the line. Once the line was established, we established the line in homozygosity, to determine whether the insertion of the tag affected *Sp6* function.

Next, we designed new primers to amplify a smaller region to facilitate the discrimination of similar size PCR product in 3% agarose gel electrophoresis. This approach allowed us to differentiate the WT allele (expected fragment of 326bp) from the

mutant allele, with the V5 sequence (expected fragment of 368bp) by conventional PCR (see M&M 3.12).

Phenotypic characterization of *Sp6:V5^{emMar}* mouse line

Mice homozygous for the *Sp6:V5* allele (*Sp6^{V5/V5}*) were viable and fertile and displayed no obvious phenotype indicating that the Sp6 tagged protein was functional.

The V5 antibody provides a useful resource for future studies requiring the detection of Sp6. To completely validate the line, we examined whether the V5 tag did impact the distribution or level of expression of Sp6 by immunohistochemistry (IHC) and immuno-fluorescence (IF) with the antiSp6 antibody (Sp6 rabbit polyclonal antibody from Proteintech, Ref: #21234-1-AP) and with the antiV5 antibody (V5 tag monoclonal antibody from eBioscience, Ref: TCM5). Unexpectedly, although Sp6 was detected both in IF and IHC assays (Fig. 38), the V5 tag was not detected in any assay. We performed IHC using two different monoclonal antiV5 antibodies (V5 tag monoclonal antibody (TCM5) from eBioscience, Mouse anti-V5 tag from BioRad and Anti-V5 antibody from Sigma Aldrich) and one polyclonal antiV5 antibody (Ref. 14440-1 AP from Proteintech), but all of them failed to detect the V5 tag (Fig. 38C).

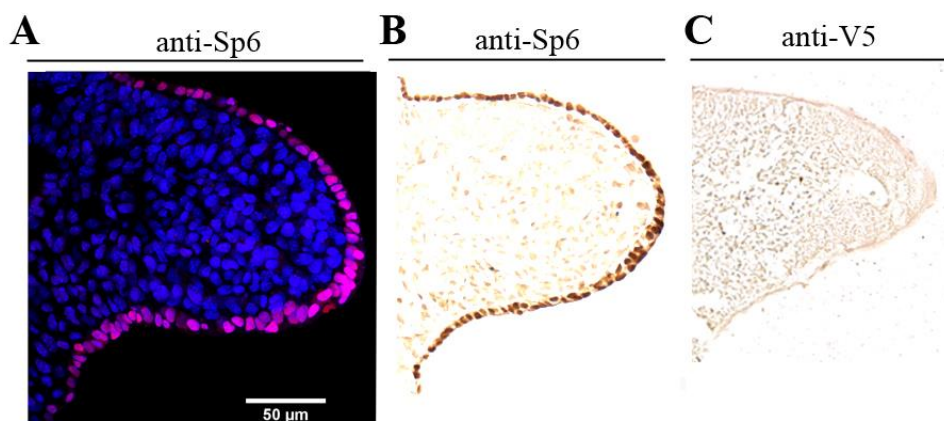


Figure 38: Immunofluorescence and immunohistochemistry in paraffin sections of FLs of *Sp6:V5* homozygous embryos at 10.5 stage. A. IF with the α Sp6 antibody detecting Sp6 in the limb ectoderm (pink). **B.** IHC with the α Sp6 antibody detecting expression in the limb ectoderm (dark brown). **C.** However, the IHC with the α V5 antibody did not give any signal.

We reasoned that the formation of Sp6 tertiary structure or even some post-translational modifications of the tag could prevent the access of the V5 antibody to the recognition site. Although V5 may not be accessible to the Ab in the fixed paraffin embedded tissue, it should be accessible in the denatured conditions of a Western blot (WB). However, all the antiV5 antibodies used failed to detect V5 in WB of E10.5 limb buds of either WT, heterozygous or homozygous embryos (Fig. 39A). In contrast, the antiSp6 antibody detected a band of ~40kDa in all these three samples (Fig. 39B).

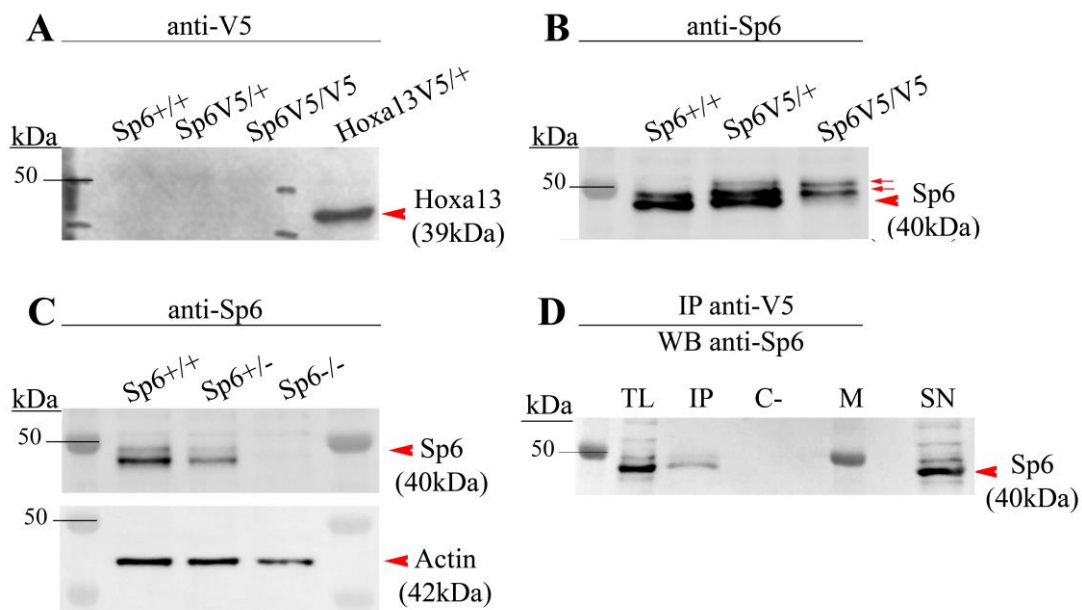


Figure 39: V5 tagged sp6 is not detected under denaturing conditions. Western blot analysis of mouse E10.5 limb buds of the genotypes indicated on top. **A.** The anti-V5 antibody detects Sp6 cell lysates of limb buds of E10.5 heterozygous (V5/+) and homozygous (V5/V5) embryos. Cell lysates of limb buds of Hoxa13:V5 heterozygotes is loaded as positive control. **B.** The anti-Sp6 antibody detects two Sp6 isoforms (A2A708-1 and Q9ESX2-1; from uniprot.org) in WT, heterozygous and homozygous E10.5 limb buds. The increase in weight of the Sp6 band in the heterozygous (V5/+) and homozygous (V5/V5) lanes indicate the presence of the V5 Tag. **C.** Western blot analysis showing the specificity of the anti-Sp6 antibody as no band is seen in the homozygous Sp6 mutant. β -Actin (Santa Cruz Ref 47778) was used as loading control. **D.** Western blot with the Sp6 antibody after immunoprecipitation (IP) with the anti-V5 nanobody of *Sp6:V5* homozygous embryos detects Sp6. TL: total lysate; IP: immunoprecipitation; C- We used cell lysates from mesencephalon of *Sp6:V5*^{V5/V5} embryos as control because this tissue

does not express *Sp6*. SN: supernatant of the immunoprecipitation that also reveals the *Sp6* band (42kDa).

Interestingly, comparison of WT, *Sp6:V5* heterozygous and homozygous samples showed a progressive increase in the size of the band indicative of the presence of the V5 tag. The specificity of the antibody against *Sp6* was confirmed in WB including limb buds from WT, heterozygous and mutant for *Sp6* (Fig. 39C)

Based on the Sanger sequencing results of *Sp6V5* homozygous mice, which showed complete and error-free insertion of the V5 tag sequence, and the WB results with the anti $Sp6$ antibody in WT, heterozygous for *Sp6V5* and homozygous samples, we can conclude that our *Sp6V5^{emMar}* mouse line has the V5 tag inserted.

Continuing with the idea that the recognition site of the antibody was not accessible for conventional antibodies, we tried to detect the V5 tag with a nanobody. Nanobodies are single-domain antibodies (sdAb) of only 15KDa, only one tenth the size of a conventional IgG antibodies (150KDa). The nanobody used was an alpaca anti-V5 V_HH, purified recombinant binding protein, which is covalently bound to magnetic agarose beads (V5-Trap Magnetic Agarose, v5tma, from ChromoTeck). Using this antibody, we performed immunoprecipitation (IP) to pulldown the *Sp6:V5* tagged protein.

The IP product was tested in an SDS-PAGE immunoblot analysis for the presence of *Sp6* with the *Sp6* antibody (*Sp6* rabbit polyclonal antibody (#21234-1-AP) from Proteintech) (Fig. 39D). A band of ~40kDa, corresponding to the size of *Sp6*, was detected in the WB further showing that V5 is bound to *Sp6* and supporting the notion that it is inaccessible for conventional antibodies. We also included in the WB the IP supernatant (SN), which usually is discarded, and found the band corresponding to *Sp6* (~40kDa) (Fig. 39D). This indicates that the IP was partial either due to the inaccessibility of the epitope or to a suboptimal technique.

4.3 APPLICATION OF THE CRISPR/CAS 9 TECHNOLOGY IN OTHER PROJECTS IN OUR LAB

4.3.1 Individual deletion of the limb-specific *Lmx1b* enhancers *LARM1* and *LARM2*.

The Nail-Patella Syndrome (NPS; MIM 161200), characterized by nail dysplasia, absent/hypoplastic patellae, chronic kidney disease, and glaucoma, is caused by *LMX1B* haploinsufficiency. *Lmx1b* is the dorsal limb determinant as it is both necessary and sufficient for dorsal limb morphology (Chen et al. 1998). *Lmx1b* expression in the limb depends on two autoregulatory enhancers termed *LARM1* and *LARM2* that were identified in a ChIP-seq for *Lmx1b* (Haro et al. 2017). The CRISPR/Cas9 removal of *LARM1* and *LARM2* together (*DelLarm1/2^{emMar}*) resulted in mice with double ventral limbs like those displayed by *Lmx1b*-nul mice but no other systemic defect, indicating that they are limb specific enhancers (Haro et al. 2021)

Most interestingly, a family with NPS lacking changes in the *LMX1B* coding region but with a 4.5 kb heterozygous deletion encompassing *LARM2* was identified indicating the pathogenicity of these enhancer (Haro et al. 2021). To further investigate the pathogenesis of the *LARM2* deletion, we generated by CRISPR-Cas9 a mouse model that replicated the 4.5 kb deletion observed in this family. In addition, we also generated the individual removal of *LARM1* to determine its involvement in *Lmx1b* regulation (Fig. 40A).

To generate individual mutants for the *LARM* enhancers, we selected two crRNAs to target the intergenic region between both enhancers and combine them with the crRNA previously used in the combined deletion of *LARM1/2*. The ones previously used were the crRNA named crRNA_355 (Sequence: TTCCCTTTTGAACCTTGCGG, chr2: + 33707449-33707471) upstream of *LARM2* and the crRNA named crRNA_372 (Sequence: TGGTCCCCAGATATTATGG, chr2: - 33699852-33699873) downstream of *LARM1*. The new crRNA selected for the individual deletion of *LARM2* was crRNA named crRNA_356 (Sequence: GGTCGGCACTGTAAATGTTG, chr2: + 33702894 - 33702916) and was used in combination with the crRNA_355. For the individual deletion of *LARM1* the new crRNA selected was the crRNA named crRNA_373 (Sequence: GGTCGGCACTGTAAATGTTG, chr2: + 33702665- 33702687) and was used in

combination with the crRNA_372. The new crRNAs selected were validated in vitro before being use for the electroporation of mouse zygotes (Fig. 40B).

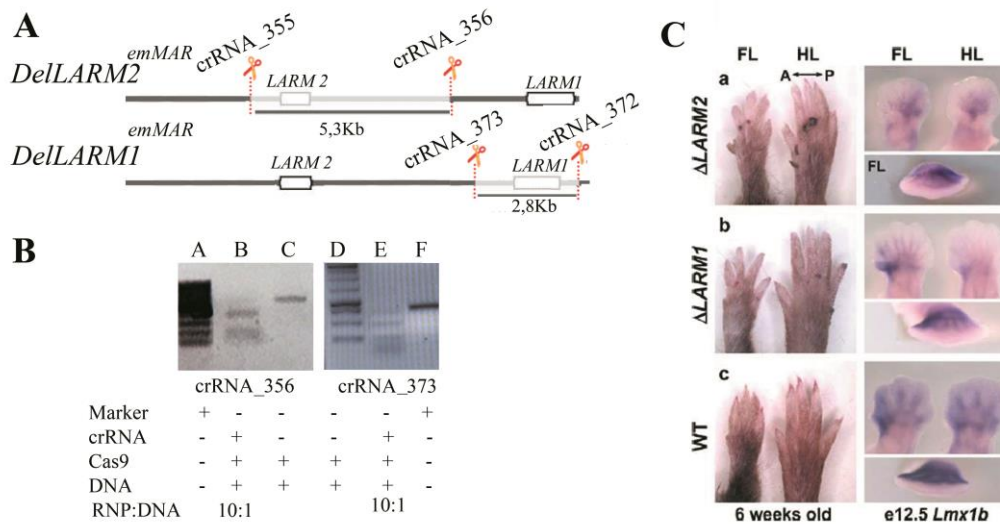


Figure 40: Individual deletion of *LARM1* and *LARM2* by CRISPR/Cas9 electroporation. **A.** Schematic representation of the *LARM1/2* locus where the crRNAs selected for each model are depicted (scissors) and the area deleted are shaded in grey. **B.** Successful in vitro digestion of the crRNA_356 and crRNA_373. Gel electrophoresis image on the left showing cleavage of the *LARM2* PCR amplified product upon incubation with the RNP formed with the crRNA_356 and for crRNA_373 upon incubation with *LARM1* PCR amplified product on the right. Lane A to F. Lane A: Marker. Lane B: Cleavage of the *LARM2* PCR amplified region (634bp) after incubation with RNP formed with the crRNA_356. The expected sizes of cleaved fragments are 347 and 287bp. Lane C: *LARM2* PCR amplified region (634bp) incubated in the absence crRNA_356 of showing no cleavage. Lane D: Marker. Lane E: Cleavage of the *LARM1* PCR amplified region (565bp) after incubation with RNP formed with the crRNA_373. The expected sizes of cleaved fragments are 185 and 380bp. Lane F: *LARM1* PCR amplified region (565bp) incubated in the absence of the crRNA_373 showing no cleavage. **C.** Dorsal views of 6-week-old mice Forelimbs and hindlimbs on the left and *Lmx1b* WMISH at E12.5 limb buds for the genotypes indicated. Note that *LARM2* homozygous mutant shows reduced anterior expression of *Lmx1b* in consistent with the appearance of footpads in the anterior part the limb concordant with the partial loss dorsalization, while *LARM1* homozygous mutant shows reduced posterior expression of *Lmx1b* consistent with the appearance of footpads in the posterior part of the limb.

We generated an animal model that replicated the mutation described in a family with 4.5Kb deleted in *LARM2* region. We established the *DelLARM2^{emMar}* mouse line carrying the deletion of *LARM2* enhancer. This animal model displays a ventral-ventral limb phenotype restricted to the anterior part of the limb coincident with the loss of *Lmx1b* expression (Fig. 40C). After that, the animal model for the KO of the *LARMI* enhancer and the *DelLARMI^{emMar}* mouse line was also established following the same procedure. In these mice the double ventral phenotype was restricted to the posterior limbs involving digits 2-5 (Haro et al. 2021).

4.3.2 Generation of a *Hoxa13* tagged knock-in mouse

To improve the detection of *Hoxa13* protein-protein interactions and given the lack of commercially available ChIP-grade antibodies for Hox proteins, a project in the lab was to generate a KI mouse model in which the endogenous *Hoxa13* gene is tagged with the V5 epitope (*Hoxa13:V5^{emMar}*) using CRISPR/cas9 electroporation of mouse zygotes and by the addition of a ssODN (Fig.41).

```

5' GCAAAGAAACAAATCCTTAAGCGTTTCTTCAAGCTGCCCTCTGC
TCCACCTTTTAATCCA TACGTAGAATCGAGACCGAGGAGAGGG
TTAGGGATAGGCTTACC GCCGGCGCCGGCGCCGGC ACTAG TAGT
CTTGAGTTTATTGATGACTTTTTTCTTTGACCCTCCTGTTCTGG
AACCA -3'

```

Figure 41: ssODN (+) used for the generation of the *Hoxa13:V5* animal model.

Both homology arms (60bp) are highlighted in green, flanking the V5 sequence in yellow. The broken crRNA sequence is highlighted in blue and the PAM sequence in purple with the changed nucleotide write in red (G>A). The STOP codon, highlighted in red, is located just after V5 sequence.

This epitope was incorporated in frame at the C terminus domain of the *Hoxa13* protein, a strategy that has been widely used for ChIP-seq studies (Koch et al. 2018). The *Hoxa13:V5* animal model was generated following the same strategy as for the generation of the *Sp6:V5^{emMar}* with the exception that a linker consisting in 3x AlaGly was added between the C-terminal end of *Hoxa13* and the V5 epitope (Fig. 42A).

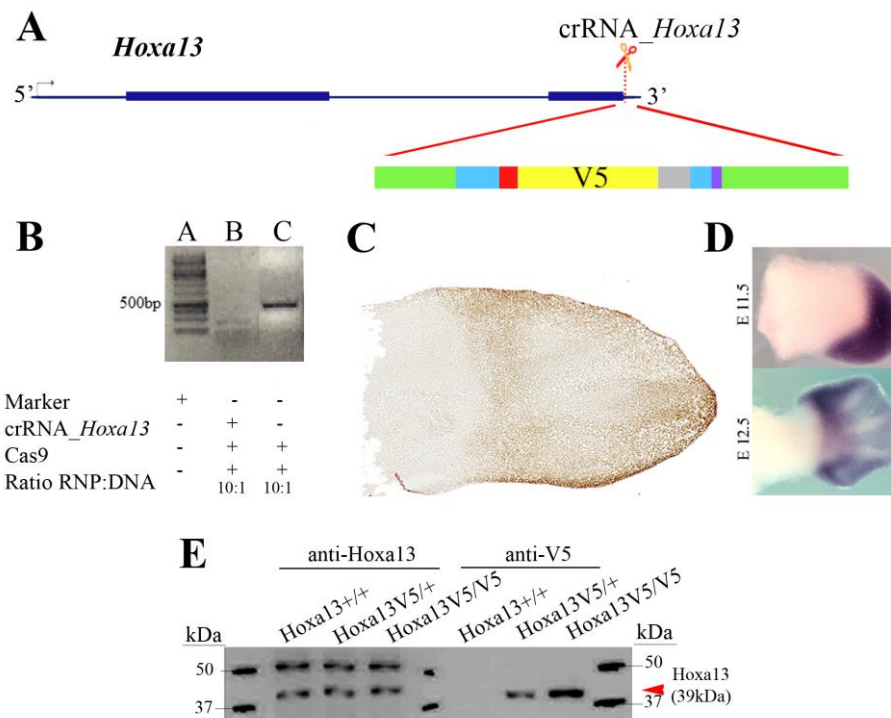


Figure 42: *Hoxa13*:V5 KI model. **A.** *Hoxa13* coding region composed of 2 exons (blue) on top. The scissors indicate the region targeted by the crRNA. Underneath the ssODN composed by the insertion of a linker region of 18bp (grey) followed by the V5 tag of 42bp (yellow) just before the Stop codon (Red). The changed PAM is indicated in purple and the homology arms in green. **B.** In vitro validation for the crRNA_ *Hoxa13*. Lane A to C. Lane A: The marker. Lane B: Incubation of the PCR amplified region targeted by the crRNA_ *Hoxa13* (405bp) with the Cas9 in the presence of crRNA_ *Hoxa13*. Expected fragments after cleavage 206 and 140 bp. Lane C: Incubation of the PCR amplified region targeted by the crRNA_ *Hoxa13* with the Cas9 in the absence of crRNA_ *Hoxa13*. **C.** anti-V5 IHC of a frontal section (cryostat) of a E11.5 mouse limb homozygous for *Hoxa13*:V5. The antibody used was V5 tag monoclonal antibody (TCM5) eBioscience, Invitrogen (#14-6796-82). V5 is detected in the distal mesenchyme of the autopod concordant with *Hoxa13* pattern of expression at this stage. **D.** *Hoxa13* WMISH in mouse limb buds of E 11.5 and E12.5. **E.** WB detection analysis of *Hoxa13*^{+/+} (39kDa); *Hoxa13*:V5^{V5/+} and *Hoxa13*:V5^{V5/V5} samples with *Hoxa13* antibody on the left and V5 antibody on the right.

The crRNA selected to target *Hoxa13* (crRNA_ *Hoxa13*), which sequence is: CCTTTTAATCCATTA ACTAG (chr6 + 52258892 - 52258911) was selected following

the same criteria as for the models above mentioned. Therefore, we introduced a modification that generates a silent mutation (G>A) in the PAM sequence of the ssODN b (Fig. 41).

Recently, it has been demonstrated that ssODN templates containing two blocking mutations, a nucleotide change in the PAM sequence and the disruption of the seed region, as in our ssODN, lead to more robust improvement in HDR efficiency (Schubert et al. 2021). The crRNA and the ssODN were designed so that the V5 tag is inserted in the 3' end of *Hoxa13* just before the stop codon with the linker region 5' to the tag (Fig. 42A). The crRNA_ *Hoxa13* was validated in vitro following the IDT protocol by the visualization of two expected fragments before the digestion of our target sequence with the RNP (Fig. 42B).

The generation of the *Hoxa13:V5^{emMar}* allele was obtained through the electroporation of mouse zygotes with the RNP formed by the crRNA_ *Hoxa13*; tracrRNA; Cas9 and a ssODN of 183bp. The line was successfully established and brought to homozygosity. Homozygous mice were viable and fertile and undistinguishable from their WT littermates. *Hoxa13:V5* was first detected by IHC in E12.5 cryostat limb sections of homozygous mutants (*Hoxa13:V5^{V5/V5}*), using the V5 antibody, in a pattern consistent with the expression of *Hoxa13* this stage (Fig. 42C-E). The antibody used to detect the V5 was the V5 tag monoclonal antibody (TCM5) from eBioscience. Detection that was further confirmed by WB with the use of *Hoxa13* antibody (Kindly provided by Dr Scot Staddler) and V5 antibodies in 4 limbs of Wild type, *Hoxa13:V5* heterozygous and homozygous mutant. While the *Hoxa13* antibody was able to detect *Hoxa13* in all the above-mentioned genotypes, the V5 failed to detect the protein.

Finally, the CRISPR/Cas9 zygote electroporation technology set up through this work has continued to be used in our laboratory for the generation of different animal models. For example, we deleted two ectodermal-specific *HOXC* enhancers, termed *EC1* and *EC2*, generating the *HoxcDelEC1-2^{emMar}* mouse line. The CRISPR-Cas9 approach also triggered an inversion of the targeted region producing the *HoxcInvEC1-2^{emMar}* allele that was the base to generate the *HoxcInvEC1-2^{emMar}* mouse line (Fernandez-Guerrero et al. 2020).

5.DISCUSSION

5. DISCUSSION

5.1. Development of a CRISPR/Cas9 based genome editing platform for generation of customized murine models

The development of this project has made it possible to establish a genome editing platform in our center, making this service available to all researchers in the field. The generation of animal models by CRISPR/Cas9 electroporation in mouse zygotes is a technique that, as we have demonstrated here, can be successfully implemented with easy and very limited resources.

Initially, the different components of the CRISPR/Cas9 system were delivered into zygotes by cytoplasmic or pronuclear microinjection (Wang et al. 2013) but this is a laborious methodology that requires practice and high skills to reduce cell damage in comparison with the zygote electroporation technique. Therefore, we decided to use the electroporation and selected the NEPA21 electroporator because the advantages over the current electroporators available in the market. The NEPA21 electroporator does not require any specific electroporation buffer, neither requires treatment of the pellucid zone prior to electroporation what increases the viability of the embryos. In addition, its efficiency is comparable to the microinjection technique (Kaneko 2017). The technique for animal knock-out system by electroporation (TAKE) method (Kaneko and Mashimo 2015) is the protocol developed for the NEPA 21 electroporator used in this project.

As expected from the power of the CRISPR technology and our selection of method for delivery, we did not encounter any major difficulties and we have rapidly set up the platform obtaining a high efficiency in the desired genomic editions.

As a result of this thesis a platform for “Transgenesis and Genomic Edition” has been integrated within the Servicio de Estabulación y Experimentación Animal (SEEA) at the University of Cantabria, specifically in the SPF (Specific Pathogen Free) section at the IBBTEC (<https://web.unican.es/unidades/scti/servicio-de-estabulaci%C3%B3n-y-experimentaci%C3%B3n-animal>). The platform is fully operative and has reached 100% efficiency in some of the latest models generated (<https://web.unican.es/unidades/scti/Documents/SEEA/Tarifas%20SEEA%202022.pdf>).

Our next step will be to set up the conditions to implement *in utero* electroporation. GONAD (Genome-editing via Oviductal Nucleic Acids Delivery) is a technique based on the electroporation of CRISPR/Cas9 system in the embryos when they are in the intact mouse oviduct (Takahashi et al. 2015). The method does not require high trained personnel in embryo isolation or embryo transfer surgeries and has the great advantage of notably reducing the number of mice required, in compliance with the 3R principles and EU regulations for animal welfare. Furthermore, this method can be a potential tool for genome editing in species other than mice.

5.2 Strategies to overcome the challenges of genotyping small INDELS

During the generation of CRISPR-aided mutagenesis, we found a limitation in our genotyping strategy due to the lack of fast and sensitive ways to detect small INDELS. The characterization of mutant mice can be difficult depending on the type of editing that has been performed. In this project, the deletion of a genomic fragment as in the *Dlx5/Dlx6* locus was rapidly assessed by regular PCR, as well as the insertion of the V5 tag using a primer designed to anneal to the V5 sequence. However, the *Jag2* KO model based on the generation of small INDELS that alters the reading frame of the gene raised problems in the genotyping strategy.

After generating a DSB, the NHEJ pathway repairs the damaged DNA. The NHEJ is error-prone and frequently generates INDELS that are often small. These small INDELS are difficult to detect by common methods based on size as they are beyond the resolution capacity of regular agarose gel electrophoresis. There are several genotyping strategies described for the detection of INDELS such as the SURVEYOR mutation detection assay (Cong et al. 2013), the Indel Detection by Amplicon Analysis (IDAA) method (Yang et al. 2015), the heteroduplex analysis (White et al. 1992; Bhattacharya and Van Meir 2019) or the PRIMA method (Probe-Induce HMA) (Kakui et al. 2021). Despite detection of the INDEL, the PCR amplification followed by Sanger sequencing (Cong et al. 2013) or by NGS are the only methods that permit the full characterization of the edited allele (Mianné et al. 2017). For genotyping the *Jag2* F0 animals, as for the other models, the genotyping strategy was based on PCR amplification followed by Sanger sequencing (Cong et al. 2013). Sequencing of the edited allele helps in the selection of the appropriate founder when several alleles are present. In general, knowing the exact modification helps to

predict which of the edited alleles is more probable to result in a null allele disrupting the open reading frame of a gene.

Genotyping by Sanger sequencing is appropriate and fast for the F0, however, it becomes untenable to maintain a colony because it would require Sanger sequencing of every mice generated. To avoid this, the heteroduplex analysis (White et al. 1992; Bhattacharya and Van Meir 2019) can be of great help, as we showed for the genotyping of the *Jag2* KO mice containing a 6nt deletion and the insertion of 1nt. Recently a new method called PRIMA has been reported (Kakui et al. 2021) based on the heteroduplex mobility assay (HMA) that uses a single-strand molecule as probe. This method seems to be rapid and cost-effective to detect a 1bp INDEL mutation. However, to resolve the difference in size between the WT and the mutant allele in the *Jag2* KO mice and prioritizing the use of agarose in contrast to polyacrylamide, the heteroduplex analysis was more convenient for us.

An alternative to eliminate the genotyping challenge of small INDELS introduced by the NHEJ repair mechanisms, is the generation of two DSBs using two crRNA flanking the essential region and remove the whole exon or even the complete gene (Chen et al. 2014; Low et al. 2016). This would allow a rapid and easy detection of the deleted allele. In addition, a donor DNA consisting in the sequences flanking both sides of the DSB and containing the desired mutation could be used to avoid short INDELS.

5.3 Disruption of the *Jag2* open reading frame by NHEJ mediated INDELS after CRISPR/Cas9 mediated DSB

The similarities in the limb phenotypes of the *Sp6* and the *Jag2* mutants prompted us to explore their possible genetic interaction during limb development and its possible implication in the SHFM syndrome. While the *Sp6* line (*B6.129-Sp6^{tm1Yoya}*) was already available in the lab, we decided to generate a KO model for *Jag2*. To this end we used CRISPR/Cas9 electroporation of zygotes directed to a single site in the coding region of the gene, based on the KO model previously published by the Gridley lab (*Jag2^{tm1Grid}*) (Jiang et al. 1998).

Among the several edited alleles obtained, we selected a *Jag2* KO allele carrying a 41bp deletion in the DSL domain (*Jag2^{emMar}*). Homozygous *Jag2^{emMar}* mice exhibited a similar phenotype to that previously described for the *Jag2* loss of function (Jiang et al. 1998). In the limb, *Jag2^{tm1Grid}* homozygous presented syndactyly of digits 2-4 with full

penetrance and variable expressivity as some cases (5 out of 13) included osseous fusions of the distal phalanges (Jiang et al. 1998). The phenotype was more severe in the hindlimbs and in several cases splitting of the terminal phalanx of digit 2 was described. While syndactyly of digit 2-4 was constant in *Jag2^{emMar}* homozygous mutants analyzed, we did not observe osseous fusions or splitting of the terminal phalanx in any of them. It is possible that the low number of mutants analyzed (n=6) might be the cause for the above-mentioned difference between both models.

The mouse *syndactylism (sm)* mutation is a spontaneous mutation initially identified because of the syndactylism phenotype (Grüneberg 1956). It was later shown that the gene mutated in *sm* mice was *Jag2* (Sidow et al. 1997). The *sm* allele carries a missense point mutation (G>A) mapping to codon 267 of the first EGF repeat of *Jag2* that results in a hypomorph allele (Sidow et al. 1997; Jiang et al. 1998). Interestingly, the variability in the penetrance and expressivity of the phenotype is observed when the genetic background is changed. Genetic background has long been proposed to be responsible for the phenotypic variability observed in mouse models generated in different strains and also in humans (Nadeau 2001). A genome-wide linkage analysis of the *Jag2 sm* identified 3 possible candidate loci acting as genetic modifiers of this hypomorph allele that could explain the observed phenotypic variability. Genetic modifiers can act either as suppressors leading to a less severe phenotype, or as enhancers making the phenotype more severe (Rahit and Tarailo-Graovac 2020). Of the three candidate modifiers of the *Jag2 sm* hypomorph allele, two were described as suppressor and one as an enhancer. One of the candidates acting as a suppressor was shown to map to a region in chromosome 11 containing several transcriptional regulators such as *Evi2* or the *HoxB* cluster. Of most interest, *Sp6* also maps to chromosome 11, ~700 Kb downstream of the *HoxB* cluster and therefore could potentially be a modifier gene of *Jag2* (Jiang et al. 1998). Therefore, a plausible explanation for the minor phenotypic differences between the *Jag2^{emMar}* and the *Jag2^{tm1Grid}* mutants is the presence of different variants of genetic modifiers between the different strains. A genetic modifier denotes a locus that can vary either in sequence or in number, in excess or in defect, between different genetic backgrounds and can alter the phenotypic outcome of a disease-causing variant (Riordan and Nadeau 2017).

It is interesting to note that while *sm* homozygous mutants generally survive and breed, both the *Jag2^{tm1Grid}* and the *Jag2^{emMar}* mutants die perinatally. In addition to the limb, *Jag2* is also expressed in other locations and most prominently in the branchial

arches. As mentioned, the perinatal death of *Jag2* mutants is due to the cleft palate phenotype. Therefore, it seems clear that the deficient function of the *Jag2* sm protein (hypomorph) is sufficient to fulfill its activity in the branchial arches but not in the limb. It would be most interesting to explore in the future the underlying mechanism accounting for this difference.

5.4 The analysis of *Jag2;Sp6* compound mutants suggests genetic interaction between both genes

Both *Sp6* and *Jag2* single homozygous mutants exhibit defects in the maturation of the AER as well as in digit patterning. The AER in these mutants is widened, as judged by the expanded domain of *Fgf8* expression, and protrudes into the mesoderm. The AER phenotype can be considered more severe in *Sp6* than in *Jag2* mutants as the former develop a double ridge phenotype with expression of *Fgf8* in two parallel rows resulting in a more pronounced widening of the limb bud. The digit skeletal phenotype is also more severe in *Sp6* than in *Jag2* mutants. We note that, while both the AER and the digit skeletal phenotype in the *Jag2^{emMar}* KO is fully penetrant, in animals lacking *Sp6* whereas the AER phenotype is fully penetrant, the syndactyl phenotype was present only in about one third of the cases making it more difficult to link these two processes (Jiang et al. 1998; Talamillo et al. 2010).

According to *Fgf8* expression in the AER and to the skeletal phenotype, double heterozygous (*Jag2^{+/-};Sp6^{+/-}*) mutants did not display an overt phenotype and animals with a single functional allele of *Sp6* in the absence of *Jag2* (*Jag2^{-/-};Sp6^{+/-}*) were indistinguishable from *Jag2* KOs. Similarly, the two mutants that were obtained lacking *Sp6* and with a single functional allele of *Jag2* (*Jag^{+/-};Sp6^{-/-}*) were indistinguishable from *Sp6* KOs. Interestingly, double homozygous mutant embryos (*Jag2^{-/-};Sp6^{-/-}*) exhibited a broader expansion of the AER with 100% of the embryos analyzed exhibiting the double ridge phenotype characteristic of the *Sp6* KO but not of the *Jag2* KO. This would indicate that *Sp6* is upstream of *Jag2* in AER regulation.

However, the hindlimbs that develop in the absence of both *Jag2* and *Sp6* (*Jag2^{-/-};Sp6^{-/-}*) displayed an skeletal phenotype not observed in either of the single KO. The bony fusion of the three phalanx elements of digits 2-4 or digits 3-4 with loss of digit 2 from the level of the metatarsal head is a phenotype more severe than that of each

individual mutation and that can be interpreted as stronger than the simple addition of the defects seen in the individual mutants. Furthermore, the variable penetrance and expressivity with left-side bias characteristics of *Sp6* KO mutants becomes fully penetrant with no lateral bias in the absence of *Jag2* (*Jag2*^{-/-};*Sp6*^{-/-}). Thus, considering the bone syndactyly phenotype, some times with oligodactyly, observed in double homozygous mutants as a new phenotype, the data supports a synergistic interaction between *Sp6* and *Jag2* (Boucher and Jenna 2013).

A point that merits some discussion is the shift from the incomplete penetrance of the skeletal phenotype of the *Sp6* null background to the full penetrance when *Jag2* is additionally lost. Genetic modifiers can change the phenotype of a disease-causing variant by genetic, biochemical, or functional interaction (Rahit and Tarailo-Graovac 2020). In the same manner that *Sp6* could act as a suppressor modifier of *Jag2*, it is also possible that *Jag2* is implicated in the variable expressivity and penetrance of the *Sp6* null skeletal phenotype.

We noticed that the skeletal phenotype of *Jag2*^{-/-};*Sp6*^{-/-} double mutant embryos morphologically reminds the SHFM phenotype. Indeed, it includes two of the main features of the SHFM namely the loss of digits and the syndactyly of remaining digits. We have previously reported the *Sp6*^{-/-};*Sp8*^{+/-} mutants are a good model for this syndrome. The limb phenotype resulting from the progressive decrease in *Sp6/Sp8* gene dosage transits from syndactyly in *Sp6* homozygous mutants, SHFM phenotype in animals lacking *Sp6* and with a single functional allele of *Sp8*, limb truncations in animals homozygous for *Sp8* and finally amelia in the double *Sp6;Sp8* KO (Haro et al. 2014). The SHFM phenotype in double *Sp6*^{-/-};*Sp8*^{+/-} mutants results from a deficit in the AER induction as the dosage of Sp transcription factors reached in this mutant is considered to be at the boundary of that required for *Fgf8* activation (Haro et al. 2014). Thus, in *Sp6*^{-/-};*Sp8*^{+/-} mutants *Fgf8* is irregularly activated in AER precursor cells eventually leading to the lack of the AER in the central portion of the limb bud. However, the SHFM-like limb phenotype of *Jag2*^{-/-};*Sp6*^{-/-} mutants correlates with an expanded AER suggesting that similar phenotypes are possible with different underlying mechanisms.

Finally, it is worth considering the implication of the interdigital tissue in the syndactyly phenotype observed in *Sp6*, *Jag2* and double mutants. Both in the *Jag2* hypomorph (Sidow et al. 1997) and in the *Sp6* mutant (Talamillo et al. 2010) the

syndactyly has been reported to be of early onset as it is already appreciable at stages previous to the establishment of the interdigital space. This is different from the late syndactyly that results from the failure of cell death to remove the interdigital mesenchyme (Lu et al. 2006). Although an in-depth study is still missing, it has been suggested that the wider AER leads to an altered limb bud architecture with thicker in the dorso-ventral axis and shorter in the anterior-posterior axis that could impact the final digit pattern.

5.5 Perinatal lethality of heterozygous prevented the establishment of the double *Dlx5/Dlx6* edited deletion

The interaction between Sp and Dlx family members is relevant for both limb and bone development (Hojo et al. 2017; Pérez-Gómez et al. 2020). Previous work in our lab, using a *Sp8:3xFLAG* KI allele determine the genome-wide distribution of Sp8 showing that Dlx mediated the binding of about one third of the direct target genes of Sp8. The goal of generating the *Dlx5/6* double deletion was to investigate the subset of Sp8 targets that require Dlx genes and their possible implication in the SHFM syndrome

Our strategy to conjointly remove *Dlx5* and *Dlx6* was similar to that followed by Lufkin and colleges to generate their *Dlx5/6* double targeted mutation (Robledo et al. 2002). Both alleles carry a deleted fragment and are null for both *Dlx5* and *Dlx6* genes. Although a very precise comparison is not possible given the incomplete description in Robledo et al. 2002, the main difference between the two mutant alleles is that the CRISPR-edited mutant (this study) removed all the fragment between the first intron of each gene while in the targeted mutant (Robledo et al. 2002) the fragment removed spanned from the second exon of each gene and the KO strategy included an *ires-LacZ-neo* cassette under *Dlx6* transcriptional control. Surprisingly, despite having designed the crRNA sites quite near of the breaking points in the *Dlx6/Dlx5* targeted allele, our deleted fragment is bigger (~16Kb) than their reported deleted fragment (~11Kb). One possible explanation for this discrepancy is the use of a different mouse genome reference to map the deletion considering the temporal distance between the two studies. Therefore, given the minimal differences between the edited and the targeted alleles, it was totally unexpected that edited allele was perinatally lethal in heterozygosis while the targeted mutant was reported as viable, fertile and without an abnormal phenotype.

Searching for an explanation for the lethality of our *Dlx5/6* heterozygous mutant, we considered the following possibilities: i) off-target effects, ii) impaired function of the remaining first exons of each gene and iii) alteration of regulatory element (long non-coding RNAs *Dlx6os2*). All these possibilities were discarded. First, the evaluation of the most common off targets predicted by the crRNA design tools did not yield any changes in the edited mice (see results, Fig. 30) so we discarded this possibility. Second, we didn't give much weight to a possible detrimental effect of the remaining transcripts (first exon of each gene), as these are usually degraded. Finally, considering the regulatory elements in the locus we noticed that the LncRNA *Dlx6os2* element was partially removed in our deleted allele while it remained unaffected in the *Dlx5/6* targeted deletion (Robledo et al. 2002). The *Dlx6os2* (chr6:6,863,797-6,865,150) (*DLX6 antisense RNA 2*) is a long non-coding RNA (LncRNA) that completely spans the first intron of *Dlx6* with no known functional open reading frames. The function of the LncRNA *Dlx6os2* has not been explored yet, but the possible negative impact of its truncation was also discarded because our mice homozygous and heterozygous for the inverted allele, which also carry the disruption of *Dlx6os2*, were viable.

Interestingly, another mouse model of SHFM type 1, generated by Levi and colleges (Merlo et al. 2002), carries a 17Kb deletion encompassing the complete coding regions of each gene (*Dlx5* and *Dlx6*) and the intervening sequences also removing the LncRNA *Dlx6os2*. Mice heterozygous for this mutation, although viable and fertile if surviving, displayed embryonic lethality with incomplete penetrance as they were recovered at reduced frequency. This embryonic lethality is consistent with our results. We obtained only a single N1 heterozygous female born alive. Indeed, we analyzed 105 N1 mice of which only 23 were heterozygous for the deletion (21.9% of heterozygous instead of 50%) reflecting intrauterine dead of heterozygotes. Taking all the above considerations into account, we think that it is reasonable to assume the background of our mice exacerbates the penetrance of the heterozygous perinatal/prenatal lethality preventing us from establishing the *Dlx5/Dlx6* DKO line.

The CRISPR-Cas9 approach also triggered an inversion of the targeted region producing the *Dlx5/6* inverted allele. Mice homozygous for this allele were viable and fertile and phenotypically indistinguishable from wild-type littermates indicating that the inverted rearrangement of the region had no functional consequence (see results, Fig.31). Given the genomic organization of *Dlx6* and *Dlx5* genes in transcriptionally convergent

orientation, the inverted rearrangement implied the generation of two chimeric proteins made of the first exon of one gene and the other two exons of the other gene. The fact that mice homozygous for the inverted allele showed no phenotypic alteration suggests that these chimeric proteins are at least partially functional.

The inverted allele also carries the inversion of the *Dlx5/6* intergenic region known to contain several regulatory elements shared by *Dlx5* and *Dlx6*. At least two enhancers have been described in this location. One is the I56i, which is a forebrain and branchial arch enhancer (Zerucha et al. 2000) and the other is I56ii, which is active in the developing forebrain and in the specific GABAergic interneurons (Ghanem et al. 2003; Poitras et al. 2010). As expected for enhancers, their inverted configuration did not carry any observable consequence.

As mentioned above, the inverted allele also disrupts the LncRNA *Dlx6os2*. Mice homozygous for the inversion were viable and displayed no overt phenotype discarding the disruption of the LncRNA as the reason behind the reduced viability of *Dlx5/6* heterozygous F0 animals.

To further continue with this aim we have recently acquired the *Dlx5/Dlx6* floxed line (Bellessort et al. 2016) in order to generate the double mutant *Sp8:3xFLAG;Dlx5/6^{ff}*. Using the *Msx2;Cre* line will allow us to overcome the lethality of the *Dlx5/6* KO. Floxed *Dlx5/Dlx6* will help us determine the targets of Sp8 that required Dlx and the relevance of this interaction between Dlx and Sp transcription factors and the involvement of this interaction in limb development.

5.6 Successfully but undetectable insertion of the V5 tag in Sp6

To test the functional activity of Sp factors in the limb ectoderm (Talamillo et al. 2010; Haro et al. 2014) and because of the limited availability of ChIP-grade antibodies for Sp8, the *Sp8:3xFLAG* KI mouse model was generated previously in our lab (Pérez-Gómez et al. 2020). This allele was instrumental to genome-wide map Sp8 binding sites in the limb ectoderm and permitted to identify the interaction between Sp and Dlx genes in limb development. In the context of our study on the SHFM and to uncover the role of Sp6 in the Dlx/Sp interactions, we decided to mark Sp6 with another tag which allowed its specific detection. Among other available small tags, such as the influenza

hemmagglutinin10 (HA) or the MYC tag, we selected V5 as it has been less extensively used and the availability of good quality antibodies.

While the homologous recombination and the establishment of the line *Sp6:V5^{em1Mar}* were successful and the insertion of the tag was in frame as determined by sanger sequencing, we encountered unexpected difficulties for detecting Sp6:V5 with the V5 antibody either by immunoblots and by IHC or IF. Three different anti-V5 monoclonal antibodies failed to detect the Sp6:V5 protein both in WB and in tissue sections (IHC and IF) while all of them detected the same tag fused to Hoxa13 (Hoxa13:V5) in another mouse model generated in our lab (*Hoxa13:V5^{emMar}*). The tag signal in Sp6 may not be detectable due to several possible situations: i) the tag is degraded during biosynthesis; ii) the tag is hidden in the fusion protein thus escaping detection by the antibody, and iii) the tag is post translationally modified becoming undetectable by the antibody.

The first situation is discarded because the WB clearly detects the difference in size between the WT and the tagged protein demonstrating its presence in the final protein.

Considering the second possibility, to uncover our tag we tried to optimize the protocol for a more efficient cell lysis and protein extraction. We tried: i) increasing the boil time of the tissue lysate from 5min. to 10min. ii) increasing the final concentration of SDS in the lysis buffer (RIPA) from 0.1% to 1%. iii) Sonication was performed to prepare our tissue lysate to unmask the tag. We sonicate 10 times in RIPA buffer. Despite the different attempts, we were unable to detect the tag.

We also tried to detect the tag using a single domain antibody or nanobody against V5. The nanobodies are tiny, recombinantly produced antigen binding VHH fragments, derived from the Alpaca heavy chain IgG antibody. Their size is about one tenth of that of a conventional antibody (15kDa instead of 150kDa), allowing them to detect recognition sites inaccessible for monoclonal or polyclonal antibodies. The V5 nanobody used in this project was bound to magnetic agarose beads and was used to immunoprecipitate the Sp6:V5-tagged fusion protein. This format of nanobody cannot be used in the WB analysis because it is covalently bound to the beads and there is not available secondary antibody to detect the Alpaca IgG. It would be necessary to buy the unconjugated V5 antibody and conjugate it with biotin for its detection. After

immunoprecipitation with the nanobody, the expected Sp6 (~40kDa) band was detected with the Sp6 antibody. The intensity of the band was low what can be explained by a partial inaccessibility of the V5 epitope, or by a suboptimal technique as a stronger band was obtained in the supernatant obtained after the IP, which usually is discarded.

Finally, we considered the possibility that a posttranslational modification of V5 made it unrecognizable by the antibody. Currently, more than 300 types of posttranslational modification have been described such as phosphorylation, glycosylation, or acetylation for example. They can alter the conventional structure of the protein, its molecular mass or even its charge. The last four amino acids of Sp6 are Alanine-Serine-Serine-Asparagine where the asparagine is identified as polar, without charge and as a N-glycosylation target. On the other hand, the last four amino acids of the V5 tag are Leucine-Aspartic-Serine-Threonine where the threonine is identified as well as polar without charge but in this case, it is a target of O-glycosylation and phosphorylation. Perhaps, these amino acids resulted in a new posttranslational modification.

Considering that a major difference between the Hoxa13:V5 mouse model and Sp6:V5 mouse model is the use of a linker between the protein and the tag, we currently wonder whether the detection problems might have been avoided by the introduction of a linker sequence of amino acids between the protein and the epitope tag, technique that has been previously shown to be useful for tagging a given gene (Sabourin et al. 2007) and that we used in the Hoxa13:V5 model with fantastic results. The Hoxa13:V5 line was generated due to the lack of ChIP grade Hox specific antibodies in the context of a project directed to investigate Hoxa13 interactions both at protein and genomic level.

To conclude, the field of biology is undergoing an incredible revolution due to the infinite possibilities that CRISPR/Cas9 offers for genomic editing. As we have seen in this thesis, it is necessary to meticulously design the genome editing models. Features like crRNA selection, ssODN design and genotyping strategies must be carefully considered. Despite the huge efficiency of the CRISPR, the establishment of the line and characterization of the model faces many challenges that are difficult to anticipate and not always easy to overcome as we have experienced in several of our models.

6. CONCLUSIONS / CONCLUSIONES

6. CONCLUSIONS

1. We have established an effective CRISPR/Cas9-mediated genome editing service based on the electroporation of the mouse zygote for disease modeling and other experiments involving elucidation of gene function

2. The electroporation method of delivering genome-editing components into zygotes shows comparable efficiency to the cytoplasmic or pronuclear microinjection, the standard method to date, with advantages as higher rates of embryo survival, easier implementation, and less cost.

3. Using our platform, we have generated a new *Jag2* edited allele (*Jag2^{emMar}*) based in NHEJ after a single DSB that lacks 41 nucleotides. This mutation disrupts the reading frame and results in a complete loss of function allele. As expected, another edited allele that lacked 3 nucleotides in frame generated a silence mutation.

4. Homozygous *Jag2^{emMar}* mutants exhibit the phenotypic features previously described in the targeted KO (Jiang et al. 1998) including the pronounced syndactyly and the cleft palate that results in perinatal death.

5. The phenotypic characterization of *Jag2;Sp6* double mutants showed that double homozygous (*Jag2^{-/-};Sp6^{-/-}*) display traits not present in any individual mutant suggesting synergic interaction between these two genes.

6. The limb phenotype of *Jag2^{-/-};Sp6^{-/-}* double mutants is reminiscent of the SHFM with loss of one digit and fusion of others. The connection between the Notch pathway and the SHFM deserves further investigation.

7. The difficulty in genotyping small INDELS by conventional PCR excludes the single DSB as an election method to generate KOs.

8. Despite obtaining the desired allele conjointly removing *Dlx5* and *Dlx6*, the intrauterine lethality and low fertility of heterozygous animals prevented us from establishing the *Dlx5/6* mutant line.

9. The *Dlx5/6* inverted allele does not produce any phenotype in homozygosis indicating that the resulting Dlx6:Dlx5 chimeric proteins are functional, at least partially.

Conclusions

10. We have generated a tagged *Sp6:V5* allele using the corresponding donor with two homology arms and the tag (V5).

11. Despite the presence of V5 being detected by Sanger sequencing and molecular weight in immunoblots, it is inaccessible to detection by the anti-V5 antibodies. This suggests that either it is hidden by the Sp6 protein or posttranslationally modified.

12. The *Sp6:V5^{em1Mar}* line in homozygosis shows no phenotype demonstrating that the Sp6:V5 protein is functional.

6. CONCLUSIONES

1. Hemos establecido un servicio de edición genómica basado en la electroporación de CRISPR/Cas9 en embriones de ratón para la generación de modelos animales para el estudio de enfermedades o cualquier otro experimento que conlleve el estudio de la función génica.

2. La electroporación de Cas9/crRNA/tracrRNA como RNP en cigotos de una célula nos ha permitido editar el genoma con una tasa de eficiencia comparable a la obtenida mediante la técnica de la microinyección. Además, si comparamos ambas técnicas, la electroporación presenta mayor tasa de viabilidad de los embriones, su puesta a punto es más sencilla y conlleva menores costes que la microinyección.

3. Gracias a la plataforma de edición genómica establecida hemos generado un nuevo alelo para *Jag2* (*Jag2^{emMar}*) basándonos en la generación de un corte de doble cadena cuya reparación a través de la ruta NHEJ eliminó 41 nucleótidos. Esta mutación alteró la pauta de lectura del gen produciendo una pérdida de función total. Además, la eliminación de 3 nucleótidos, que no alteraba la pauta de lectura del gen, producía una mutación silenciosa.

4. Los mutantes *Jag2^{emMar}* homocigotos presentan el fenotipo previamente descrito para el KO de *Jag2* (Jiang et al. 1998) incluyendo la pronunciada sindactilia y el paladar hendido que resulta en una muerte perinatal.

5. La caracterización fenotípica de los dobles mutantes *Jag2;Sp6* muestra que el doble mutante (*Jag^{-/-};Sp6^{-/-}*) presenta un fenotipo diferente al que encontramos en los mutantes simples sugiriendo una interacción genética sinérgica entre ambos genes.

6. El fenotipo del doble mutante *Jag2^{-/-};Sp6^{-/-}* recuerda al fenotipo del síndrome de mano hendida, con la pérdida de un dedo y la fusión de otros. La posible conexión entre la vía de Notch y el síndrome de la mano hendida necesita una investigación más exhaustiva.

7. La dificultad de genotipar los INDELS que produce el sistema CRISPR/Cas9 cuando generamos un modelo KO produciendo un solo corte de doble cadena, excluye esta técnica para esta aplicación.

Conclusiones

8. A pesar de que se obtuvo el alelo portador de la delección conjunta de *Dlx5* y *Dlx6*, la muerte intrauterina y la baja fertilidad de los ratones dobles heterocigotos para *Dlx5* y *Dlx6* (*Dlx5/Dlx6*^{+/-}) nos ha impedido establecer la línea.

9. El alelo invertido de *Dlx5/6* no produce ningún fenotipo en homocigosis indicando que las proteínas quiméricas resultantes *Dlx6:Dlx5* son funcionales, al menos parcialmente.

10. Hemos generado el alelo marcado *Sp6:V5* usando una hebra donante que contenía dos brazos de homología y la etiqueta V5

11. A pesar de demostrarse la presencia de V5 por secuenciación Sanger y por peso molecular en inmunoblot, no se consigue su detección con anticuerpos. Esto sugiere que o bien V5 está escondido por Sp6 o que ha sufrido alguna modificación postraduccional.

12. La línea *Sp6:V5*^{emIMar} ha sido establecida en homocigosis y no muestra ningún fenotipo, demostrando que la proteína *Sp6:V5* es funcional, al menos parcialmente.

7. REFERENCES

7. REFERENCES

- Acampora D., Merlo G.R., Paleari L., Zerega B., Postiglione M.P., Mantero S., Bober E., Barbieri O., Simeone A., Levi G.** 1999. Craniofacial, vestibular and bone defects in mice lacking the Distal-less-related gene *Dlx5*. *Development*. 126:3795–3809.
- Ackerman C.M., Myhrvold C., Thakku G.S., Freij C.A., Metsky H.C., Yang D.K., Ye S.H., Boehm C.K., Kosoko-Thoroddse T.-S.F., Kehe J., Nguyen T.G., Carter A., Kulesa A., Barnes J.R., Dugan V.G., Hung D.T., Blainey P.C., Sabeti P.C.** 2020. Massively multiplexed nucleic acid detection with Cas13. *Nature*. 582.
- Ahmad M., Abbas H., Haque S., Flatz G.** 1987. X-chromosomally inherited split-hand/split-foot anomaly in a Pakistani kindred. *Hum. Genet.* 75:169–173.
- Alghadban S., Bouchareb A., Hinch R., Hernandez-Pliego P., Biggs D., Preece C., Davies B.** 2020. Electroporation and genetic supply of Cas9 increase the generation efficiency of CRISPR/Cas9 knock-in alleles in C57BL/6J mouse zygotes. *Sci. Rep.* 10:1–12.
- Anderson S.A., Qiu M., Bulfone A., Eisenstat D.D., Meneses J., Pedersen R., Rubenstein J.L.R.** 1997. Mutations of the Homeobox Genes *Dlx-1* and *Dlx-2* Disrupt the Striatal Subventricular Zone and Differentiation of Late Born Striatal Neurons. 19:27–37.
- Andersson E.R., Sandberg R., Lendahl U.** 2011. Notch signaling: Simplicity in design, versatility in function. *Development*. 138:3593–3612.
- Badura-stronka M., Latos-biele A., Stronka M., Jamsheer A.** 2014. Heterozygous *DLX5* Nonsense Mutation Associated with Isolated Split-Hand / Foot Malformation with Reduced Penetrance and Variable Expressivity in Two Unrelated Families. *Birth Defects Res A Clin Mol Teratol.* 1.
- Barrangou R., Fremaux C., Deveau H., Richards M., Boyaval P., Moineau S., Romero D.A., Horvath P.** 2007. CRISPR Provides Acquired Resistance Against Viruses in Prokaryot. *Science* (80-.). 315:1709–1713.

- Barrow J.R., Thomas K.R., Boussadia-Zahui O., Moore R., Kemler R., Capecchi M.R., McMahon A.P.** 2003. Ectodermal Wnt3 β -catenin signaling is required for the establishment and maintenance of the apical ectodermal ridge. *Genes Dev.* 17:394–409.
- Bell S.M., Schreiner C.M., Waclaw R.R., Campbell K., Pottert S.S., Scottt W.J.** 2003. Sp8 is crucial for limb outgrowth and neuropore closure. *Proc. Natl. Acad. Sci. U. S. A.* 100:12195–12200.
- Bellessort B., Le Cardinal M., Bachelot A., Narboux-Nême N., Garagnani P., Pirazzini C., Barbieri O., Mastracci L., Jonchere V., Duvernois-Berthet E., Fontaine A., Alfama G., Levi G.** 2016. Dlx5 and Dlx6 control uterine adenogenesis during post-natal maturation: Possible consequences for endometriosis. *Hum. Mol. Genet.* 25:97–108.
- Bendall A.J.** 2016. Direct Evidence of Allele Equivalency at the Dlx5 / 6 Locus. *276:272–276.*
- Beumer K.J., Trautman J.K., Mukherjee K., Carroll D.** 2013. Donor DNA Utilization During Gene Targeting with Zinc-Finger Nucleases. *Genetics.*
- Bhattacharya D., Van Meir E.G.** 2019. A simple genotyping method to detect small CRISPR-Cas9 induced indels by agarose gel electrophoresis. *Sci. Rep.* 9:1–7.
- Blattner A., Huber A.R., Röthlisberger B.** 2010. Homozygous nonsense mutation in WNT10B and sporadic Split-Hand/Foot Malformation (SHFM) with autosomal recessive inheritance. *Am. J. Med. Genet. Part A.* 152:2053–2056.
- Boel A., De Saffel H., Steyaert W., Callewaert B., De Paepe A., Coucke P.J., Willaert A.** 2018. CRISPR/Cas9-mediated homology-directed repair by ssODNs in zebrafish induces complex mutational patterns resulting from genomic integration of repair-template fragments. *Dis Model Mech.*
- Boles R.G., Pober B.R., Gibson L.H., Willis C.R., McGrath J., Roberts D.J., Yang-Feng T.L.** 1995. Deletion of chromosome 2q24-q31 causes characteristic digital anomalies: case report and review. .

- Bolotin A., Quinquis B., Sorokin A., Dusko Ehrlich S.** 2005. Clustered regularly interspaced short palindrome repeats (CRISPRs) have spacers of extrachromosomal origin. *Microbiology*. 151:2551–2561.
- Boucher B., Jenna S.** 2013. Genetic interaction networks: Better understand to better predict. *Front. Genet.* 4:1–16.
- Boulet A.M., Moon A.M., Arenkiel B.R., Capecchi M.R.** 2004. The roles of Fgf4 and Fgf8 in limb bud initiation and outgrowth. *Dev. Biol.* 273:361–372.
- Brouns S.J.J., Jore M.M., Lundgren M., Westra E.R., Slijkhuis R.J.H., Snijders A.P.L., Dickman M.J., Makarova K.S., Koonin E. V., Oost and J. van der.** 2008. Small CRISPR RNAs Guide Antiviral Defense in Prokaryotes. *Science*. 317:784–790.
- Brunner H.G., Hamel B.C.J., Bokhoven H. Van.** 2002. The p63 gene in EEC and other syndromes. *Med Genet.*
- Byrne S.M., Church G.M.** 2015. Crispr-mediated Gene Targeting of Human Induced Pluripotent Stem Cells. *Curr Protoc Stem Cell Biol.* 2015:1–28.
- C Rodriguez-Esteban, Schwabe J.W., Peña J.D. La, Foy B., Eshelman B., Izpisua Belmonte J.C.** 1997. Radical fringe positions the apical ectodermal ridge at the dorsoventral boundary of the vertebrate limb. *Nature*. 386.
- Campo M. Del, Jones M.C., Veraksa A.N., Curry C.J., Jones K.L., Mascarello J.T., Ali-kahn-catts Z., Drumheller T., McGinnis W.** 1999. Monodactylous Limbs and Abnormal Genitalia Are Associated with Hemizygoty for the Human 2q31 Region That Includes the HOXD Cluster. :104–110.
- Chen F., Pruett-Miller S.M., Huang Y., Gjoka M., Duda K., Taunton J., Collingwood T.N., Frodin M., Davis G.D.** 2011. High-frequency genome editing using ssDNA oligonucleotides with zinc-finger nucleases. *Nat Methods*.
- Chen H., Lun Y., Ovchinnikov D., Kokubo H., Oberg K.C., Pepicelli C. V, Gan L., Lee B., Johnson R.L.** 1998. Limb and kidney defects in Lmx1b mutant mice suggest an involvement of LMX1B in human nail patella syndrome. *Nat. Genet.*

- Chen J.S., Ma E., Harrington L.B., Da Costa M., Tian X., Palefsky J.M., Doudna J.A.** 2018. CRISPR-Cas12a target binding unleashes indiscriminate single-stranded DNase activity. *Science* (80-.). 360:436–439.
- Chen S., Lee B., Lee A.Y.F., Modzelewski A.J., He L.** 2016. Highly efficient mouse genome editing by CRISPR ribonucleoprotein electroporation of zygotes. *J. Biol. Chem.* 291:14457–14467.
- Chen X., Xu F., Zhu C., Ji J., Zhou X., Feng X., Guang S.** 2014. Dual sgRNA-directed gene knockout using CRISPR/Cas9 technology in *Caenorhabditis elegans*. *Nature*.
- Chylinski K., Makarova K.S., Charpentier E., Koonin E. V.** 2014. Classification and evolution of type II CRISPR-Cas systems. *Nucleic Acids Res.* 42:6091–6105.
- Cohn M.J., Izpisua-Belmonte J.C., Abud H., Heath J.K., Tickle C.** 1995. Fibroblast Growth Factors Induce Additional Limb Development from the Flank of Chick Embryos. 80:739–746.
- Cong L., Ran F.A., Cox D., Lin S., Barretto R., Hsu P.D., Wu X., Jiang W., Marraffini L. a.** 2013. Multiplex genome engineering using CRISPR/Cas systems. *Science.* 339:819–823.
- Conte D., Garaffo G., Lo Iacono N., Mantero S., Piccolo S., Cordenonsi M., Perez-Morga D., Orecchia V., Poli V., Merlo G.R.** 2016. The apical ectodermal ridge of the mouse model of ectrodactyly *Dlx5;Dlx6*^{-/-} shows altered stratification and cell polarity, which are restored by exogenous *Wnt5a* ligand. *Hum. Mol. Genet.* 25:740–754.
- Crackower M.A., Scherer S.W., Rommens J.M., Hui C.C., Poorkaj P., Soder S., Cobben J.M., Hudgins L., Evans J.P., Tsui L.C.** 1996. Characterization of the split hand/split foot malformation locus SHFM1 at 7q21.3-q22.1 and analysis of a candidate gene for its expression during limb development. *Hum. Mol. Genet.* 5:571–9.
- Crossley P.H., Martin G.R.** 1995. The mouse *Fgf8* gene encodes a family of polypeptides and is expressed in regions that direct outgrowth and patterning in the

developing embryo. *Development*.

- Davis C.A., Holmyard D.P., Millen K.J., Joyner A.L.** 1991. Examining pattern formation in mouse, chicken and frog embryos with an En-specific antiserum. *Development*.
- Dealy C.N., Brown A.M.C.** 1993. Wnt-5a and Wnt-7a are expressed in the developing chick limb bud in a manner suggesting roles in pattern formation along the proximodistal and dorsoventral axes. *43:175–186*.
- Deb K., Reese J., Paria B.C.** 2006. Methodologies to study implantation in mice. *Methods Mol. Med.* 121:9–34.
- Deltcheva E., Chylinski K., Sharma C.M., Gonzales K.** 2011. CRISPR RNA Maturation by Trans-Encoded Small RNA and Host Factor RNase III. *Nature.* 471:602–607.
- Doudna J.A.** 2020. The promise and challenge of therapeutic genome editing. *Nature.* 578:229–236.
- Dudley A.T., Ros M.A., Tabin C.J.** 2002. A re-examination of proximodistal patterning during vertebrate limb development. .
- Duijf P.H.G., van Bokhoven H., Brunner H.G.** 2003. Pathogenesis of split-hand/split-foot malformation. *Hum. Mol. Genet.* 12:R51-60.
- Eggan K., Akutsu H., Loring J., Jackson-Grusby L., Klemm M., Rideout W.M., Yanagimachi R., Jaenisch R.** 2001. Hybrid vigor, fetal overgrowth, and viability of mice derived by nuclear cloning and tetraploid embryo complementation. *Proc. Natl. Acad. Sci. U. S. A.* 98:6209–6214.
- Eisenstat D.D., Liu J.K., Mione M., Zhong W., Yu G., Anderson S.A., Ghattas I., Puelles L., Rubenstein J.L.** 1999. DLX-1, DLX-2, and DLX-5 expression define distinct stages of basal forebrain differentiation. *Com neurol.*
- Ellies D.L., Langille R.M., Martin C.C., Akimenko M.A., Ekker M.** 1997. Specific craniofacial cartilage dysmorphogenesis coincides with a loss of *dlx* gene expression in retinoic acid-treated zebrafish embryos. *mech dev.*

- Elliott A.M., Evans J.A.** 2006. Genotype – Phenotype Correlations in Mapped Split Hand Foot Malformation (SHFM) Patients. *Am. J. Med. Genet.* 1427:1419–1427.
- Elliott A.M., Reed M.H., Chudley A.E., Chodirker B.N., Evans J.A.** 2006. Clinical and epidemiological findings in patients with central ray deficiency: Split hand foot malformation (SHFM) in Manitoba, Canada. *Am. J. Med. Genet. Part A.* 140A:1428–1439.
- Faiyaz-Ul-Haque M., Zaidi S.H.E., King L.M., Haque S., Patel M., Ahmad M., Siddique T., Ahmad W., Tsui L.-C., Cohn D.H.** 2005. Fine mapping of the X-linked split-hand/split-foot malformation (SHFM2) locus to a 5.1-Mb region on Xq26.3 and analysis of candidate genes. *Clin. Genet.* 67:93–97.
- Fallon J.F., López A., Ros M.A., Savage M.P., Olwin B.B., Simandl B.K., Fallon J.F., Lopez A., Ros M.A., Savage M.P., Olwin B.B., Simandl B.K.** 1994. FGF-2 : Apical Ectodermal Ridge Growth Signal for Chick Limb Development
Published by : American Association for the Advancement of Science
Stable URL : <http://www.jstor.org/stable/2883834> JSTOR is a not-for-profit service that helps scholars , researcher. 264:104–107.
- Farboud B., Jarvis E., Roth T.L., Shin J., Corn J.E., Marson A., Meyer B.J., Patel N.H., Hochstrasser M.L.** 2018. Enhanced genome editing with cas9 ribonucleoprotein in diverse cells and organisms. *J. Vis. Exp.* 2018:1–13.
- Fernandez-Guerrero M., Yakushiji-kaminatsui N., Lopez-delisle L., Zdral S.** 2020. Mammalian-specific ectodermal enhancers control the expression of Hoxc genes in developing nails and hair follicles. 117:30509–30519.
- Fernandez-Teran M., Ros M.A.** 2008. The Apical Ectodermal Ridge : morphological aspects and signaling pathways. *Int. J. Dev. Biol.* 871:857–871.
- Francis J.C., Radtke F., Logan M.P.O.** 2005. Notch1 signals through Jagged2 to regulate apoptosis in the apical ectodermal ridge of the developing limb bud. *Dev. Dyn.* 234:1006–1015.
- Gardner C.A., Barald K.F.** 1992. Expression Patterns of Engrailed-Like Proteins in the Chick Embryo. 388.

- Garneau J.E., Dupuis M.È., Villion M., Romero D.A., Barrangou R., Boyaval P., Fremaux C., Horvath P., Magadán A.H., Moineau S.** 2010. The CRISPR/cas bacterial immune system cleaves bacteriophage and plasmid DNA. *Nature*. 468:67–71.
- Gasiunas G., Barrangou R., Horvath P., Siksnys V.** 2012. Cas9-crRNA ribonucleoprotein complex mediates specific DNA cleavage for adaptive immunity in bacteria. *Proc. Natl. Acad. Sci. U. S. A.* 109:2579–2586.
- Geurts A.M., Cost G.J., Freyvert Y., Zeitler B., Jeffrey C., Choi V.M., Jenkins S.S., Wood A., Cui X., Meng X., Vincent A., Lam S., Michalkiewicz M., Schilling R., Kalloway S., Weiler H., Ménoret S., Anegón I., Davis G.D., Zhang L., Rebar E.J., Gregory P.D., Urnov F.D., Jacob H.J., Buelow R.** 2009. Knockout Rats Produced Using Designed Zinc Finger Nucleases. *Science* (80-). 325:2009–2011.
- Ghanem N., Jarinova O., Amores A., Long Q., Hatch G., Park B.K., Rubenstein J.L.R., Ekker M.** 2003. Regulatory roles of conserved intergenic domains in vertebrate Dlx bigene clusters. *Genome Res.* 13:533–543.
- Gilbert L.A., Larson M.H., Morsut L., Liu Z., Gloria A., Torres S.E., Stern-
ginossar N., Brandman O., Whitehead H., Doudna J.A., Lim W.A., Jonathan S.** 2013. CRISPR-Mediated Modular RNA-Guided Regulation of Transcription in Eukaryotes. *Cell.* 154:442–451.
- Goodman F.R., Majewski F., Collins A.L., Scambler P.J.** 2002. A 117-kb Microdeletion Removing HOXD9 – HOXD13 and EVX2 Causes Synpolydactyly. :547–555.
- Gootenberg J.S., Abudayyeh O.O., Lee J.W., Essletzbichler P., Dy A.J., Joung J., Verdine V., Donghia N., Daringer N.M., Freije C.A., Myhrvold C., Bhattacharyya R.P., Livny J., Regev A., Koonin E. V., Hung D.T., Sabeti P.C., Collins J.J., Zhang F.** 2017. Nucleic acid detection with CRISPR-Cas13a/C2c2. *Science* (80-). 356:438–442.
- Gordon J.W., Ruddle F.H.** 1981. Integration and stable germ line transmission of genes injected into mouse pronuclei. *Science* (80-). 214:1244–1246.

- Grabarek J.B., Plusa B., Glover D.M., Zernicka-Goetz M.** 2002. Efficient delivery of dsRNA into zona-enclosed mouse oocytes and preimplantation embryos by electroporation. *genesis*.
- Graf R., Li X., Chu V.T., Rajewsky K.** 2019. sgRNA Sequence Motifs Blocking Efficient CRISPR/Cas9-Mediated Gene Editing. *Cell Rep.* 26:1098-1103.e3.
- Grüneberg H.** 1956. Genetical studies on the skeleton of the mouse XVIII. Three genes for syndactylism. *Jorunal Genet.*
- Guerrini L., Costanzo A., Merlo G.R.** 2011. A symphony of regulations centered on p63 to control development of ectoderm-derived structures. *J. Biomed. Biotechnol.* 2011:13.
- Guo Q., Loomis C., Joyner A.L.** 2003. Fate map of mouse ventral limb ectoderm and the apical ectodermal ridge. 264:166–178.
- Gurrieri F., Prinós P., Tackels D., Kilpatrick M.W., Allanson J., Genuardi M., Vuckov A., Nanni L., Sangiorgi E., Garofalo G., Nunes M.E., Neri G., Schwartz C., Tsipouras P.** 1996. A split hand-split foot (SHFM3) gene is located at 10q24→25. *Am. J. Med. Genet.* 62:427–436.
- Hale C.R., Zhao P., Olson S., Duff M.O., Graveley B.R., Wells L., Terns R.M., Terns M.P.** 2009. RNA-Guided RNA Cleavage by a CRISPR RNA-Cas Protein Complex. *Cell.*
- Haro E., Delgado I., Junco M., Yamada Y., Mansouri A., Oberg K.C., Ros M.A.** 2014. Sp6 and Sp8 Transcription Factors Control AER Formation and Dorsal-Ventral Patterning in Limb Development. *PLoS Genet.* 10:1004468.
- Haro E., Petit F., Pira C.U., Spady C.D., Lucas-toca S., Yorozuya L.I., Gray A.L., Escande F., Jourdain A., Nguyen A., Fellmann F., Good J., Francannet C., Manouvrier-hanu S., Ros M.A., Oberg K.C.** 2021. Identification of limb-specific Lmx1b auto-regulatory modules with Nail-patella syndrome pathogenicity. *Nat. Commun.*:1–11.
- Haro E., Watson B.A., Feenstra J.M., Tegeler L., Pira C.U., Mohan S., Oberg K.C.**

2017. Lmx1b-targeted cis-regulatory modules involved in limb dorsalization. *Development*.
- Harrison S.M., Houzelstein D., Dunwoodie S.L., Beddington R.S.** 2000. Sp5, a new member of the Sp1 family, is dynamically expressed during development and genetically interacts with Brachyury. *Dev. Biol.*
- Heikinheimo M., Lawshé A., Shackleford G.M., Wilson D.B., MacArthur C.A.** 1994. Fgf-8 expression in the post-gastrulation mouse suggests roles in the development of the face, limbs and central nervous system. *mech dev*.
- Hoyo H., Ohba S., He X., Lai L.P., McMahon A.P., Broad-cirm E., Angeles L.** 2017. Sp7/Osterix is restricted to bone-forming vertebrates where it acts as a Dlx co-factor in osteoblast specification. *37:238–253*.
- Horii T., Arai Y., Yamazaki M., Morita S., Kimura M., Itoh M., Abe Y., Hatada I.** 2014. Validation of microinjection methods for generating knockout mice by CRISPR/Cas-mediated genome engineering. *Sci. Rep.* 4:1–6.
- Hsu M., Chang Y., Truong V.A., Lai P.** 2019. CRISPR technologies for stem cell engineering and regenerative medicine One cut Two cuts. *Biotechnol. Adv.* 37.
- Iacono N. Lo, Mantero S., Chiarelli A., Garcia E., Mills A.A., Morasso M.I., Costanzo A., Levi G., Guerrini L., Merlo G.R.** 2008. Regulation of Dlx5 and Dlx6 gene expression by p63 is involved in EEC and SHFM congenital limb defects. *Development.* 135:1377–1388.
- Ianakev P., Kilpatrick M.W., Toudjarska I., Basel D., Beighton P., Tsiouras P.** 2000. Split-hand/split-foot malformation is caused by mutations in the p63 gene on 3q27. *Am. J. Hum. Genet.* 67:59–66.
- Irvine K.D., Vogt T.F.** 1997. Dorsal-ventral signaling in limb development. *Curr. Opin. Cell Biol.* 9:867–876.
- J C Ramer, Mowrey P.N., Robins D.B., Ligato S., Towfighi J., Ladda R.L.** 1990. Five children with del (2)(q31q33) and one individual with dup (2)(q31q33) from a single family: review of brain, cardiac, and limb malformations. *Med Genet.*

- Jaenisch R., Mintz B.** 1974. Simian virus 40 DNA sequences in DNA of healthy adult mice derived from preimplantation blastocysts injected with viral DNA. *Proc. Natl. Acad. Sci. U. S. A.* 71:1250–1254.
- Jansen R., Van Embden J.D.A., Gaastra W., Schouls L.M.** 2002. Identification of genes that are associated with DNA repeats in prokaryotes. *Mol. Microbiol.* 43:1565–1575.
- Jiang R., Lan Y., Chapman H.D., Shawber C., Norton C.R., Serreze D. V, Weinmaster G., Gridley T.** 1998. Defects in limb, craniofacial, and thymic development in Jagged2 mutant mice. .
- Jinek M., Chylinski K., Fonfara I., Hauer M., Jennifer A.** 2012. A programmable dual RNA-guided DNA endonuclease in adaptive bacterial immunity. *Science* (80- .). 337:816–821.
- Johnson C.G., Chen T., Furey N., Hemmingsen M.G., Bissig K.D.** 2020. Somatic Liver Knockout (SLiK): A Quick and Efficient Way to Generate Liver-Specific Knockout Mice Using Multiplex CRISPR/Cas9 Gene Editing. *Curr. Protoc. Mol. Biol.* 130:e117.
- Kakui H., Yamazaki M., Shimizu K.K.** 2021. PRIMA: a rapid and cost-effective genotyping method to detect single-nucleotide differences using probe-induced heteroduplexes. *Sci. Rep.* 11:1–10.
- Kaneko T.** 2017. Genome editing in mouse and rat by electroporation. *Methods in Molecular Biology.* p. 81–89.
- Kaneko T., Mashimo T.** 2015. Simple genome editing of rodent intact embryos by electroporation. *PLoS One.* 10:e0142755.
- Kaneko T., Sakuma T., Yamamoto T., Mashimo T.** 2014. Simple knockout by electroporation of engineered endonucleases into intact rat embryos. *Sci. Rep.* 4:6382.
- Kawakami Y., Esteban C.R., Matsui T., Rodríguez-león J., Kato S., Carlos J., Belmonte I.** 2004. Sp8 and Sp9 , two closely related buttonhead-like transcription

- factors , regulate Fgf8 expression and limb outgrowth in vertebrate embryos. *Development*. 8:4763–4774.
- Kellner M.J., Koob J.G., Gootenberg J.S., Abudayyeh O.O., Zhang F.** 2019. SHERLOCK: nucleic acid detection with CRISPR nucleases. *Nat. Protoc*. 14:2986–3012.
- Khan S., Basit S., Fk Z., Ali N., Ali G., Ansar M., Ahmad W.A.** 2012. A novel homozygous missense mutation in WNT10B in familial split-hand / foot malformation. *Clin. Genet*. 13:48–55.
- Kidder B.** 2014. In Vitro Maturation and In Vitro Fertilization of Mouse Oocytes and Preimplantation Embryo Culture. *Methods Mol Biol*. 1150:141–152.
- Koch B., Bianca Nijmeijer, Kueblbeck M., Cai Y., Walther N., Ellenberg J.** 2018. Generation and validation of homozygous fluorescent knock-in cells using CRISPR/Cas9 genome editing. *Nat. Protoc*. 176:139–148.
- Korzh V., Strähle U.** 2002. Marshall Barber and the century of microinjection: From cloning of bacteria to cloning of everything. *Differentiation*. 70:221–226.
- Kouwenhoven E.N., van Bokhoven H., Zhou H.** 2015. Gene regulatory mechanisms orchestrated by p63 in epithelial development and related disorders. *Biochim. Biophys. Acta - Gene Regul. Mech*. 1849:590–600.
- Kouwenhoven E.N., va Heeringen S.J., Tena J.J., Oti M., Dutilh B.E., Alonso M.E., de la Elisa C.M., Smeenk L., Rinne T., Parsaulian L., Bolat E., Jurgelenaite R., Huynen M.A., Hoischen A., Veltman J.A., Brunner H.G., Roscioli T., Oates E., Wilson M., Manzanares M., José L.G.S., Stunnenberg H.G., Lohrum M., van Bokhoven H., Zhou H.** 2010. Genome-wide profiling of p63 DNA-binding sites identifies an element that regulates gene expression during limb development in the 7q21 shfm1 locus. *PLoS Genet*. 6:1001065.
- Kraus P., Lufkin T.** 2006. Dlx Homeobox Gene Control of Mammalian Limb and Craniofacial Development. 1374:1366–1374.
- Labun K., Montague T.G., Krause M., Cleuren Y.N.T., Valen E.** 2019.

CHOPCHOP v3 : expanding the CRISPR web toolbox beyond genome editing H
akon. *Nucleic Acids Res.* 47:171–174.

**Latella M.C., Teresa M., Salvo D., Cocchiarella F., Benati D., Grisendi G.,
Comitato A., Marigo V., Recchia A.** 2016. In vivo Editing of the Human Mutant
Rhodopsin Gene by Electroporation of Plasmid-based CRISPR / Cas9 in the
Mouse Retina. :1–12.

Lee Niswander, Martin G.R. 1993. FGF-4 and BMP-2 have opposite effects on limb
growth. *Nature.*

Leonetti M.D., Sekine S., Kamiyama D., Weissman J.S., Huang B. 2021. A scalable
strategy for high-throughput GFP tagging of endogenous human proteins. *PNAS.*

Lewandoski M., Sun X., Martin G.R. 2000. Fgf8 signalling from the AER is essential
for normal limb development. 26:460–463.

Li, J.F. N., J.E. A., , J. M., M. Z., D. B., J. C., Sheen J. 2013. Multiplex and
homologous recombination-mediated genome editing in *Arabidopsis* and *Nicotiana
benthamiana* using guide RNA and Cas9. *Nat. Biotechnol.*

Liang X., Potter J., Kumar S., Ravinder N., Chesnut J.D. 2017. Enhanced
CRISPR/Cas9-mediated precise genome editing by improved design and delivery
of gRNA, Cas9 nuclease, and donor DNA. *J Biotechnol.*

Lin L., Luo Y. 2019. Tracking CRISPR's Footprints. .

Liu J.K., Ghattas I., Liu S., Chen S., Rubenstein J.L. 1997. Dlx genes encode DNA-
binding proteins that are expressed in an overlapping and sequential pattern during
basal ganglia differentiation. *Dev dyn.*

Low B.E., Kutny P.M., Wiles M. V. 2016. Simple, Efficient CRISPR-Cas9-Mediated
Gene Editing in Mice: Strategies and Methods. *Mouse Model. Drug Discov.*

Lu P., Minowada G., Martin G.R. 2006. Increasing Fgf4 expression in the mouse
limb bud causes polysyndactyly and rescues the skeletal defects that result from
loss of Fgf8 function. *Development.* 133:33–42.

- Maeder M.L., Samantha J Linder, Vincent M Cascio, Yanfang Fu, Quan H Ho, J Keith Joung.** 2013. CRISPR RNA-guided activation of endogenous human genes Morgan. *Nat Methods.* 10:977–979.
- Mahmood R., Bresnick J., Hornbruch A., Morton N., Colquhoun K., Martin P., Lumsden A., Dicksont C., Mason I.** 1995. A role for FGF-8 in the initiation and maintenance of vertebrate limb bud outgrowth. 5.
- Makarova K.S., Brouns S.J.J., Horvath P., Sas D.F., Wolf Y.I.** 2011. Evolution and classification of the CRISPR-Cas systems. *Nat. Rev. Microbiol.* 9:467–477.
- Makarova K.S., Koonin E. V.** 2015. Annotation and Classification of CRISPR-Cas Systems. *Methods Mol Biol.:*1–27.
- Mali P., Esvelt K.M., Church G.M.** 2013a. Cas9 as a versatile tool for engineering biology. *Nat Methods.* 10:957–963.
- Mali P., Yang L., Esvelt K.M., Aach J., Guell M., DiCarlo J.E., Norville J.E., Church G.M.** 2013b. RNA-guided human genome engineering via Cas9. *Science* (80-.). 339:823–826.
- Mariani F. V, Ahn C.P., Martin G.R.** 2008. Genetic evidence that FGFs play an instructive role in limb proximal-distal patterning. 453:401–405.
- Marinić M., Aktas T., Ruf S., Spitz F.** 2013. An Integrated Holo-Enhancer Unit Defines Tissue and Gene Specificity of the Fgf8 Regulatory Landscape. *Dev. Cell.* 24:530–542.
- Marraffini L.A., Sontheimer E.J.** 2008. CRISPR interference limits horizontal gene transfer in staphylococci by targeting DNA. *Science* (80-.). 322:1843–1845.
- Matson A.W., Hosny N., Swanson Z.A., Hering B.J., Burlak C.** 2019. Optimizing sgRNA length to improve target specificity and efficiency for the GGTA1 gene using the CRISPR/Cas9 gene editing system. *PLoS One.* 14:1–16.
- McGuinness T., Matthew H.P., Smiga S., Jason E.L., Danwen X., Bulfone A., Kingsley C., Qiu M., Kuei Liu J., L.R.Rubenstein J.** 1996. Sequence, Organization, and Transcription of the Dlx-1 and Dlx-2 Locus. *Genomics.*

- Merlo G.R., Paleari L., Mantero S., Genova F., Beverdam A., Palmisano G.L., Barbieri O., Levi G.** 2002. Mouse Model of Split Hand / Foot Malformation Type I. *genesis*. 101:97–101.
- Mianné J., Codner G.F., Caulder A., Fell R., Hutchison M., King R., Stewart M.E., Wells S., Teboul L.** 2017. Analysing the outcome of CRISPR-aided genome editing in embryos : Screening , genotyping and quality control. *Methods*. 122:68–76.
- Mikuni T., Nishiyama J., Sun Y., Kamasawa N., Yasuda R.** 2016. High Throughput, High Resolution Mapping of Protein Localization in Mammalian Brain by In Vivo Genome Editing. *Cell*.
- Mills A.A., Zheng B., Wang X.J., Vogel H., Roop D.R., Bradley A.** 1999. p63 is a p53 homologue required for limb and epidermal morphogenesis. *Nature*. 398:708–713.
- Miura H., Gurumurthy C.B., Sato T., Sato M., Ohtsuka M.** 2015. CRISPR/Cas9-based generation of knockdown mice by intronic insertion of artificial microRNA using longer single-stranded DNA. *Sci. Rep*.
- Miura H., Quadros R.M., Gurumurthy C.B., Ohtsuka M.** 2018. Easi-CRISPR for creating knock-in and conditional knockout mouse models using long ssDNA donors. *Nat. Protoc*.
- Mojica F., Díez-Villaseñor C., García-Martínez J., Soria E.** 2005. Intervening sequences of regularly spaced prokaryotic repeats derive from foreign genetic elements. *J. Mol. Evol*. 60:174–182.
- Mojica F., Díez-Villaseñor C., Soria E., Juez G.** 2000. Biological significance of a family of regularly spaced repeats in the genomes of Archaea, Bacteria and mitochondria. *Mol Microbiol*. 36:244–246.
- Mojica F.J.M., Díez-Villaseñor C., García-Martínez J., Almendros C.** 2009. Short motif sequences determine the targets of the prokaryotic CRISPR defence system. *Microbiology*.:733–740.

- Moon A.M., Boulet A.M., Capecchi M.R.** 2000. Normal limb development in conditional mutants of *Fgf4*. *127*:989–996.
- Moon A.M., Capecchi M.R.** 2000. *Fgf8* is required for outgrowth and patterning of the limbs. *Nat. Genet.* *23*:1–7.
- Myat A., Henrique D., Ish-Horowicz D., Lewis J.** 1996. A chick homologue of *Serrate* and its relationship with *Notch* and *Delta* homologues during central neurogenesis. *Dev. Biol.*
- Nadeau J.H.** 2001. Modifier genes in mice and humans. *Nat. Rev. Genet.*
- Nakamura S., Stock D.W., Wydner K.L., Bollekens J.A., Takeshita K., B M Nagai, Chiba S., Kitamura T., Freeland T.M., Zhao Z., J Minowada, J B Lawrence, Weiss K.M., Ruddle F.H.** 1996. Genomic analysis of a new mammalian distal-less gene: *Dlx7*. *Genomics.*
- Nakamura T., Unda F., De-Vega S., Vilaxa A., Fukumoto S., Yamada K.M., Yamada Y.** 2004. The Krüppel-like Factor *Epiprofin* Is Expressed by Epithelium of Developing Teeth, Hair Follicles, and Limb Buds and Promotes Cell Proliferation. *J. Biol. Chem.* *279*:626–634.
- Nguyen T.M., Zhang Y., Pandolfi P.P.** 2020. Virus against virus: a potential treatment for 2019-nCov (SARS-CoV-2) and other RNA viruses. *Cell Res.* *30*:189–190.
- Nishimasu H., Ran F.A., Hsu P.D., Konermann S., Shehata S.I., Dohmae N., Ishitani R., Zhang F., Nureki O.** 2014. Crystal Structure of *Cas9* in Complex with Guide RNA and Target DNA. *Cell.* *156*:935–949.
- Niswander L.** 2003. Pattern formation: old models out on a limb. *Nat. Rev. Genet.*
- Nunes M.E., Schutt G., Kapur R.P., Luthardt F., Kukulich M., Byers P., Evans J.P.** 1995. A second autosomal split hand/split foot locus maps to chromosome 10q24-q25. *Hum. Mol. Genet.* *4*:2165–2170.
- Nunez J., Chen J., Pommier G., Cogan J., Replogle J., Adriaens C., Ramadoss G., Shi Q., Hung K., Samelson A., Pogson A., Kim J., Chung A., Leonetti M., Chang H., Kampmann M., Bernstein B., Hovestadt V., Gilbert L., Weissman**

J. 2021. Genome-wide programmable transcriptional memory by CRISPR-based epigenome editing. *Cell*.

Ohtsuka M., Sato M., Miura H., Takabayashi S., Matsuyama M., Koyano T., Arifin N., Nakamura S., Wada K., Gurumurthy C.B. 2018. i-GONAD: a robust method for in situ germline genome engineering using CRISPR nucleases. *Genome Biol*.

Oliveros J.C., Tabas-madrid D., San-le D., Montoliu L., Cubas P., Pazos F. 2016. Breaking-Cas — interactive design of guide RNAs for CRISPR-Cas experiments for ENSEMBL genomes. *Nucleic Acids Res.* 44:267–271.

Ozcelik T., Porteus M.H., Rubenstein J.L., Francke U. 1992. DLX2 (TES1), a homeobox gene of the Distal-less family, assigned to conserved regions on human and mouse chromosomes 2. *Genomics*.

Paix A., Folkmann A., Goldman D.H., Kulaga H., Grzelak M.J., Rasoloson D., Paidemarry S., Green R., Reed R.R., Seydoux G. 2017. Precision genome editing using synthesis-dependent repair of Cas9-induced DNA breaks. *Proc. Natl. Acad. Sci. U. S. A.* 114:E10745–E10754.

Pan Y., Liu Z., Shen J., Kopan R. 2005. Notch1 and 2 cooperate in limb ectoderm to receive an early Jagged2 signal regulating interdigital apoptosis. 286:472–482.

Pérez-Gómez R., Fernández-Guerrero M., Campa V., Lopez-Gimenez J.F., Rada-Iglesias A., Ros M.A. 2020. Sp8 regulatory function in the limb bud ectoderm. *BioRxiv*.

Poitras L., Yu M., Lesage-Pelletier C., MacDonald R.B., Gagné J.-P., Hatch G., Kelly I., Hamilton S.P., Rubenstein J.L.R., Poirier G.G., Ekker M. 2010. An SNP in an ultraconserved regulatory element affects Dlx5/Dlx6 regulation in the forebrain. *Development*.

Presnell J.S., Schnitzler C.E., Browne W.E. 2015. KLF/SP transcription factor family evolution: Expansion, diversification, and innovation in eukaryotes. *Genome Biol. Evol.* 7:2289–2309.

- Qi L.S., Larson M.H., Gilbert L.A., Doudna J.A., Weissman J.S., Arkin A.P., Lim W.A.** 2013. Repurposing CRISPR as an RNA-Guided Platform for Sequence-Specific Control of Gene Expression. *Cell*. 152:1173–1183.
- Qiu M., Bulfone A., Ghattas I., Meneses J.J., Christensen L., Sharpe P.T., Presley R., Pedersen R.A., Rubenstein J.L.** 1997. Role of the Dlx homeobox genes in proximodistal patterning of the branchial arches: mutations of Dlx-1, Dlx-2, and Dlx-1 and -2 alter morphogenesis of proximal skeletal and soft tissue structures derived from the first and second arches. *Dev Biol*.
- Raas-Rothschild A., Manouvrier S., Gonzales M., Farriaux J.P., Lyonnet S., Munnich A.** 1996. Refined mapping of a gene for split hand-split foot malformation (SHFM3) on chromosome. *JMed Genet.*:996–1001.
- Rahit K.M.T.H., Tarailo-Graovac M.** 2020. Genetic Modifiers and Rare Mendelian Disease. *Genes (Basel)*.
- Richardson C.D., Ray G.J., DeWitt M.A., Curie G.L., Corn J.E.** 2016. Enhancing homology-directed genome editing by catalytically active and inactive CRISPR-Cas9 using asymmetric donor DNA. *Nat. Biotechnol.*
- Riddle R.D., Ensini M., Nelson C., Tsuchida T., Jessell T.M., Tabin C.** 1995. Induction of the LIM homeobox gene Lmx1 by WNT7a establishes dorsoventral pattern in the vertebrate limb. *Cell*.
- Riley B.B., Savage M.P., Simandl B.K., Olwin B.B., Fallon J.F.** 1993. Retroviral expression of FGF-2 (bFGF) affects patterning in chick limb bud. *Development*.
- Rinne T., Brunner H.G., Bokhoven H. Van, Brunner H.G., Bokhoven H. Van.** 2007. p63-Associated disorders. *Cell cycle*. 4101.
- Riordan J.D., Nadeau J.H.** 2017. From Peas to Disease: Modifier Genes, Network Resilience, and the Genetics of Health. *Am. J. Hum. Genet.*
- Robledo R.F., Rajan L., Li X., Lufkin T.** 2002. The Dlx5 and Dlx6 homeobox genes are essential for craniofacial, axial, and appendicular skeletal development. *Genes Dev*. 16:1089–1101.

- Roscioli T., Taylor P.J., Bohlken A., Donald J.A., Masel J., Glass I.A., Buckley M.F.** 2004. The 10q24-linked split hand/split foot syndrome (SHFM3): Narrowing of the critical region and confirmation of the clinical phenotype. *Am. J. Med. Genet.* 124A:136–141.
- Rowe D.A., Fallon J.F.** 1982. The proximodistal determination of skeletal parts in the developing chick embryo. *J. Embryol. Exp. Morphol.* Vol. 68:1–7.
- S Sifakis, Basel D., Ianakiev P., Kilpatrick M., Tsipouras P.** 2001. Distal limb malformations: underlying mechanisms and clinical associations. *Clin. Genet.*
- Sabourin M., Tuzon C.T., Fisher T.S., Zakian V.A.** 2007. A flexible protein linker improves the function of epitope-tagged proteins in *Saccharomyces cerevisiae*. *Yeast.* 24:39–45.
- Sapranaukas R., Gasiunas G., Fremaux C., Barrangou R., Horvath P., Siksnys V.** 2011. The *Streptococcus thermophilus* CRISPR/Cas system provides immunity in *Escherichia coli*. *Nucleic Acids Res.* 39:9275–9282.
- Saunders J.W.J.** 1948. The proximo-distal sequence of origin of the parts of the chick wing and the role of the ectoderm. *Exp. Zool.*
- Schaeper N.D., Prpic N.M., Wimmer E.A.** 2010. A clustered set of three Sp-family genes is ancestral in the Metazoa: Evidence from sequence analysis, protein domain structure, developmental expression patterns and chromosomal location. *BMC Evol. Biol.* 10.
- Schubert M.S., Thommandru B., Woodley J., Turk R., Yan S., Kurgan G., McNeill M.S., Rettig G.R.** 2021. Optimized design parameters for CRISPR Cas9 and Cas12a homology-directed repair. *Sci. Rep.* 11:1–15.
- Schuster-Gossler K., Cordes R., Gossler A.** 2007. Premature myogenic differentiation and depletion of progenitor cells cause severe muscle hypotrophy in Delta1 mutants. *Proc. Natl. Acad. Sci. U. S. A.* 104:537–542.
- Semenova E., Jore M.M., Datsenko K.A., Semanova A., Westra E.R., Wanner B., Van Der Oost J., Brouns S.J.J., Severinov K.** 2011. Interference by clustered

regularly interspaced short palindromic repeat (CRISPR) RNA is governed by a seed sequence. *Proc. Natl. Acad. Sci. U. S. A.* 108:10098–10103.

- Seruggia D., Montoliu L.** 2014. The new CRISPR-Cas system: RNA-guided genome engineering to efficiently produce any desired genetic alteration in animals. *Transgenic Res.*
- Shamseldin H.E., Faden M.A., Alashram W., Alkuraya F.S.** 2011. Identification of a novel DLX5 mutation in a family with autosomal recessive split hand and foot malformation. *J. Med. Genet.* 49:16–20.
- Shawber C., Boulter J., Lindsell C.E., Weinmaster G.** 1996. Jagged2: A Serrate-like gene expressed during rat embryogenesis. *Dev. Biol.* 180:370–376.
- Shen B., Zhang X., Du Y., Wang J., Gon J., Zhang X., Tate P.H., Li H., Huang X., Zhang W.** 2013. Efficient Knockin Mouse Generation by ssDNA Oligonucleotides and Zinc-Finger Nuclease Assisted Homologous Recombination in Zygotes. *PLoS One.*
- Shilo B., Sprinzak D.** 2017. The lipid-binding side of Notch ligands. *EMBO J.* 36:2182–2183.
- Shmakov S., Abudayyeh O.O., Makarova K.S., Wolf Y.I., Jonathan S., Semenova E., Minakhin L., Joung J., Konermann S., Severinov K., Zhang F., Koonin E. V.** 2015. Discovery and functional characterization of diverse Class 2 CRISPR-Cas systems. *mol cell.* 60:385–397.
- Sidow A., Bulotsky M.S., Kerrebrock A.W., Bronson R.T., Daly M.J., Reeve M.P., Hawkins T.L., Birren B.W., Jaenisch R., Lander E.S.** 1997. Serrate2 is disrupted in the mouse limb-development mutant syndactylism. .
- Simeone A., Acampora D., Pannese M., D’Esposito M., Stornaiuolo A., Gulisano M., Mallamaci A., Kastury K., Druck T., Huebner K., Boncinelli E.** 1994. Cloning and characterization of two members of the vertebrate Dlx gene family. *Proc. Natl. Acad. Sci. U. S. A.* 91:2250–2254.
- Soshnikova N., Zechner D., Huelsken J., Mishina Y., Behringer R.R., Taketo**

- M.M., Iii E.B.C., Birchmeier W.** 2003. Genetic interaction between Wnt/b-catenin and BMP receptor signaling during formation of the AER and the dorsal-ventral axis in the limb. *Genetic interaction between.* :1963–1968.
- Sowińska-Seidler A., Socha M., Jamsheer A.** 2014. Split-hand/foot malformation - molecular cause and implications in genetic counseling. *J. Appl. Genet.* 55:105–115.
- Stock D.W., Elliest D.L., Zhao Z., Ekkert M., Ruddle F.H., Weiss K.M.** 1996. The evolution of the vertebrate *Dlx* gene family. *93:10858–10863.*
- Sumiyama K., Irvine S.Q., Ruddle F.H.** 2003. The role of gene duplication in the evolution and function of the vertebrate *Dlx*/distal-less bigene clusters. *J Struct Funct Genomics.*
- Sun X., Lewandoski M., Meyers E.N., Liu Y.H., Jr R.E.M., Martin G.R.** 2000. Conditional inactivation of *Fgf4* reveals complexity of signalling during limb bud development. *Nat. Genet.*
- Sun X., Mariani F. V, Martin G.R.** 2002. Functions of FGF signalling from the apical ectodermal ridge in limb development. *Nature.* 418:501–508.
- Sun X., Meyers E.N., Lewandoski M., Martin G.R.** 1999. Targeted disruption of *Fgf8* causes failure of cell migration in the gastrulating mouse embryo. *Genes Dev.* 13:1834–1846.
- Suske G., Bruford E., Philipson S.** 2005. Mammalian SP/KLF transcription factors: Bring in the family. *Genomics.* 85:551–556.
- Tabebordbar M., Zhu K., Cheng J.K.W., Chew W.L., Widrick J.J., Yan W.X., Maesner C., Wu E.Y., Xiao R., Ran F.A., Cong L., Zhang F., Vandenberghe L.H., Church G.M., Wagers A.J.** 2016. In vivo gene editing in dystrophic mouse muscle and muscle stem cells. *Science (80-.).* 351:407–411.
- Tackels-Horne D., Toburen A., Sangiorgi E., Gurrieri F., De Mollerat X., Fischetto R., Causio F., Clarkson K., Stevenson R., Schwartz C.** 2001. Split hand/split foot malformation with hearing loss: First report of families linked to the SHFM1

locus in 7q21. *Clin. Genet.* 59:28–36.

Takabayashi S., Aoshima T., Kabashima K., Aoto K., Ohtsuka M., Sato M. 2018. i-GONAD (improved genome-editing via oviductal nucleic acids delivery), a convenient in vivo tool to produce genome-edited rats. *Sci. Rep.* 8:1–12.

Takahashi G., Gurumurthy C.B., Wada K., Miura H., Sato M., Ohtsuka M. 2015. GONAD: Genome-editing via Oviductal Nucleic Acids Delivery system: A novel microinjection independent genome engineering method in mice. *Sci. Rep.* 5:1–11.

Talamillo A., Delgado I., Nakamura T., De-Vega S., Yoshitomi Y., Unda F., Birchmeier W., Yamada Y., Ros M.A. 2010. Role of Epiprofin, a zinc-finger transcription factor, in limb development. *Dev. Biol.* 337:363–374.

Temtamy S.A., McKusick V.A. 1978. The genetics of hand malformations. *Birth Defects Orig. Artic. Ser.* 14:i–xviii, 1–619.

Tesson L., Usal C., Ménoret S., Leung E. 2011. Knockout rats generated by embryo microinjection of TALENs. 29:695–696.

Theisen A., Rosenfeld J.A., Shane K., McBride K.L., Atkin J.F., Gaba C., Hoo J., Kurczynski T.W., Schnur R.E., Coffey L.B., Zackai E.H., Schimmenti L., Friedman N., J M.Z., Ball S., Pagon R., Lucas i A., Brasington C.K., Spence J.E., Sparks S., O V.B., Smith W., Friedberg T., Wyatt P.R., Aust M., Tervo R., Crowley A., Skidmore D., Lamb A.N., Ravnan B., Sahoo T., Schultz R., Torchia B.S., Sgro M., Shaffer D.C. I L.G. 2011. Refinement of the Region for Split Hand / Foot Malformation 5 on 2q31 . 1. 99207:262–271.

Treichel D., Becker M., Gruss P. 2001. The novel transcription factor gene Sp5 exhibits a dynamic and highly restricted expression pattern during mouse embryogenesis. *mech dev.* 101:175–179.

Treichel D., Schöck F., Jäckle H., Gruss P., Mansouri A. 2003. mBtd is required to maintain signaling during murine limb development. *Genes Dev.* 17:2630–2635.

Truett G.E., Heeger P., Mynatt R.L., Truett A.A., Walker J.A., Warman M.L. 2000. Preparation of PCR-quality mouse genomic dna with hot sodium hydroxide

and tris (HotSHOT). *Biotechniques*. 29:52–54.

Ugur S.A., Tolun A. 2008. Homozygous WNT10b mutation and complex inheritance in Split-Hand/Foot Malformation. *Hum. Mol. Genet.* 17:2644–2653.

Ullah A., Hammid A., Umair M., Ahmad W. 2017. A Novel Heterozygous Intragenic Sequence Variant in DLX6 Probably Underlies First Case of Autosomal Dominant Split-Hand / Foot Malformation Type 1. *45320:79–84*.

Vargesson N., Patel K., Lewis J., Tickle C. 1998. Expression patterns of Notch1, Serrate1, Serrate2 and Delta1 in tissues of the developing chick limb. *Mech. Dev.*

Vaudin P., Delanoue R., Davidson I., Silber J., Zider A. 1999. TONDU (TDU), a novel human protein related to the product of vestigial (vg) gene of *Drosophila melanogaster* interacts with vertebrate TEF factors and substitutes for Vg function in wing formation. *Development*. 126:4807–4816.

Wang H., Yang H., Shivalila C.S., Cheng A.W., Shi L., Jaenisch R. 2013. One-step generation of mice carrying reporter and conditional alleles by CRISPR/Cas-mediated genome engineering. *Cell*. 154:1370–1379.

Wang X., Xin Q., Li L., Li J., Zhang C., Qiu R., Qian C., Zhao H., Liu Y., Shan S., Dang J., Bian X., Shao C., Gong Y., Liu Q. 2014. Exome sequencing reveals a heterozygous DLX5 mutation in a Chinese family with autosomal-dominant split-hand / foot malformation. *22:1105–1110*.

Wefers B., Bashir S., Rossius J., Wurst W., Kühn R. 2017. Gene editing in mouse zygotes using the CRISPR / Cas9 system. *Methods*. 121–122:55–67.

White M.B., Carvalho M., Derse D., O'Brien S.J., Dean M. 1992. Detecting Single Base Substitutions as Heteroduplex Polymorphisms. *306:301–306*.

Witte F., Dokas J., Neuendorf F., Mundlos S., Stricker S. 2009. Comprehensive expression analysis of all Wnt genes and their major secreted antagonists during mouse limb development and cartilage differentiation. *Gene Expr. Patterns*. 9:215–223.

Xie K., Yang Y. 2013. RNA-guided genome editing in plants using a CRISPR-Cas

system. *Mol plant*.

- Xu J., Liu Z., Ornitz D.M.** 2000. Temporal and spatial gradients of Fgf8 and Fgf17 regulate proliferation and differentiation of midline cerebellar structures. *Development*.
- Yang A., Schweitzer R., Sun D., Kaghad M., Walker N., Bronson R.T., Tabin C., Sharpe A., Caput D., Crum C., Mckeon F.** 1999. p63 is essential for regenerative proliferation in limb , craniofacial and epithelial development. *398*:3–7.
- Yang H., Wang H., Jaenisch R.** 2014. Generating genetically modified mice using CRISPR/Cas-mediated genome engineering. *Nat. Protoc*.
- Yang Z., Steentoft C., Hauge C., Hansen L., Thomsen A.L., Niola F., Vester-Christensen M.B., Frödin M., Clausen H., Wandall H.H., Bennett E.P.** 2015. Fast and sensitive detection of indels induced by precise gene targeting. *Nucleic Acids Res.* 43.
- Yoshimi K., Kunihiro Y., Kaneko T., Nagahora H., Voigt B., Mashimo T.** 2016. SsODN-mediated knock-in with CRISPR-Cas for large genomic regions in zygotes. *Nat. Commun.* 7:2–11.
- Zerucha T., Stühmer T., Hatch G., Park B.K., Long Q., Yu G., Gambarotta A., Schultz J.R., Rubenstein J.L.R., Ekker M.** 2000. A highly conserved enhancer in the Dlx5/Dlx6 intergenic region is the site of cross-regulatory interactions between Dlx genes in the embryonic forebrain. *J. Neurosci.* 20:709–721.
- Zhan T., Rindtor N., Betge J., Ebert M.P.** 2018. CRISPR/Cas9 for cancer research and therapy. Elsevier. *Seminars i*.
- Zhang F., Abudayyeh O.O., Gootenberg J.S., Sciences C., Mathers L.** 2020. A protocol for detection of COVID-19 using CRISPR diagnostics. *Bioarchive.*:1–8.
- Zhang J., Li X., Neises A., Chen W., Hu L.** 2016. Different Effects of sgRNA Length on CRISPR-mediated Gene Knockout Efficiency. *Nat. Publ. Gr.*:1–10.

8. AGRADECIMIENTOS

AGRADECIMIENTOS

Millones de gracias a todos esos pilares que, de una manera u otra, me han sujetado durante estos años de tesis doctoral. Sin vosotros, esto no hubiera sido posible.

Gracias a Marian, por ser un referente para mí. Su “cabeza” sin duda es envidiable, pero quisiera resaltar su capacidad para hacer “equipo” en el laboratorio, haciéndonos a todos partícipes de cada momento y consiguiendo sacar de nosotros el máximo (ni más ni menos que lo que ella nos da cada día). Gracias por confiar en mi para hacer la tesis contigo.

Gracias a Endika, por estar conmigo codo con codo los primeros años de la tesis y por intentar sacar siempre un hueco para ayudarme, que además sé que no siempre fue fácil.

Gracias a Laura, esa maravilla de técnico que tiene nuestro laboratorio. Sin duda, tu curiosidad y tus ganas de aprender y mejorar siempre son dignas de admiración (jamás las pierdas). Gracias por toda la ayuda que me has dado estos años, pero gracias y mil gracias más por nuestras largas charlas, por escucharme, por apoyarme, por todo.

Gracias a Alex, “mi compañero de enfrente”, ese que me ha hecho compañía hasta tarde en el labo tantas veces, que me ha movido la cajonera dejándome sin espacio otras tantas y que sabe frenarme cuando empiezo a modificar cosas a última hora sin sentido. Sé que llegarás lejos, aunque a veces cueste, así que disfruta del camino, haz lo que te gusta y “step by step”.

Gracias a todo el lab, Sofía, Irene, Miguel, Lau por estar siempre dispuestos a echar una mano. Gracias Maria Félix, porque su experiencia vale millones. Gracias a toda la gente que ha pasado por el laboratorio, aunque haya sido de manera breve, porque siempre han aportado algo.

Gracias a Cristina, a Marc y a Rocio, porque sin duda, gracias a vosotros (junto con Laura) mis primeros años de tesis fueron realmente increíbles. Muchas horas de trabajo, pero también muchas risas, ¿Qué sería de nosotros sin las risas?

Gracias al laboratorio de Rada: Patri, María, Víctor, Thais, Sara, Marianna (etc etc etc). Por la pandemia dejamos de unirnos en los “Lab meetings” y aunque Víctor esté encantado con el sistema online, quería que supierais que se os echa de menos.

Gracias al laboratorio de Piero: Marta, Dalia, Lorena, Berta y Rocío, por siempre estar dispuestas a ayudar.

Agradecimientos

Gracias al personal del SEEA. Gracias a su director Miguel, a Mar, Patri y Marta, por todo su trabajo día a día, pero sobre todo gracias a Bea por ayudarme siempre, juntas hemos hecho esto posible.

Gracias a mis evaluadores, Álvaro Rada y Ramón Merino, por ayudarme año tras año a mejorar.

Gracias a Judith, por intentar organizarme los horarios en la clínica para no morir en el intento. Y gracias a Irene, que en lo poco que llevamos juntas presiento que este es el comienzo de una larga historia.

Por último, pero no menos importante, quiero dar especialmente las gracias a mi familia y a mis amigos. Compaginar una tesis doctoral con un trabajo requiere muchos sacrificios, y probablemente la gente que más quieres se lleva la peor parte, que es estar a veces en un segundo plano.

Por ello, quiero dar las gracias a mis amigos, por contar siempre conmigo para todo, pese a recibir tantas veces un “yo no puedo ir” por respuesta.

Gracias a mi familia de Solares, por la tortilla de los miércoles y los tupper hasta arriba que tantas veces me han salvado la vida.

Quiero dar las gracias a mis abuelas y a mi abuelo, por estar menos con ellos de lo que debería y siempre entenderlo.

Gracias en especial a mis padres y a mi hermana, sin duda ellos son uno de mis pilares fundamentales en la vida. Gracias por escucharme y por apoyarme, por decirme que frene, que me cuide, pero a la vez siempre empujarme a seguir, porque si alguna vez me caía, sabía que vosotros seríais mi red.

Y como postre, dejo las gracias para mi futuro marido. Sé que no han sido unos años fáciles, sobre todo el final, pero tú siempre has estado a mi lado sin queja alguna, ayudándome, escuchándome, acompañándome los fines de semana que me tocaba quedarme en casa trabajando y dándome en cada momento ese empujoncito que necesitaba. Gracias. Qué bonita casualidad la nuestra.

“Carpe Diem”

